A Surfacelet-based Method for Constructing Geometric Models of Microstructure

A Dissertation
Presented to
The Academic Faculty

By

Namin Jeong

In Partial Fulfillment
of the Requirements for the Degree
Doctor of Philosophy in the
School of Mechanical Engineering

Georgia Institute of Technology
December 2015

A Surfacelet-based Method for Constructing Geometric Models of Microstructure

Approved by:

Dr. David W. Rosen, Advisor
School of Mechanical Engineering
Georgia Institute of Technology

Dr. Hamid Garmestani
School of Materials Science and Engineering
Georgia Institute of Technology

Dr. Xiaoming Huo
School of Industrial & Systems Engineering
Georgia Institute of Technology

Dr. Surya Kalidindi
School of Mechanical Engineering
Georgia Institute of Technology

Dr. David L. McDowell
School of Mechanical Engineering
Georgia Institute of Technology

Dr. Yan Wang
School of Mechanical Engineering
Georgia Institute of Technology

Date Approved: November 16, 2015

Soli Deo Gloria

ACKNOWLEDGEMENTS

A dissertation marks the end of a long academic journey. It would not have been possible to complete this journey without the supports. I am grateful to a number of people who have provided their generous help during the course of this work.

Firstly, I would express my sincere appreciation to my advisor Dr. David W. Rosen for his guidance, patience, and encouragement. He waited me to find direction with enormous encouragement and provided great insight for me to finish this long journey. His relentless support and guidance cannot be overestimated. It is great opportunity to be your student.

I would like to extend my appreciation to my reading committee members, Dr. David McDowell, Dr. Hamid Garmestani, Dr. Xiaoming Huo, Dr. Surya Kalidindi, and Dr. Yan Wang for providing great feedback and invaluable insight. I have benefitted greatly from your time, knowledge, and advice.

I also would like to thank my lab friends, Chad A. Hume, Dr. Jane Kang, Sang-in Park, Dr. Amit Jariwala, Dr. Wencho Zhou, Narumi Watanabe, Jonathan Holmes, Ying Zhang, Xiayun Zhao, Patric Chang, and Jason Nguyen. They supported me to go through it and provided constructive discussion time. It was unforgettable and enjoyable time to be with you. I will miss the time we spent together.

I would like to thank my church members, Chong's family, Choi's family, Seungmin Lee, Young Joo Lee, Eunyoung Ahn, and Jinhee Kim for their warm-hearted support and encouragement. I will always remember the moment we have made.

I owe my family, my parents, parents-in-law, sister, brothers, sisters-in-law, immense gratitude for their unconditional love and support that have helped me go through the most difficult times. Without their support and sacrifice, I would not have gone so far.

Last but not least, I am deeply indebted to my husband Jaemin and my son Ian. Thank you for your endless love, support, and encouragement for me to go through it. Jaemin, you are always great my husband and my love. You are the one.

TABLE OF CONTENTS

LIST OF TABLES

LIST OF FIGURES

SUMMARY

Integration of material composition, microstructure, and mechanical properties with geometry information enables many product development activities, including design, analysis, and manufacturing. To address such needs, models of material composition have been integrated into CAD systems, creating systems called heterogeneous CAD modeling. In order to support the heterogeneous CAD system, extensive process-structure-property relationships have to be captured and integrated into current CAD system. A new method for reverse engineering of materials will be presented such that microstructure models can be constructed and used in the heterogeneous CAD system.

Reverse engineering of material consists of three parts: image analysis, structure-property-process relationship, and repository. In this research, an image processing method, which comprises the Radon transform and the wavelet transform, will be used in order to recognize geometric features from a microstructure image. Recognizing geometric features can be obtained by combinations of three techniques, masking, clustering, and high frequency component on wavelet transform, that are integrated with the Radon transform. Then, recognized geometric features can be used to construct an explicit geometric model of microstructure. The proposed work will provide an explicit mathematical method to recognize and to quantify microstructure features from an image. In addition, explicit geometric models of microstructure can be automatically constructed and utilized to get effective mechanical properties, establishing structure-property relationship of the material. In order to demonstrate this, polymer nano-composite sample and metal alloy sample will be used.

CHAPTER 1
INTRODUCTION

1.1 Geometry Representation in CAD

In the early 1960s, a revolutionary computer program, “Sketchpad” was developed. The program introduced a novel method of human-computer interaction using computer graphic. Since then, a computer-aided design program is rapidly developed, assisting product design process. The process covers from the design stage to the fabrication stage. These activities include manufacturing planning, fabrication, product performance analysis, and manufacturing process simulations. The parametric representation is the type of geometric models that are used in CAD system. Parametric equations use coordinates of the points as functions of variables to represent curve. Additionally, explicit geometric models for linear and conic geometry are used to model complicated geometry. An explicit geometric model indicates a geometric modeling represented as an explicit equation. It can be directly used in CAD system to model geometric features or can be converted to a parametric form. Most CAD programs have been built upon a surface modeling paradigm where a solid object is defined as an object enclosed by a set of discrete boundaries. This is known as Boundary Representation or Brep.

Material composition and microstructure play important roles in mechanical properties. However, the current CAD system has limitation to represent multiple materials with a modeling part. This fundamentally limits for a designer to use only one material for an entire part.

1.2 Heterogeneous CAD system

For many years, practitioners in the additive manufacturing (AM) industry have cited the lack of suitable engineering materials as a major challenge. Others note the large variability and

unpredictability of mechanical properties in AM processed materials. Computer-aided design (CAD) tools that integrate material information with geometry would address these issues. Furthermore, the capability of deriving mechanical properties from the material and geometry information would greatly aid part design and engineering [1]. Models of material composition and geometry are integrated in the new CAD system, called heterogeneous CAD system.

Heterogeneous CAD modeling integrates parameters related to material composition, microstructure, and mechanical properties with geometry information; in so doing it supports many product development activities, including design, analysis, and manufacturing. However, in existing methods, the distribution of material compositions is modeled parametrically using volume fraction. This approach focuses on macro-scale part models, while neglecting the microstructure of the models. Furthermore, such material composition models only represent the designer's desire or specification, but the physical behaviors of the actual materials are needed to be recognized. To deal with this problem, developing a heterogeneous CAD system, which supports integration of microscopic material models into CAD models, is becoming important.

1.3 Structure-property relationship of microstructure

In order to support the heterogeneous CAD system, extensive process-structure-property relationships have to be captured and integrated into current CAD system such as CATIA and Pro-Engineer. The relationships will allow detailed compositions of actual materials to be captured. In order to do this, structure-property relationships at the micro scale are the focus of this research. A new method for reverse engineering of materials is presented such that microstructure models can be constructed and used as CAD representations to support heterogeneous part modeling. Figure 2 schematically shows the method for reverse engineering

of material. A material sample is sliced and imaged at appropriate resolutions to capture the geometric features of its microstructure. This is defined as the structure, represented by lines, angles, curves, and other geometric primitives. Those geometric features are related to each other, of the prepared surface of a material sample at the microscopic level. For example, fibers are represented as simple lines or cylinders, as shown in Figure 1a. Figure 1b also shows that grain boundaries can be expressed by the lines with different angles. The geometric structure can even be illustrated by irregular shapes such as small elliptical shapes, convex sets or non-convex sets of shape objects, as shown in Figure 1c.

Capturing these geometric features from a microstructure image enables structure-property relationships to be constructed at the desired level of scale. Before performing image analysis, one specifies material compositions (i.e., which colors or shades correspond to which materials). An image processing technique is performed to extract the geometry of material's microstructure (e.g., grain or particle size, shape, orientation) and to correlate it with material compositions. In order to obtain structure-property relationships, the extracted geometry features are integrated into CAD systems. By constructing a microstructure model, the effective mechanical properties of microstructure (e.g., Poisson's ratio, elastic modulus etc.) can be calculated. Therefore, structure-property relationships are established. As a result, one will have the ability to construct heterogeneous models of materials that can be integrated into CAD system and used for mechanical part design.

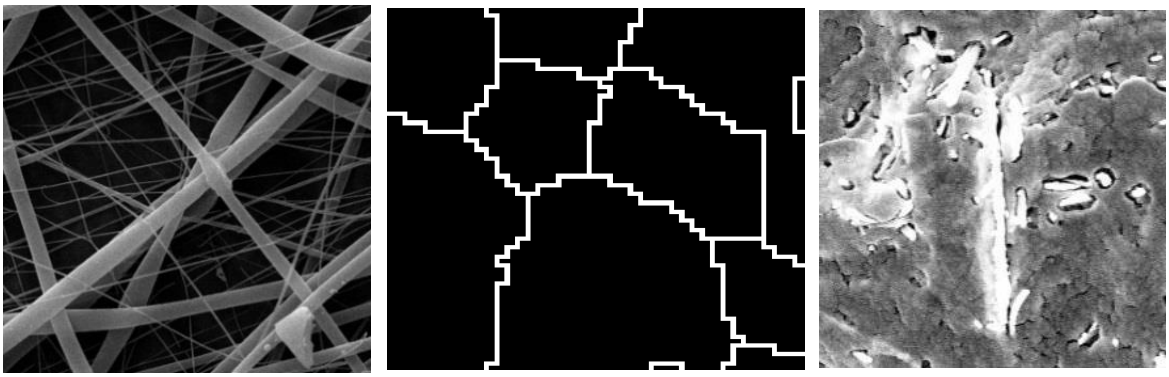

a. Nano scale fiber b. Grain boundary c. Irregular shape of microstructure

Figure 1. Geometric feature of microstructure

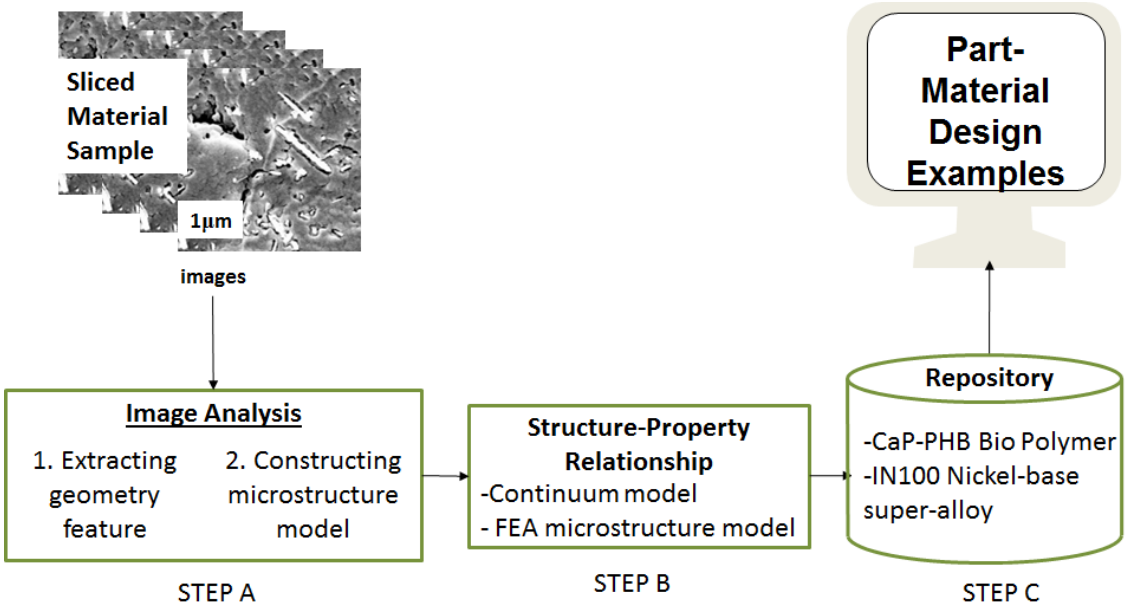

Figure 2. Proposed reverse engineering of material process

1.4 Scope of the research

The principal goal of this dissertation is the development of methods to construct structure-property relationship of microstructure for a heterogeneous CAD system. The principal research goal is to be achieved by two sub-goals, shown in Figure 2 step A: 1) To extract the geometric features from microstructure image using image processing techniques, and 2) To construct

grain boundaries using extracted geometric feature from previous step. By achieving two sub-goals, the structure-property relationship of microstructure can be established, shown in Figure 2 step B. As shown in Figure 2 step C, structure-property relationships of each material are determined and stored in repository of the Heterogeneous CAD system. This research will propose a method to complete the goal, focusing on the specific microstructure, such as 2D polymer composite with fiber shown in Figure 1 a, 2D and 3D grain boundaries of metal alloy shown in Figure 1 b. Furthermore, this research recognizes geometric entities in the image and connects these entities in order to construct grains with explicit geometric model of the material microstructure. Then, this research will demonstrate that it is possible to compute effective mechanical properties by applying material properties. By accomplishing this, the process will help to establish the heterogeneous CAD system, which represents both geometry and property. Therefore, this CAD system enables designers to have much larger degree of freedom in the CAD systems.

This research uses reverse engineering for microstructure models. The microstructure is difficult to test its mechanical property directly different. Due to the size of the microstructure model, properties of microstructure are difficult to define directly, so reverse engineering aids to estimate properties of microstructure depending on its structure. In this research, step A in Figure 2 will be extensively investigated in this research. Result of the step A will be used as an input of step B to validate structure-property relationship.

1.5 Research focus in the dissertation

1.5.1 Research questions and hypothesis in the dissertation

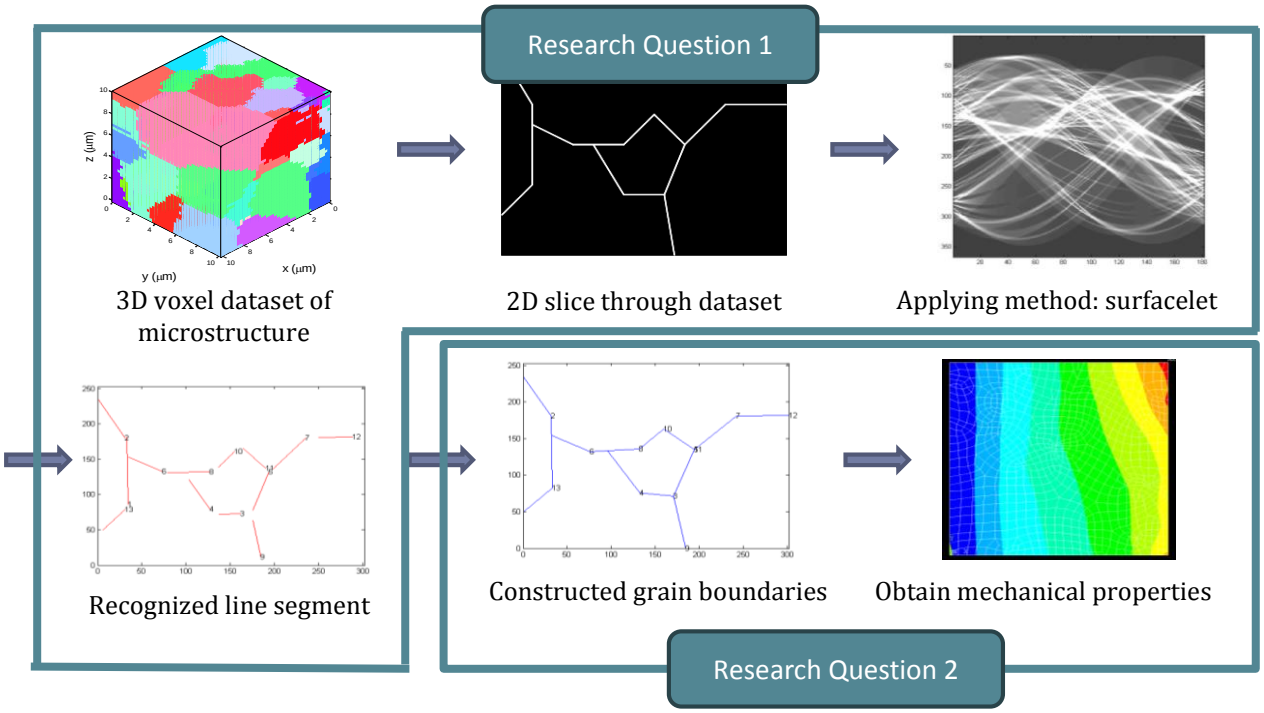

Figure 3. Overall research step

The research question 1 is

"Can an entire geometric feature in the microstructure image be extracted as an explicit geometric model using the surfacelet method?"

Current CAD system uses explicit geometric representation for modeling. In order to integrate heterogeneous CAD modeling into current CAD system, extraction of geometric feature using explicit representation form is needed. Research question 1 is related to extracting geometric features from 2D or 3D image. This research question can be answered by proofing 2 hypotheses. The first hypothesis is about linear geometric features.

Hypothesis 1.a: *"A surfacelet based method that includes the Radon transform can be used to detect linear features using infinite lines, for 2D images, or bounded planes, for 3D datasets, and this can provide an explicit geometric model of these microstructure features."*

A linear feature is the simplest shape in geometric features. Length, position and orientation information is required to be extracted. The information can be obtained using image processing technique such as the Radon transform or wavelet transform. This information allows having explicit geometric feature. Except linear feature, non-linear geometric feature will be extracted by proofing hypothesis 1.b.

Hypothesis 1.b: *"Non-linear geometry features, such as circles or circular arcs, can be recognized by the cylindrical surfacelet based method, which can be used to represent cylindrical singularities. The cylindrical surfacelet based method extracts circular or cylindrical microstructure features as explicit geometry model from 2D or 3D dataset."*

Microstructure includes not only linear features but also non-linear features, such as cylinders or circles. A cylindrical surfacelet based method enables users to extract 2D and 3D non-linear features from the microstructure. The cylinderlet based method uses a cylinder shape to extract the curvature boundary of the microstructure feature.

As shown in Figure 3, research question 2 focuses on establishing of structure-property relationship.

The research question 2 is

"Can the structure-property relationship of microstructures be established using the microstructure model from recognized geometry features?"

In order to solve this question, the hypothesis is proposed.

"Recognized 2D linear features can be used to construct grain boundaries, which are used to form a microstructure model of grains. The microstructure model will be utilized as input to a computational engineering analysis tool so that effective mechanical properties can be calculated. By pursuing these processes, one can establish the structure-property relationship of microstructure"

Integration of microstructure, material composition, and mechanical properties with geometry information aids many product development activities. Structure-property relationships enable users to model heterogeneous CAD systems, which support not only geometry information but also material composition. By using features extracted from research question #1, a microstructure model can be constructed. In order to calculate the effective mechanical properties of a given microstructure, the constructed microstructure model will be used as an input to a computational engineering analysis tool, such as ANSYS or NASTRAN. This process will enable us to achieve the structure-property relationship.

CHAPTER 2
LITERATURE REVIEW

2.1 Heterogeneous modeling

Heterogeneous materials are composed of different constituent materials. It displays continuously changing composition and/or microstructure. These materials have increasingly been used in engineering applications [2]. Current CAD systems have limited ability to model heterogeneous materials. Recently, several studies of heterogeneous material modeling systems have been explored. Kumar and Dutta presented a set-based approach for spatial discretization of the solid interior by including variations in composition along with the geometry [3]. Their implementation was restricted to polynomial functions. Kumar and Wood proposed a finite element based method for modeling and optimizing material density distributions using particular design objectives and constraints [4]. They proposed a method that used a four-node mesh and its associated interpolation functions. The method needed to be improved for describing arbitrary heterogeneous solids. In order to achieve heterogeneous modeling, some researchers used a mesh-free method, which does not rely on any form of spatial decomposition of the geometry. Wahlborg and Ganter implemented an implicit approach to heterogeneous solid modeling (H-ISM) [5]. Their work used Boolean operators to construct heterogeneous models with both solid and material spaces. Pratap and Crawford presented work that used existing research based on implicit procedural methods [6]. They extended that work in order to build a tool to design volumetric material information. However, because these methods were focused on macro-structure, modeling and representing the microstructure of heterogeneous objects is beyond these studies.

2.2 Microstructure quantification

Several researchers investigated microstructure quantification as means of representing microstructures for subsequent computational materials design applications. The term 'local state' means that any specific location in the microstructure is mathematically defined at the length scale of interest by averaging the information over all the length scales below the selected length scale. Local state distribution codifies volume fraction information. This is the best statistical measure of microstructure. Common metrics (e.g., particle, pore, or grain size distribution, etc.) can be expressed mathematically as local state distributions for potential correlations with properties. Schmid, Casey, and Starkey proposed the orientation distribution function (ODF) using quartz-pole figure data [7]. They proposed a description of the crystallographic texture of polycrystalline materials. ODF is one of the most studied local state distributions in metal alloy for representing processing/property relationships. By using ODF, each distinct lattice orientation can be explained as an independent local state. In quantifying microstructure, the spatial distribution of local states in the material internal structure would be limited even if the user had defined the local states of interest and the corresponding local state space.

Research on *n*-point correlations or *n*-point statistics has been conducted by several researchers like Torquato, Adams, Garmestani, and Saheli [2, 8]. *N*-point correlations provide a rigorous statistical framework to define the spatial correlations of local states in the microstructure. Since distributions on local state spaces reflect the probability density associated with finding a specific local state of interest, *h*, at a point selected randomly in the microstructure, they often are termed the 1-point statistics. 2-point correlations are expanded versions of the basic concept that capture the probability density associated with finding local states *h* and *h*' at each end of finite-length vectors thrown randomly into a microstructure image. These correlations

are only exactly defined over an ensemble of microstructure realizations, but can be approximated if the ability to process many material samples is limited [9]. These *n*-point correlation methods seek to represent microstructures probabilistically, rather than supporting direct microstructure feature extraction. This approach also uses indirect feature extraction and needs further work to be represented explicitly.

2.3 Feature extraction on microstructure

An important capability in ICME is microstructure reconstruction. In the literature this has two meanings: generate geometric models of specific grains from 2D or 3D images or the generation of geometric models of microstructures that are statistically consistent with measured microstructure characteristics. In this paper, we will present a reverse engineering of materials method that focuses on the first, but enables the second as well. To extract geometric features from 2D images, Leavers and Boyce showed that the Radon transform could be used to encode the data associated with analytically defined shape primitives in the image [10]. They developed a convolution filter for locating feature-indicative regions in transform space and an analytical model for computing feature characteristics. Leavers improved the method for extracting straight lines and extended the method to extract circular arcs and other conics [11].

Recently, Niezgoda and Kalidindi developed a size invariant Hough framework to detect arbitrary 3D shapes and applied the method to extract grains from 3D microstructure datasets [9]. They generalized the concept of a Hough filter by implementing size parameters of interest, such as diameters, in the complex phase. Although successful at recognizing some individual grains, they did not demonstrate the extraction of grain boundaries for all grains in a dataset, which is our objective. Furthermore, the method has limitation to produce an explicit geometric model of the microstructure.

2.3.1 Radon transform

Several researches have been proposed method of extracting geometry in the desired image. Leavers and Boyce showed that a two-dimensional transform space could be used to encode the data associated with analytically defined shape primitives in the image space [10]. They proposed that the form of the distributions in transform space associated with the shape primitives in image space may be deduced and used to derive convolution filters with which to locate those distributions. Leavers used the Radon transform to decompose a binary edge image into its constituent shape primitives where those shape primitives are straight lines and arcs of conic sections[11]. She proposed a technique that makes explicit certain geometric properties and spatial relations between the shape primitives which are then used to code for representation of shape.

2.3.2 Hough transform

Recently, Niezgoda and Kalidindi developed a size invariant Hough framework to detect arbitrary shapes [9]. They generalize the concept of a Hough filter by implementing other parameters of interest in the complex phase. The research focused on exploring the application of a phase-coded generalized Hough transform.

CHAPTER 3
MATHEMATICAL APPROACH

This research will focus on development of methods to achieve heterogeneous CAD system. In order to do that, an image processing method will be used. In this chapter, mathematical approaches of related image processing methods will be explained.

3.1 Radon transform

Generally, the Radon transform is based on a function of integrals over straight lines. It is also an integral transform whose inverse is used to reconstruct an image from medical CT scans [12]. The inverse Radon transform is used to reconstruct the original image from the sensor data obtained during the imaging step. Since the Radon transform is based on integrals over straight lines, if geometric features with linear geometry exist in the object to be imaged, those linear features can be recognized readily. This capability has been used in many applications in image compression [13], image reconstruction [14], and feature recognition [15].

The Radon transform is defined as the line integral along each line, *L*, in the XY plane:

$$R_f(L) = \int_L f(x)|dx| \quad (1)$$

or

$$\boldsymbol{R_f(\alpha, b) = \int_{-\infty}^{\infty} f\big((usin\alpha + bcos\alpha), (-ucos\alpha + bsin\alpha)\big)du} \quad (2)$$

If a parametric model of a line is used:

$$p(u) = ((u\sin\alpha + b\cos\alpha), (-u\cos\alpha + b\sin\alpha)) \quad (3)$$

where *u* is the parameter along the line, α is the angle of the line, and *b* is its distance from the origin. The Radon transform can be extended to three or higher dimensions. In three-dimensional cases, the linear geometry is a plane [14].

3.2 Wavelet transform

In the domain of 2D shape representations, wavelets are among the most popular multi-resolution representations. Similar to Fourier analysis, wavelet analysis represents and approximates signals (or functions). However, instead of sinusoidal functions in Fourier analysis, the functional space for wavelet analysis is decomposed based on a scaling function *j(t)* and a wavelet function *y(t)* with the one-dimensional variable t for multi-resolution analysis. Wavelets are self-similar and can be scaled up and down. More specifically, the wavelet function

$$y_{\alpha,b}(t) = \alpha^{-1/2} y(\alpha^{-1}(t-b)) \quad (4)$$

is scaled by a scaling (dilation) factor *a* and translated by a translation factor *b*. Although certain forms (e.g. Haar, Daubechies, Morlet, etc.) have been used extensively, *y(t)* is actually general and can be customized for specific problems. The most important feature of wavelets is that they are localized in both real (time) and reciprocal (frequency) spaces due to the property of regularity and vanishing moments. In the geometric modeling domain, the wavelet transforms were used to describe planar curves with multiple resolutions [16].

3.3 Surfacelet

The surfacelet transform is a generalization of the radon transform so that the integral is applicable to 2D curves or 3D surfaces of any shapes. The simplest surfacelet is the ridgelet

transform, which is the 1D wavelet transform of the surface integral resulting from the Radon transform (Equation 2) as in Equation 5 [17]:

$$\text{2D: } \Psi_{b,\alpha} = \langle R_f(\alpha, b), y(\alpha, b)) \rangle \quad (5a)$$

$$\text{3D: } \Psi_{b,\alpha,b} = \langle R_f(\alpha, b, b), y(\alpha, b, b)) \rangle \quad (5b)$$

Equation 5 can be generalized for other types of surfacelets. The surfacelet transform can be rewritten as a general surfacelet basis function by modifying Equation 4 as

$$y_{a,b,\boldsymbol{p}}(r) = a^{-1/2} y(a^{-1} r_{b,p}(r)) \quad (6)$$

where $\mathbf{r} = (x,y,z)$ is the location in the domain Ω in the Euclidean space, $y{:}R \rightarrow R$ is a wavelet function, $r_{b,p}$: $R^3 \rightarrow R$ is a surface function so that $\rho_{b,p}=(x,y,z)=0$ implicitly defines a surface, with the translation factor b and the shape parameter vector $p \in R^m$ determining the location and shape of surface singularities, respectively. For example, the 2D ridgelet is formed by introducing angular element $\alpha \in [0,\pi)$ into the wavelet function as

$$y_{a,b,\alpha}(r) = y_{a,b}(x\cos\alpha + y\sin\alpha) = a^{-1/2} y(a^{-1}(x\cos\alpha + y\sin\alpha - b)) \quad (7)$$

The 2D ridgelet is shown schematically in Figure 4a.

The 3D ridgelet represents plane singularities and is defined as

$$y_{a,b,\alpha,\beta}(r) = a^{-1/2} y(a^{-1}(\cos\beta\cos\alpha \cdot x + \cos\beta\sin\alpha \cdot y + \sin\beta \cdot z - b)) \quad (8)$$

where α is rotation about the Z axis, $\beta \in [0,\pi)$is a new angular parameter about the local X axis, and b is a translation along the local Y-axis, as shown in Figure 4b. Here the shape parameter vector is **p** = (α,β). Similarly, a surfacelet that represents cylindrical singularities can be defined as

$$y_{a,b,c,\alpha,\beta,r_1,r_2}(r) = a^{-1/2} y\left(a^{-1}\begin{bmatrix} r_1(\cos\beta\cos\alpha \cdot x + \cos\beta\sin\alpha \cdot y + \sin\beta \cdot z - b)^2 + \\ r_2(-\sin\alpha \cdot x + \cos\alpha \cdot y)^2 \end{bmatrix}\right) \quad (9)$$

where parameters r_1 and r_2 describe the major and minor radii of the cylindrical shape.

The parameters of surfacelets can be geometrically interpreted as follows. For 3D ridgelets as in Figure 4b, any point on a plane $cos\, b \cos\alpha \cdot x + cosbsin\alpha \cdot y + \sin b \cdot z = t$ has the same evaluation of the wavelet function $y(\alpha^{-1}(t-\beta))$. Therefore, the isosurfaces of Equation 8 are planes. The cylindrical surfacelet is shown in Figure 4c, where the isosurfaces of Equation 9 are seen as cylinders. The 2D version of cylinderlets is shown in Figure 4d.

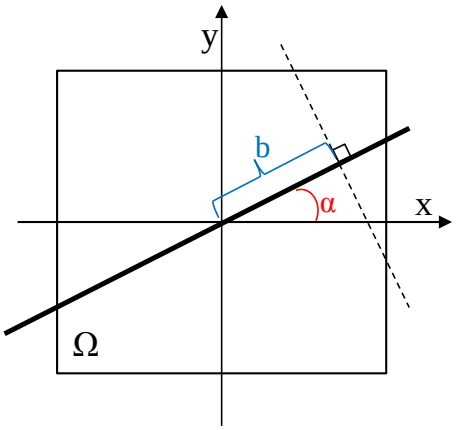

(a) 2D ridgelet

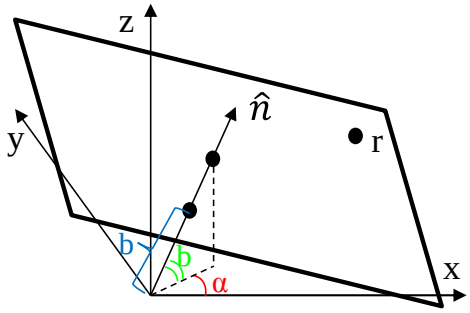

(b) 3D ridgelet

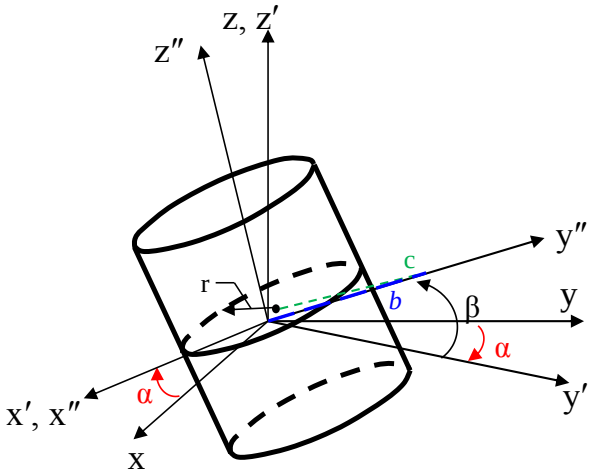

(c) 3D cylindrical and ellipsoidal surfacelets

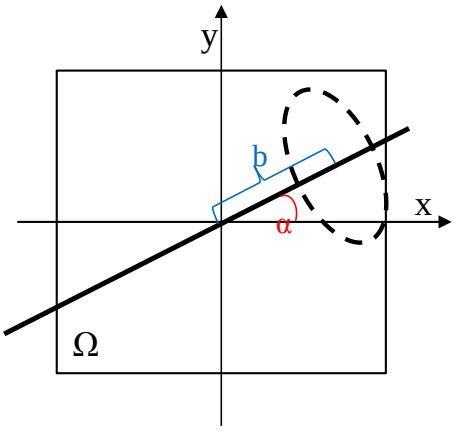

(d) 2D cylindrical and ellipsoidal surfacelets

Figure 4. Geometric interpretation of Surfacelet

3.4 Summary

Image processing methods are introduced and explained mathematically in this chapter. These approaches will be used in this research so that heterogeneous CAD system can be achieved. The main method, the surfacelet transform, is consisted of the Radon transform and wavelets transforms are used to recognize feature in the image.

CHAPTER 4
FEATURE RECOGNITION METHOD
FOR MICROSTRUCTURE FEATURE

In order to accomplish the heterogeneous CAD system, the first requirement that needs to be fulfilled is structure-property relationships. Due to the size the model, properties of microstructure are difficult to define directly so reverse engineering aids to estimate properties of microstructure depending on its structure. As the first step of a reverse engineering, geometric features of the microstructure needed to be extracted from an image. This chapter will explain the feature recognition method using surfacelet based method. In order to define geometric features, one of the main research task is finding appropriate peak value from the transformation coefficient domain. This will be explained in this chapter.

4.1 Feature recognition method

This research is intended to develop a new method for reverse engineering of materials. Specifically, the research will be focus on the extracting both linear and non-linear geometric features from the image. Both 2D and 3D microstructure images will be investigated to show recognized geometric features, as shown in Figure 2 step A-1. Then, microstructure model will be constructed, which is related to Figure 2 step A-2. The result of Figure 2 step A will be used as input information of Figure 2 step B to show structure-property relationship.

Materials with well-defined microstructure features, such as fibers or particles, can be recognized using a surfacelet method. A number of parameters are required in the method to represent recognized features. For example, linear feature like fibers can be characterized using their position, orientation, and sizes (diameter and length). In a 2D image, fibers can be

recognized using 2D ridgelets, which provide orientation and location information directly. By analyzing features of the surfacelet transform result, the rest of the information about the fiber can be obtained. Similarly, grain boundaries often have linear shapes and so can be recognized by 2D ridgelets in 2D images and by 3D ridgelets if 3D voxel datasets are analyzed.

Circular features in 2D image can be recognized using 2D Cylinderlet based method. By using this method, coordinates of the center of circular arcs as well as radii can be recognized. [18].

As a pre-processing step of the surfacelet based method, gradient of image is required in order to facilitate recognition of grain boundaries in the image. The gradient of a scalar function is denoted $\nabla \mathrm{f}$ where ∇ denotes the vector differential operator del. In two dimensional Cartesian coordinate system, the gradient is

$$\nabla \mathrm{f} = \frac{\partial f}{\partial x} i + \frac{\partial f}{\partial y} j$$

where i, j are the standard unit vectors. For example of 2D microstructure grain image, each grain has same intensity value, the gradient of inside of grain is zero. When gradient is calculated different two grains, it gives non-zero value. By calculating gradient of an image, an input image is represented as binary image, which highlights grain boundaries. By doing that, it is easy to recognize grain boundaries using the surfacelet based method.

Microstructure features can be extracted using surfacelet representations, which are computed by first applying the Radon transform or a Radon-like transform to the image, to convert line or edge singularities to point singularities. Then, post processing of the Radon or Radon-like transform will be performed. The feature recognition method is presented in Figure 5, which is step A in Figure 2. It starts from 2D image or 3D voxel domain. Microstructure features can be found computationally using surfacelet representations. As shown in Figure 4 surfacelet method can be interpolated as different name depends on geometric features. For example, if linear

features are focused on the 2D image domain then 2D ridgelet method will be used. Surfacelet method yields explicit geometric representation of microstructure features, which allow constructing microstructure model. A Constructed microstructure model is used for establishing structure-property relationships of microstructure.

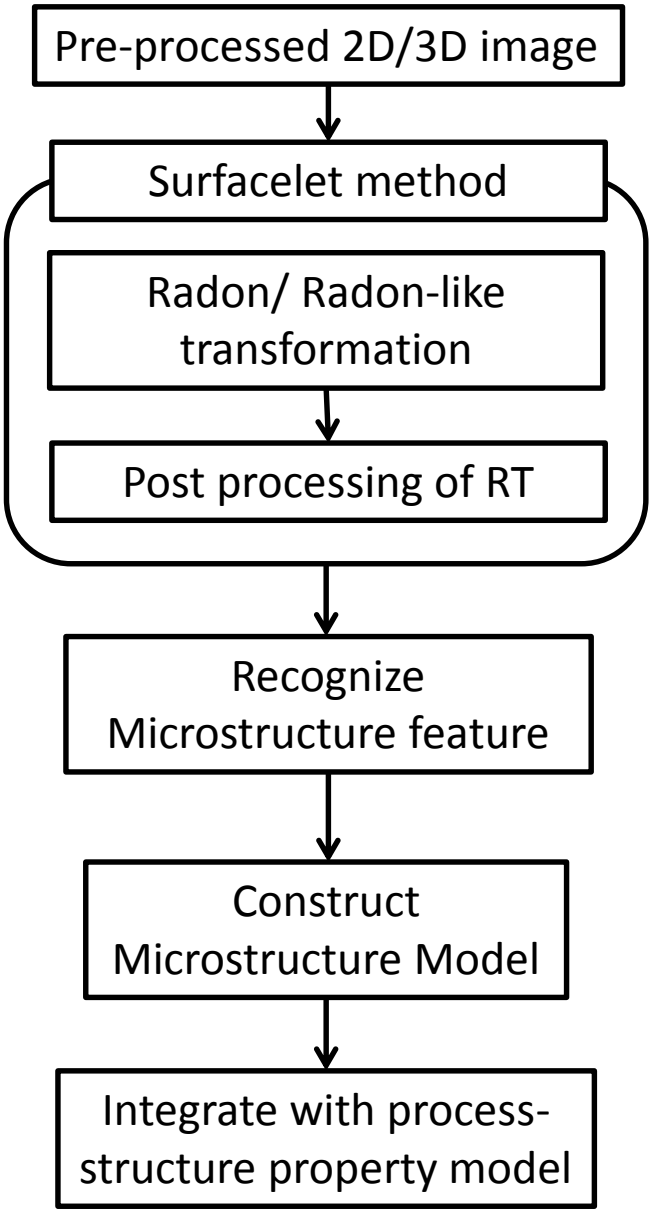

Figure 5. Microstructure feature recognition method

4.2 Surfacelet based method

The first research question focuses on extracting geometric feature from microstructure image. In this research, geometric features are classified by 4 categories, 2D linear, 3D linear, 2D non-linear, and 3D non-linear feature. Linear features will be extracted by using ridgelet while cylindrical surfacelet is used to extract non-linear features.

A linear feature is the simplest shape in geometric features. In 2D microstructure, four parameters, length, position and orientation, can be identified by using surfacelet transform. 2D Radon transform uses 2 parameters α and b, which correspond to angle of the line, and b is its distance from the origin respectively. In 3D microstructure, 3D ridgelet transform will be used to extract 3D linear feature, as shown in Figure 4b, which uses 3 parameters. 3D ridgelet generates 3D coefficient set. In order to identify peak bright points in the 3D coefficient sets, plane overlaying method will be used.

In order to calculate position, length, and orientation of the linear feature in 2D, it is essential to analyze the Radon transform domain. The Radon transform is consisted with plenty of butterfly wings overlapped each other randomly. The first task of recognizing geometric feature is to recognize peak value in the Radon transform domain. This will be mentioned in section 4.3. The next step of this research is to determine parameters of geometric feature using butterfly wing in the Radon transform, which will be explained in next chapter.

4.3 Recognize peak value

In order to identify geometric features it is essential to recognize peak value in the Radon transform domain. In this section, the mean of recognizing peak value will be explained using example of 2D linear case.

2D Feature extraction can be obtained computationally using the 2D Radon transform. The 2D Radon transform generates 2D coefficient sets, as shown in Figure 6. By finding peaks in the coefficient sets in the result of the Radon transform, geometric feature information can be extracted. . Following is an algorithm for finding peak values from the Radon transform coefficient domain.

Given: the Radon transform domain containing intensity values of entire image, threshold value (th)

Ouput: high intensity values (α, b)

1. Calculate the first derivative on the intensity values in the Radon transform coefficient domain. The equation is

$$\nabla \mathrm{f} = \frac{\partial f}{\partial \alpha}\,\hat{\imath} + \frac{\partial f}{\partial b}\hat{\jmath}$$

where $\frac{\partial f}{\partial \alpha}$ is the gradient of α direction and $\frac{\partial f}{\partial b}$ is the gradient of b direction. The first derivative of the Radon transform domain indicates the direction information where the change of intensity values occurs at the point compared to the previous pixel.

2. Calculate the second derivative on the intensity values in the Radon transform coefficient domain. The equation is

$$\nabla^2 \mathrm{f} = \frac{\partial^2 f}{\partial \alpha^2}\,\hat{\imath} + \frac{\partial^2 f}{\partial b^2}\hat{\jmath}$$

This also provides the direction of the slope, which is the first derivative, to define maximum intensity value occurs at the gradient changes sign.

The challenge is that often a feature, such as a fibers or grain boundary, will be represented by several of these bright points close to one another in the Radon transformed parameter space. This type of representation will be called over-representing features. This is often observed with long fibers or grain boundaries; two or three neighboring angles (α, β) will have large transform values. Conversely, a single peak in the Radon transform may correspond to more than one microstructure feature; for example, if two fibers were collinear and were represented by a single peak, this feature would be called under-represented features. In order to solve these issues, this work will apply three techniques to the Radon, Radon-like, and wavelets transform in order to can obtain linear geometric features from microstructure images. A simple 2D example of an over and under-represented feature is shown in Figure 7. In order to solve this problem, additional techniques are needed to choose accurate peak point in the Radon transform.

2D linear microstructure features can be found computationally using the surfacelet method, shown in section 3. In order to extract 2D linear feature, four parameters need to be specified, length, orientation, and position(x, y). These parameters can be determined by finding peaks in the Radon transform. The peaks are observed as bright points in renderings of coefficient sets, which are the result of applying the Radon transform. Combinations of the three techniques mentioned below are used to obtain accurate results.

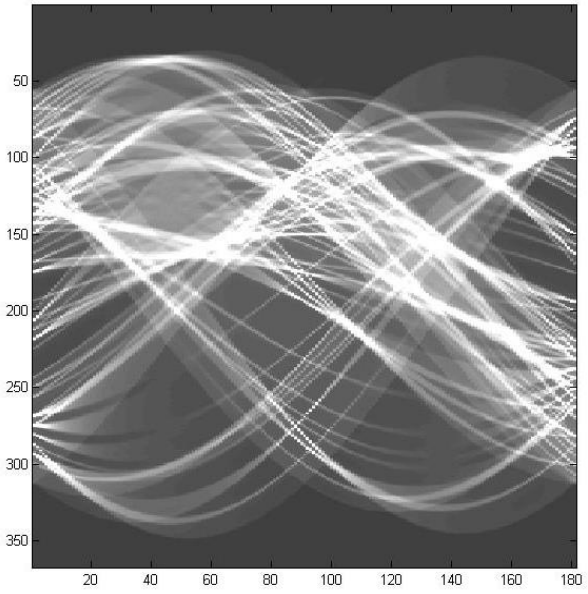

Figure 6. Complicated results of the Radon transform

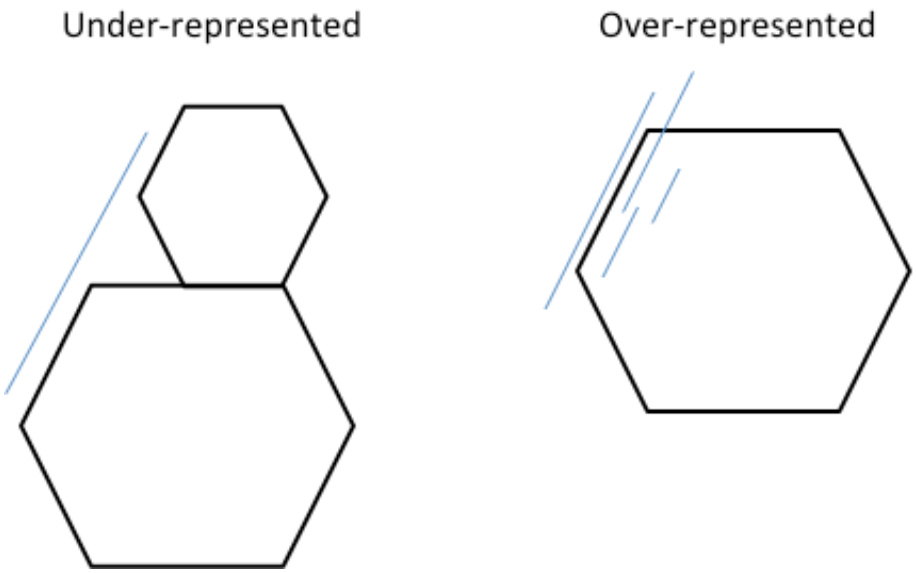

Figure 7. Simple example of an over and under-represented feature

4.3.1 Masking

Masking is the one of the methods that identifies peaks, which correspond to linear features in the image. The distribution of the Radon or Radon-like transform has the appearance of a

butterfly with its wings extended in the (α) direction as shown in Figure 8. The wings of the butterfly are only connected points forming distinct line segments in the image space. They exhibit a dense packing of curves around the maximum value in transform space [11]. Equation (10) is a 3 x 3 convolution mask of the form.

$$\begin{pmatrix} 0 & -2 & 0 \\ 1 & 2 & 1 \\ 0 & -2 & 0 \end{pmatrix} \quad (10)$$

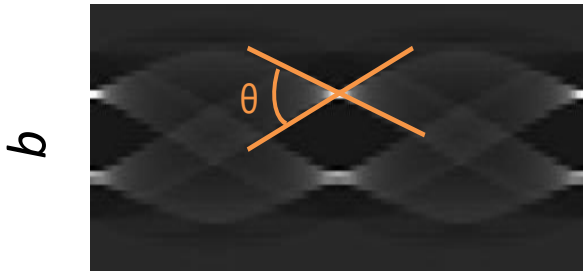

b

α

Figure 8. Shape of butterfly wings in the Radon transforms

Equation (10) emphasizes the peak by multiplying 2 to the peak value. On the other hand, the pixels above and below the peak point will be de-emphasized by multiplying by -2. The matrix dimension can be expanded depending on the size of the transform coefficient matrix, or it can be rotated depending on the shape of the butterfly wing. By using this mask, peaks in transform space can be found and over-representation can be avoided.

4.3.2 Clustering

If the image contains complicated geometric features, the result of the Radon transform can be produced as in Figure 6. Numerous butterfly wings are rotated and overlapped. It is difficult to find linear features by detecting all peak values. If several bright spots, high peak values, are located near one another, they can often be considered to represent one microstructure feature (this is an example of an over-represented feature). These peak values will be clustered together

using a k-means clustering method based on pair-wise distances between peaks. K-mean clustering is popular method for cluster analysis in data mining [19]. This is the process of partitioning entire peak values in the Radon transform into a small number of clusters. Among the peak values in the cluster, we take the largest value in the clustering area. By using clustering for the complicated result, the peaks of the linear features can be chosen.

4.3.3 High frequency component on wavelet result

The wavelet transform is one of the main transformation in Surfacelet transforms. The wavelet transform contains both low and high frequency coefficients, which represent respectively low and high resolution information about the image. The high resolution component contains abundant information to extract linear features, and it emphasizes large gradients in the image [20]. These emphasized gradients help to extract information to recognize geometric features. Two factors, point singularities and large gradient, hold promise for recognizing peaks.

4.4 Summary

This chapter describes feature recognition method; Surfacelet based method, for extracting geometric features. In general, the surfacelet based method includes the Radon or Radon-like transform followed by post-processing of the Radon transform domain. In order to help selecting the peak value, 3 techniques are used as a post processing step. By using post-processing, it facilitate to select appropriate peak values, which correspond to the linear features in the image domain for 2D case. By using the surfacelet based method with 3 techniques, geometric features can be extracted systematically and quantitatively. Therefore, the surfacelet based method provides consistent result when it runs, generating an explicit microstructure model.

This chapter helps to answer a research question 1, which is related to extracting linear geometric feature.

"Can an entire geometric feature in the microstructure image be extracted as an explicit geometric model using the surfacelet method?"

The surfacelet based method is proposed to answer this research question. By using masking, clustering, and high frequency component of the wavelet transform, it is possible to select appropriate peak values, which correspond to linear feature in the image domain. Detail approaches of analyzing the result of peak value will be explained in chapter 5.

CHAPTER 5
RESEARCH QUESTION 1: 2D LINEAR FEATURE EXTRACTION

This chapter will elaborately explain two approaches of extracting of 2D linear features in the microstructure image. The butterfly wing approach analyzes the Radon transform domain to determine position and length of linear features while line overlaying methods superimposes a line of pixels onto original microstructure image. Other than selecting peak value, one of the other important research task is analyzing the peak values. In this chapter, the way of identifying geometric features using selected peak values will be described. This chapter will use 2D linear geometric features to explain two approaches.

5.1 Approach 1: Butterfly wing method

5.1.1 Define Angle of the Linear Feature

Determining the angle of the linear geometric feature is illustrated with a simple example of a fiber –reinforced composition material. Figure 9a shows the sample microstructure, with vertical and horizontal fibers spaced 100 μm apart. The surfacelet transform is applied to the sample's image. The Radon transform of the microstructure results in four sets of non-zero coefficients, as four bright spots shown in Figure 9b, which illustrates the efficiency of surfacelet representation for microstructures with linear elements. Angle of the four fibers from Figure 9a are identified by coefficients of (α,b) = (0,50), (0,150), (90,50), and (90,150). The α values correspond to the angles of 0 and 90 degrees, while the b values correspond to the positions of the fibers. Using the Radon transform, it is possible to recognize angle of the fibers in the image.

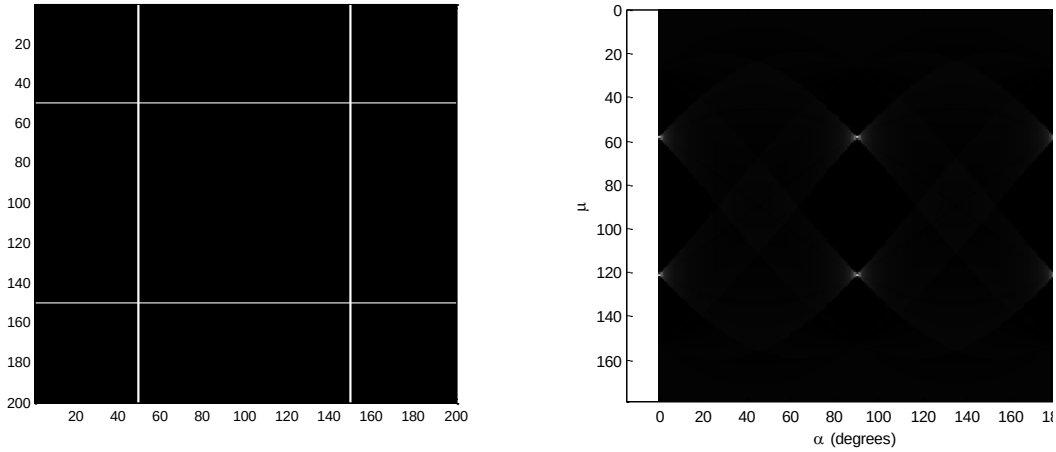

a) Fiber-reinforced composite microstructure b) Radon transform

Figure 9. Simple synthetic fiber-reinforced microstructure and surfacelet representations

5.1.2 Define Length/Position of the linear feature

Consider the linear microstructure feature shown in Figure 10. The Radon transform of the linear feature can be illustrated using Figure 11, where θ is the angle of the linear feature (which is α + 90 degrees), and the linear feature is represented by the perpendicular line to the linear feature at a distance, b, from the origin and its angle, α. P_0 represents the foot of the perpendicular from the origin to the linear geometric feature. If we take the maximum Δα value, the Radon transform would give two displacement values, $b_{u1}$and b_{u2}, which are the foot of the perpendicular from the origin to the lines 1 and 2 that pass through the linear feature end points, Q and R. As shown in Figure 10, the cross points of the line 1, 2 and the linear feature make a right triangle (ΔQRS). The height of the triangle can be expressed as equation (11).

$$\overline{\mathrm{QS}} = b_{u1} - b_{u2} \qquad (11)$$

By using Δ α and height of a right triangle, length of the linear segment can be calculated.

$$length = \overline{\mathrm{QR}} = \overline{\mathrm{QS}} * \sin(\Delta\alpha) \qquad (12)$$

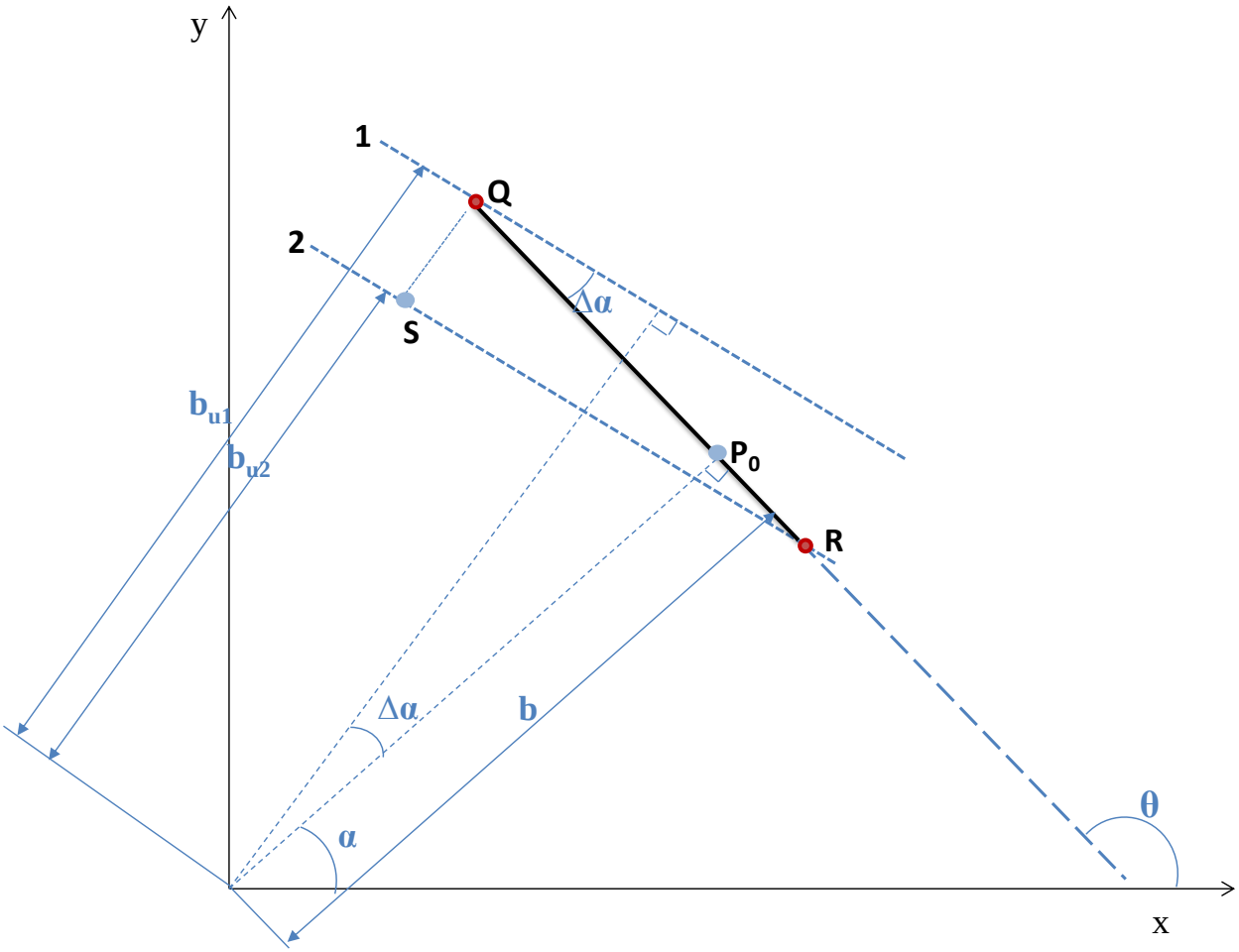

Figure 10. Schematic of linear feature of characterization

Based on the research conducted by Leaver and Boyce the position of line segment along its angle θ, can be determined [10]. The length of the contributing point from the foot of the perpendicular, *p*, is as follows:

$$p = tan(\psi) \tag{13}$$

where $tan(\psi)$ is the slope of a bounding curve of the butterfly wing as shown in Figure 11b. Therefore, we obtain the lengths of the linear lines $\overline{QP_0}$and $\overline{P_0R}$

$$p_1 = \overline{QP_0} = tan(\psi_1),\ p_2 = \overline{P_0R} = tan(\psi_2) \tag{14}$$

Having found p_1 and p_2, the linear feature length can be computed as the sum of these quantities:

$$Length = p_1 + p_2 \quad (15)$$

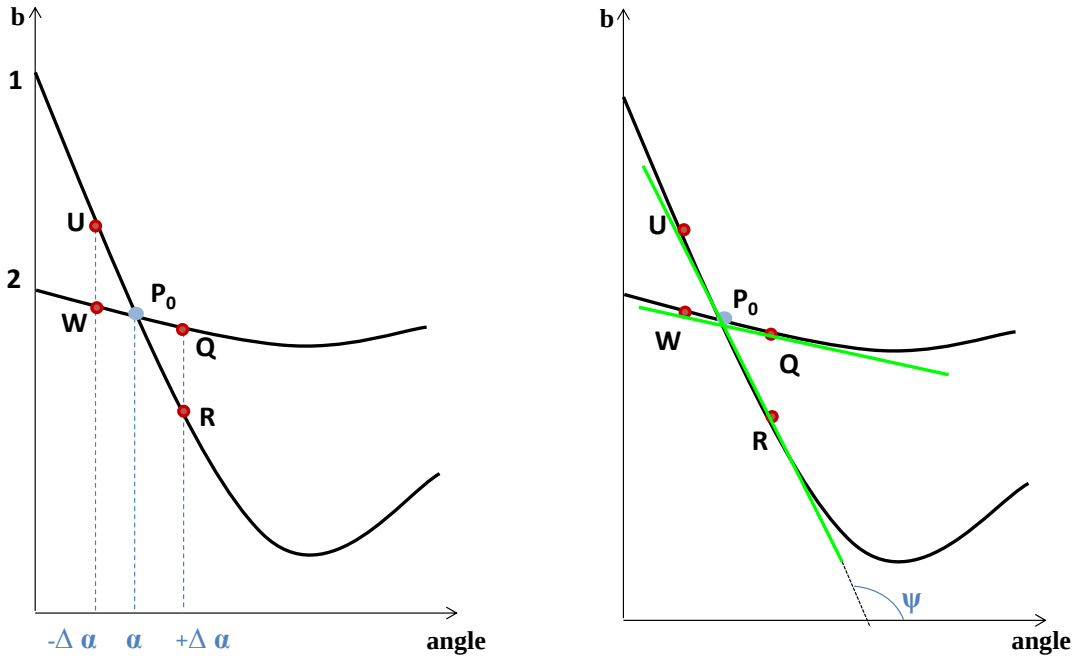

(a) Cross points of butterfly wings (b) slope of butterfly wings

Figure 11. The butterfly wing of the Radon transforms

5.1.3 Butterfly wing analysis

When we deal with simple linear feature, defining parameters of linear feature is straightforward. However, if an image contains complicated geometric features, the Radon transform produces un-organized overlapped butterfly wings. This impedes to identify cross points of butterfly wings, Q, R, U and W shown in Figure 11 a. This section explains how to isolate butterfly wings using peak values in the complicated Radon transform domain.

5.1.3.1 Terminology

- Alpha (α): angle parameter, x-axis on the Radon transform domain
- Angle step (Δα): distance between peak point and edge of the butterfly wing

- B index (b): distance parameter, y-axis on the Radon transform domain
- Segment parameter (Δb): number of pixels that searches cross points of the butterfly wing. Vertically arrayed pixels at Δα. The segment parameter is aligned at α ± Δα and it searches edge of the butterfly wing.

5.1.3.2 Cross point of the butterfly wing

In order to find out cross points of the butterfly wing, shown in Figure 11 a, correct peak values need to be selected. Proposed techniques in section 5.2 enable to choose accurate peak values in the complicated Radon transform domain. Then user takes small number of pixels from pre-selected peak value (α , b) in x-axis direction, which is ±Δ α. As shown in Figure 12, red dot represents peak value in the butterfly wing, and yellow dots represent offset value from the peak value, (α +Δ α , b) and (α -Δ α , b).

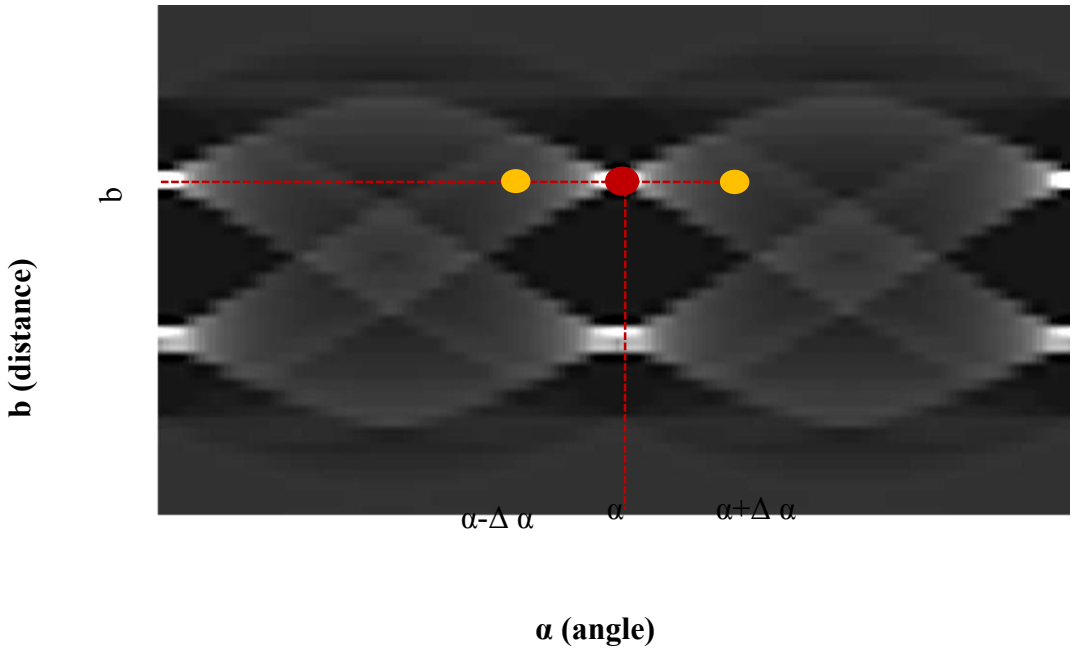

Figure 12. Angle step in the butterfly wing and offset value (yellow dot)

Since the Radon transform has abundant overlapped butterfly wings, it would be better to search around the offset value (yellow dot) for identifying cross points of the butterfly wing. In order to do that, several pixels are vertically taken from the offset value, yellow dot. These pixels are called segment parameter; Δb. Segment parameters are stacked from the offset value to both up and down direction ($2x\ \Delta b$) as shown in Figure 13. This range reduces search area to find cross point of the butterfly wing. Then, find maximum value in the range determined in previous step ($2x\ \Delta b$). A threshold value is set as some percentage of the maximum value (e.g. 0.8*max($2x\ \Delta b$)). Next, all pixels with a magnitude greater than this threshold value are extracted. The extracted range is called "Defined Range", as shown in Figure 14. Both ends of the defined range indicate cross point of the butterfly wing and by obtaining those reconstructed line segment can be calculated.

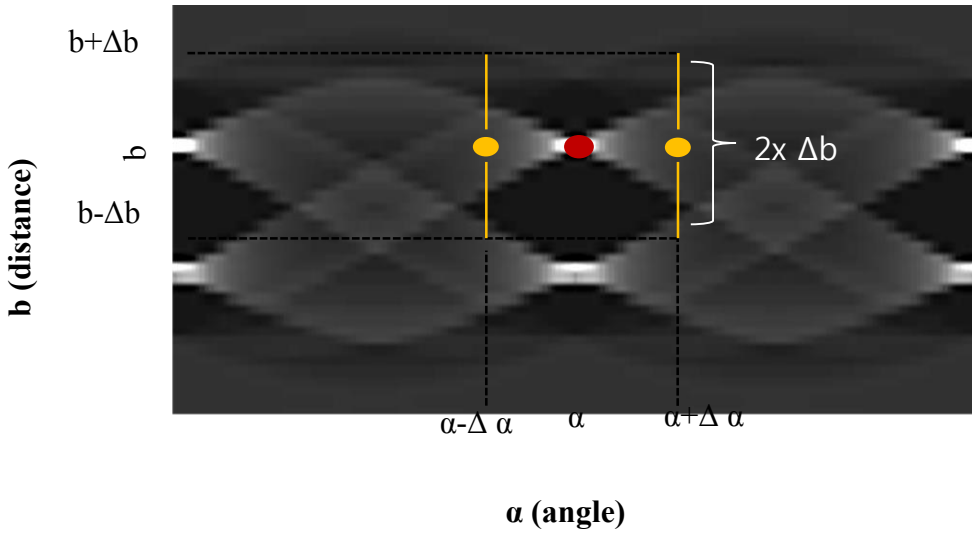

Figure 13. Find broad range using segment parameter, Δb.

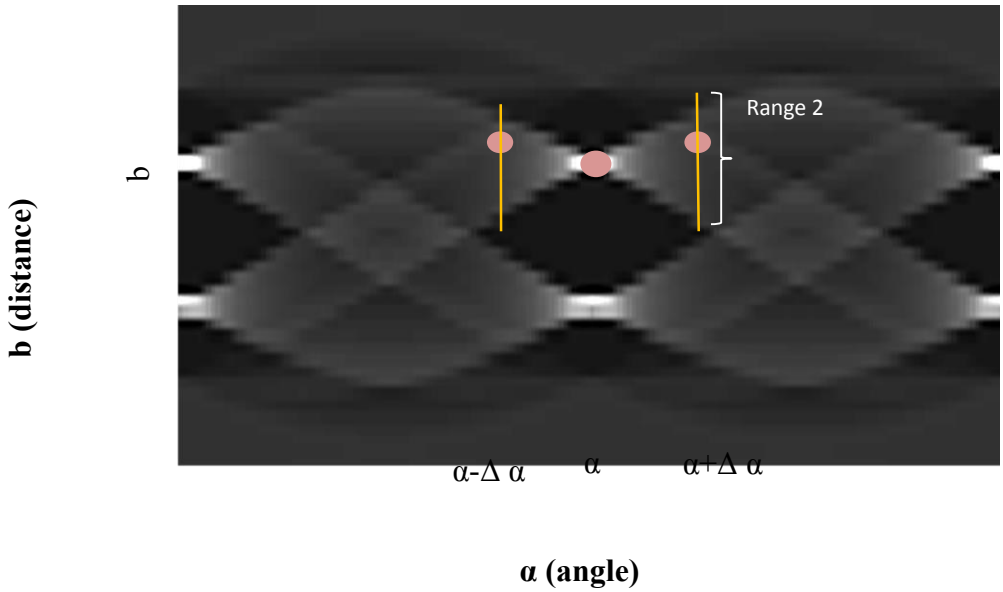

Figure 14. Determine Defined Range using peak threshold

5.2 Approach 2: Line overlaying method

As an alternative to the "butterfly wing" analysis method, the line overlay method can be used to extract line segments from images, given peaks recognized in the Radon transform. Conceptually, the line overlay method is similar to the Radon transform in that a line of pixels is superimposed on the original image and used to extract line segments from the image. The line of pixels corresponds to one of the Radon transform lines; i.e., line L in Figure 4 a which corresponds to a (α, *b*) pair that is selected for each peak. The steps of the method are as follows:

Given: a peak (α, *b*), a gray scale threshold (*th*), a maximum gap (gap_{max}), and a minimum line segment length, l_{min}.

Find: all line segments consisting of image pixels brighter than *th* along the line corresponding to (α, *b*) that is at least l_{min} long and that can span gaps of no more than gap_{max} wide.

1. Generate a line of pixels coordinates at (α, *b*).
2. Extract pixel values from the image along those pixel coordinates.
3. Extract pixel coordinates which have intensity values greater than *th*.
4. Divide the extracted pixel coordinates into line segments that span gaps no larger than gap_{max}.
5. Keep each line segment that is at least l_{min} long.

5.3 Comparison of two approaches

Linear features are recognized by two different approaches, butterfly wing method and line overlaying method. Those two approaches use 1) Radon transform, 2) Radon transform with masking, 3) Radon transform with high frequency component of the wavelet transform in order to extract geometric features. In order to choose appropriate peak values in the coefficient matrix, clustering technique is used.

Three combinations of butterfly wing methods provide calculated length and positions of linear features, which are reasonably close to those from the original image. Angles of the linear features are recognized accurately, while length and position are extracted with small errors. This is because the length and position calculation of linear features highly depends on accurately identifying the cross points of the butterfly wings in the Radon transform, which can be difficult in complex Radon transforms and for noisy images. In addition, the limited resolution

of Radon transforms causes the points U, W, Q, and R in Figure 11 to be identified with significant error in some cases.

The line overlaying method also uses three techniques so that it calculates length, position and angle of the linear features. The line overlaying method works somewhat better than the surfacelet based methods in terms of accuracy of length and position of the linear features. The same peak finding method is used; however, by overlaying Radon lines on the image, it directly overlays the peak value (α, *b*) information onto the original image so that the lengths and positions can be calculated easily by finding the white pixels (linear features) in the original image.

5.4 Summary

This chapter completes how to recognize geometric feature in 2D image domain. Orientation, position, and length of 2D linear geometric features are determined by using proposed approaches, butterfly wing method and line overlaying method. Including chapter 4 and 5, research question 1 can be answered, which is related to extracting linear geometric feature.

> ***"Can an entire geometric feature in the microstructure image be extracted as an explicit geometric model using the surfacelet method?"***

The surfacelet based method is proposed to answer this research question. By using masking, clustering, and high frequency component of the wavelet transform, it is possible to select appropriate peak values, which correspond to linear feature in the image domain (chapter 4). Then, analyzing peak values using 2 approaches allows recognizing geometric feature completely (chapter 5). Therefore, the surfacelet based method allows extracting explicit geometric model of microstructure.

CHAPTER 6
RESULTS OF RECOGNITION OF 2D LINEAR FEATURE

In this section, the results of recognition of the 2D microstructure linear feature will be described. The proposed methods are used to extract geometric features. In order to demonstrate the capability of the proposed method, Calcium-Phosphate Fiber, IN100 metal alloy, and Titanium Alloy examples are used, which include linear geometric features as grain boundaries and form grains.

6.1 Calcium-Phosphate Fiber

Nano-scale fibers can strengthen biopolymers for bioengineering applications. Here, we study a synthetic nanocomposite with 5 weight-percent fibers that is based on a nanofiber filled biodegradable polymer, polyhydroxybutyrate (PHB), with calcium-phosphate (CaP) nanofibers [21]. I use a synthetic microstructure since we can directly control fiber length, position, and orientation in order to compare with the feature recognition results. It is assumed that fibers are randomly distributed, a sample microstructure is shown in Figure 15 that consists of nine fibers.

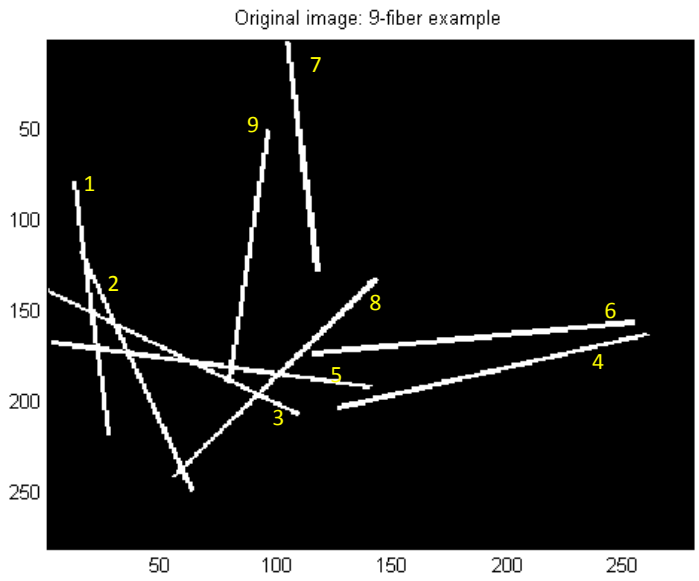

Figure 15. Calcium phosphate fiber

Specific steps for finding geometric features are shown in Figure 4. Followings are steps of finding Calcium-Phosphate fibers using the surfacelet based method.

Step 1. Pre-processed 2D image

An image of Calcium-Phosphate fiber is taken by SEM. Then, it is converted to binary image so that grain boundaries are easily recognized.

Step 2. Apply the Radon transform onto an image

The surfacelet transform which contains the Radon transform is applied on the image shown in Figure 15. A straight line in the Radon transform adds intensity values of pixels, traversing entire image domain with angle α and distance *b*. The Radon transform is represented equation (2) mentioned Chapter 3. Summations are mapped onto the Radon coefficient matrix.

$$\boldsymbol{R_f(\alpha, b) = \int_{-\infty}^{\infty} f\big((usin\alpha + bcos\alpha), (-ucos\alpha + bsin\alpha)\big)du} \quad (2)$$

For example, fiber 9 shown in Figure 15 produces intensity value 35273 and is mapped onto the coefficient matrix at (174,254), where 174 represents α, which is the angle of fiber 9 from the x-axis. Also, 254 refer to b, which is its distance from the origin shown in Figure 16. The peak value, (174,254), corresponds to fiber 9 and it is plugged in equation (2), where *u* is the parameter along the linear feature (fiber 9) in the image.

$$R_f(174,254) = \int_{-\infty}^{\infty} f\Big((usin(174) + 254 * \cos(174)), \big(-ucos(174) + 254 * sin(174)\big)\Big)du = 35273$$

Step 3. Post processing of the Radon transform

The surfacelet-based method calculates the intensity value for entire image domain then; converts to an intensity value to map to Radon transform coefficient domain. When the straight line is overlapped white fibers, the intensity value can be high. It is important that finding a high intensity value, which corresponds to a linear feature. The high intensity values, called 'peak values', are selected by using a threshold value. If an intensity value is higher than the threshold value, then it is considered that it represents a linear feature. However, it is not easy to select peak value efficiently due to the over/ under representation case. In order to solve these problems, three techniques mentioned section 4.3 are used.

A mask technique allows to select appropriate peak value by emphasizing a peak value while de-emphasizing neighbor pixels. When a mask is applied on the coefficient matrix at (174,254), which is corresponding fiber 9, the intensity value of the peak has

increased 26.7%, which is 44715, while upper and below pixels of the peak value are decreased 108.9% and 65.8% respectively.

In addition to mask, a high frequency component on the wavelet transform can be also used to aid to select the peak value. The high frequency component on the wavelet transform is applied to the Radon transform, enhancing detail feature of the Radon transform coefficient domain. Therefore, the peak value, which is bright spot, can be highlighted.

Even though the peak values have been found in the complicated Radon coefficient matrix, the high intensity values can be located close to each other, representing the same geometric feature, which is called over represented case. The clustering technique allows avoiding over-represented case. After computing clusters, the method selects the pixel with the largest intensity value as the peak. If the peak value is larger than a threshold value, the point is selected as a microstructure feature.

By performing three steps, linear geometric features can be reconstructed.

Figure 16 shows results of several variations of the surfacelet based feature recognition methods. These methods enable to select peaks corresponding to fibers. All fibers are recognized at the red circles in Figure 16 a using the regular surfacelet method, at the bright convergence spots in Figure 16 (b) using masking, and at the white circles in Figure 16 (c) using high frequency component of wavelet transform. Each indicated spot corresponds to the fiber angle and location. In order to choose correct peak points, I used clustering.

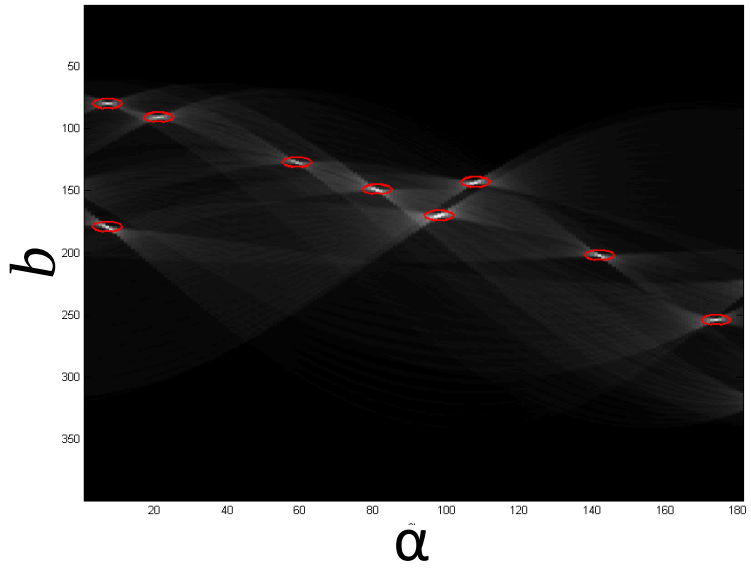

(a) Regular Radon transform

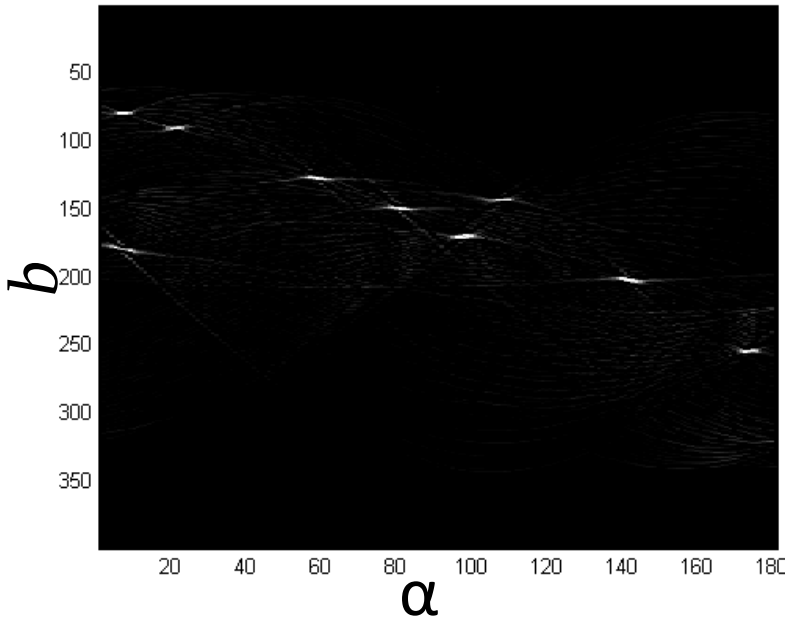

(b) Radon transform + Masking

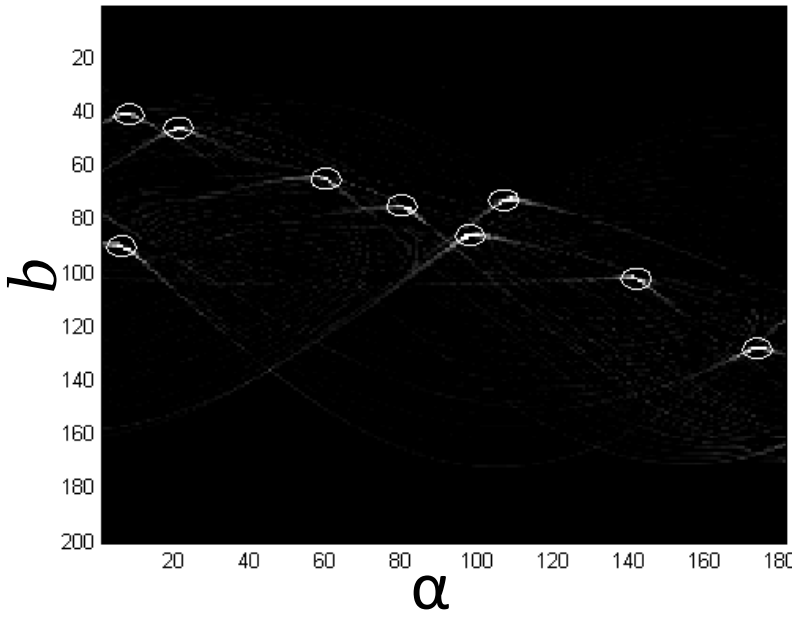

(c) Radon transform + High frequency component in wavelets

Figure 16. Result of the Radon transform with different feature recognition methods

Table 1. Peak locations (α, *b*) from different feature recognition methods

fiber	regular radon transform		radon + masking		radon + high frequency comp	
	disp.	angle	disp.	angle	disp.	angle
1	7	80	7	80	8	82
2	21	91	21	91	21	92
3	59	127	59	127	60	130
4	180	143	107	144	107	146
5	81	149	80	149	80	150
6	98	170	98	171	98	176
7	7	179	9	181	6	180
8	142	202	142	202	142	204
9	174	254	174	254	174	256

Table 1 shows the results from each method that finds peaks in the Radon transform coefficient matrix. Masking and high frequency component in wavelets give almost the same result with the regular Radon transform.

As mentioned in Section 5.1.2, we are able to calculate length and position of the fibers using these angles shown in Table 1. Since we have peak values, we can find each edge of the butterfly wings. In this example, $\Delta\alpha$ is 4 and each cross point of the butterfly wings are shown in Figure 17. For example, each of white spots corresponds to U, W, Q, and R in Figure 11 (b).

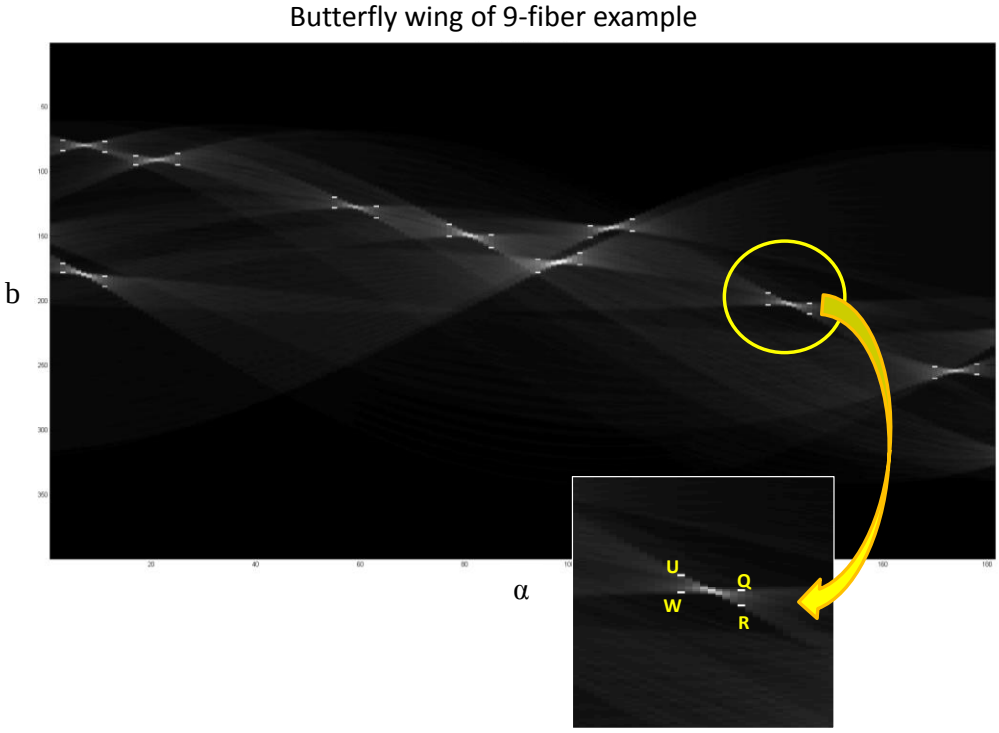

Figure 17. Result of the Radon transform with cross points of the butterfly wings for 9-fiber example

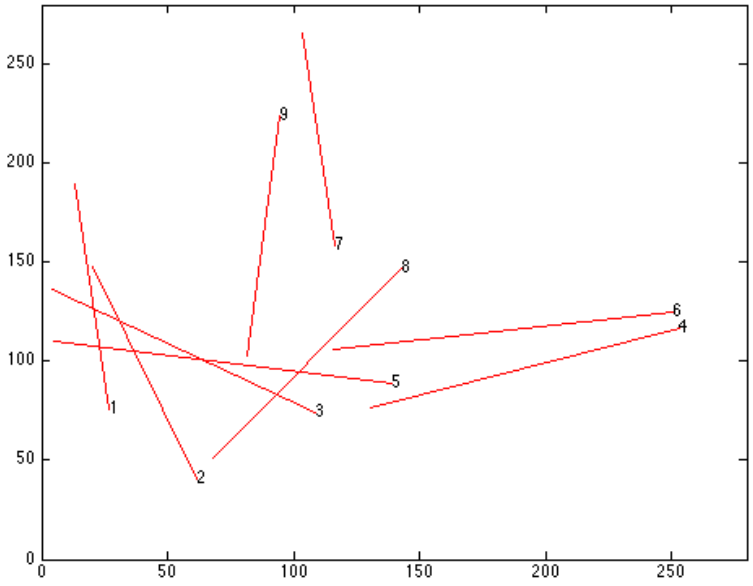

Figure 18. Reconstructed image of 9-fiber example

Table 2 Error between actual fiber and reconstructed fiber

Fiber	Length 1	Length 2	Angle %
	Height *** sin(Δφ)**	**P1 + P2**	
	Length error (%)	**Length error (%)**	
1	15.53	15.64	0.69
2	9.54	9.65	0.80
3	3.39	3.26	0.81
4	22.22	22.31	0.50
5	2.51	2.38	0.27
6	1.68	1.80	0.55
7	8.70	8.82	1.10
8	9.81	9.93	0.65
9	6.65	6.77	0.63

By using the cross points of the butterfly wings, we obtain the lengths of the fibers and its positions. Figure 18 shows the reconstructed fibers image. Line 7 is located lower than its actual location, but all the other fibers are located at their actual locations. All fiber lengths and angles are almost the same as actual fibers. Table 2 shows the error between the actual and reconstructed fibers. Note that the length 1 is the first length calculation method, given in Equation (12), while length 2 is the method given in Equation (15). These two methods to calculate length give almost the same results. Since the masking and the high frequency component of the wavelets produce similar peak values, their reconstructed images are the same.

6.2 IN100 Metal Alloy

In this chapter, grain boundaries will be recognized in a dataset obtained from a 10x10x10 μm IN100 nickel-base super-alloy sample [22], shown in Figure 19 using both the butterfly wing and the line overlay methods. Part of one the cross section through the dataset was smoothed manually, since the original dataset was too coarse (only 41x41 pixels) and was used for this example. Figure 20 shows part of the smoothed cross-section. By using surfacelet based method, the linear features were recognized.

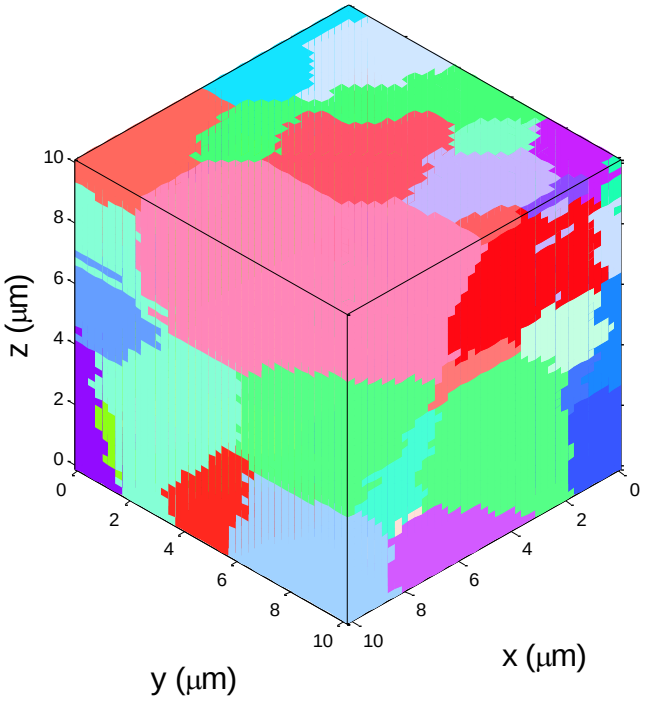

Figure 19. IN100 voxel dataset

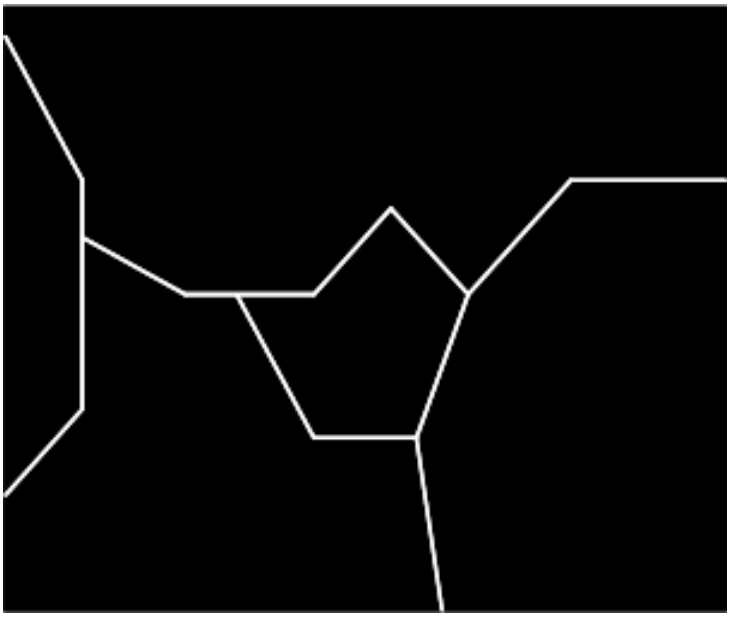

Figure 20. Cross section of part of IN100 example

Three different variations of the butterfly wing method were performed which are the regular Radon transform with clustering, the Radon transform with masking and clustering, and the Radon transform with high frequency component of wavelet and clustering. After the peaks are recognized by one of the methods, the linear feature analysis method is applied from Section 5.1.3. For each peak, the cross points of the butterfly wings are identified, which are located Δα on each side of the peak. These cross points are indicated as red dots on the Radon transform in Figure 21; one of the peaks is highlighted with labeled U, W, Q, R cross points. For the examples in this research, the Δα values are 4, 5, or 6 degrees.

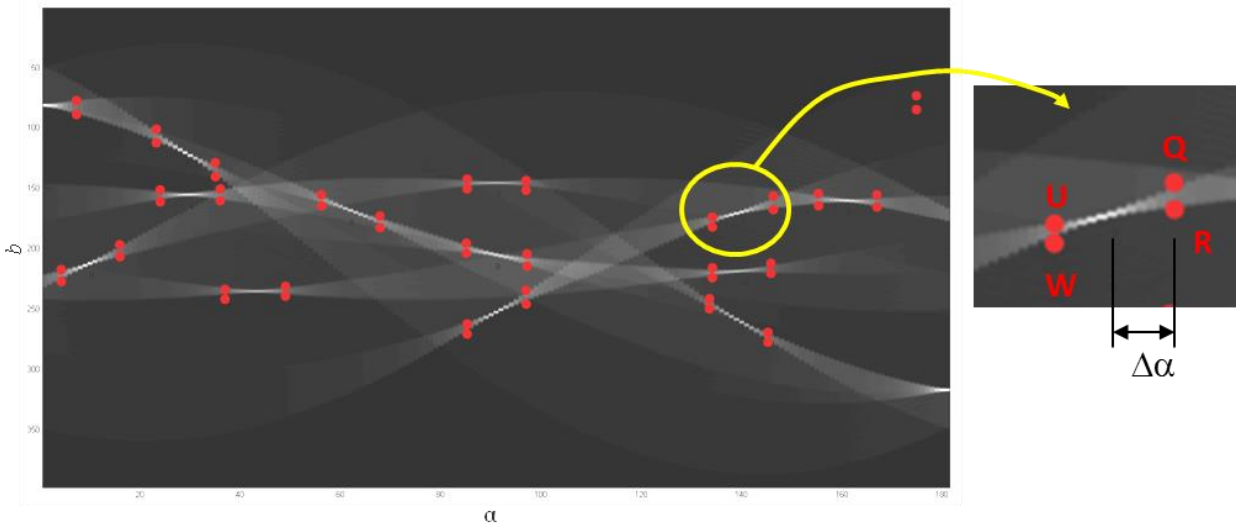

Figure 21. Result of the Radon transform with cross points of the butterfly wings for IN 100 example

Among the three variations, high frequency component of wavelet produces the most promising result. As shown in Table 3, most of the linear features are detected by the high frequency component of wavelet. After the cross points are determined, the length and positions of line segment are computed and reconstructed shown in Figure 22. However, in order to construct

grain boundaries, the line segments need to be connected. If the end points of the line segments are close to one another, they are assumed to represent the shared vertices and are connected. The positions of the shared vertices computed by averaging all shared cross point positions. The reconstructed grain boundary image is shown in Figure 23.

Table 3 Peak values from different feature recognition methods for alloy example

line segment	Regular radon		Radon + masking		Radon + high freq. comp.	
	disp.	angle	disp.	angle	disp.	angle
1	95	1	94	2	98	1
2	258	19	258	19	260	19
3	170	63	171	62	172	63
4	159	91	159	91	162	89
5	180	149	180	150	182	150
6	269	181	269	180	270	180
7	153	56	None		152	55
8	170	107	None		174	108
9	None		120	131	122	131
10	None		None		216	143
11	None		None		130	172
12	None		None		234	91
13	159	84	None		None	
14	None		140	91	None	

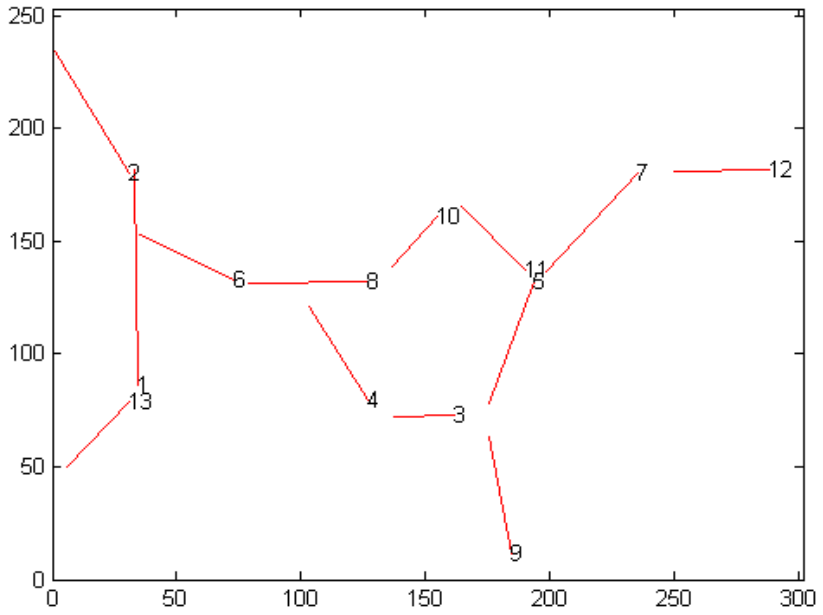

Figure 22. Reconstructed image of line segment for cross section of IN 100 example

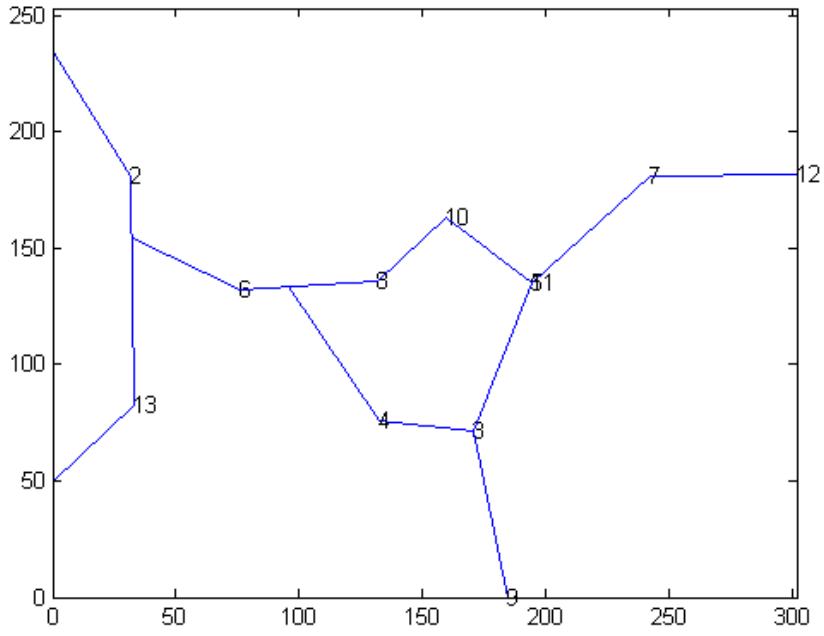

Figure 23. Reconstructed grain boundaries of IN 100 example

The line overlay method works even better, as can be seen in Figure 24. Because line segments are recognized by referencing the original image directly, the start and end points of the segments can be found with high accuracy. After ensuring that the line segments connect, grains can be recognized by finding closed loops among the line segments, as shown in Figure 24 (b).

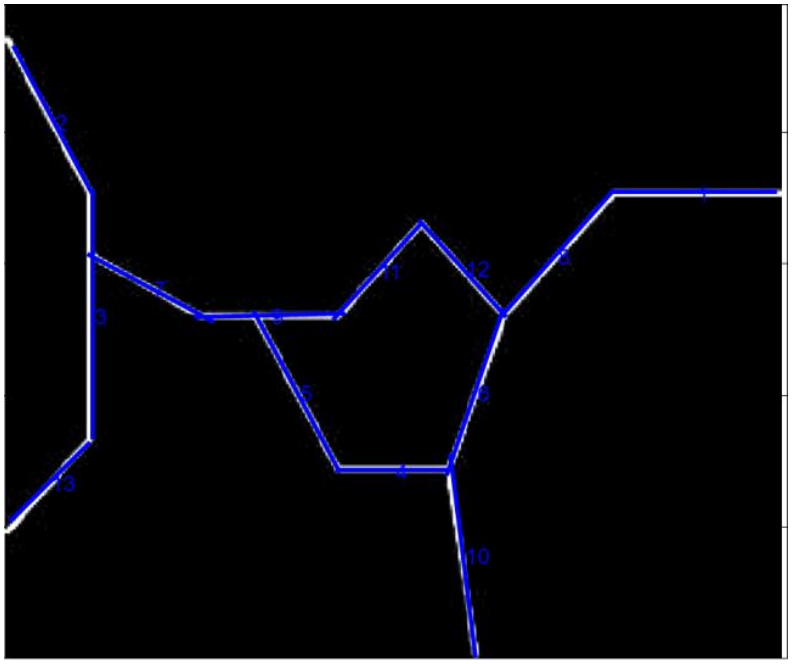

a) recognized line segments

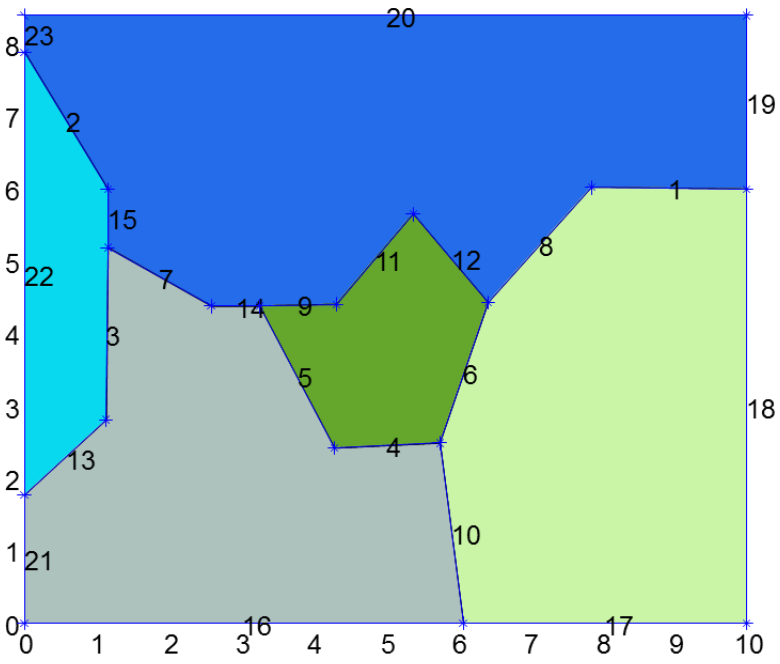

b) recognized grains

Figure 24. Line overlay method results of IN 100 example

6.3 Titanium Alloy Fabricated by Directed Energy Deposition

A research group fabricated compositionally graded titanium alloy samples using a variation of the directed energy deposition process [23]. Directed energy deposition (DED) is the ASTM standard name for processes such as Laser Engineered Net Shaping (LENS) wherein powder feedstock is injected into a focused high power laser beam to form a weld pool that, upon solidification, forms a deposit. The specific process utilized here used two feedstock streams, a burn resistant (BurTi) alloy Ti-25V-15Cr-2Al-0.2C powder and a Ti-6Al-4V (Ti64) wire. The proportions of each were varied locally and the resulting microstructures studied. Results demonstrated that only beta phase was observed and increases in the proportion of BurTi caused grain size to be reduced. Several grains in the image from a sample fabricated using 4.88

g/min BurTi powder with 0.4 g/min Ti64 wire (see Figure 25) were analyzed using the butterfly wing and the line overlay feature recognition methods.

Of the three butterfly wing methods, the Radon with masking method gives the best results. As shown in Figure 25 (b), most of the prominent grain boundaries were recognized. The size of the image is approximately 300x150 μm. Small errors are observable in the calculations of line segment position and length. It is likely that unrecognized grain boundaries are due to noise in the image. The noise and the limited resolution of the Radon transform cause the errors for recognizing the geometric features.

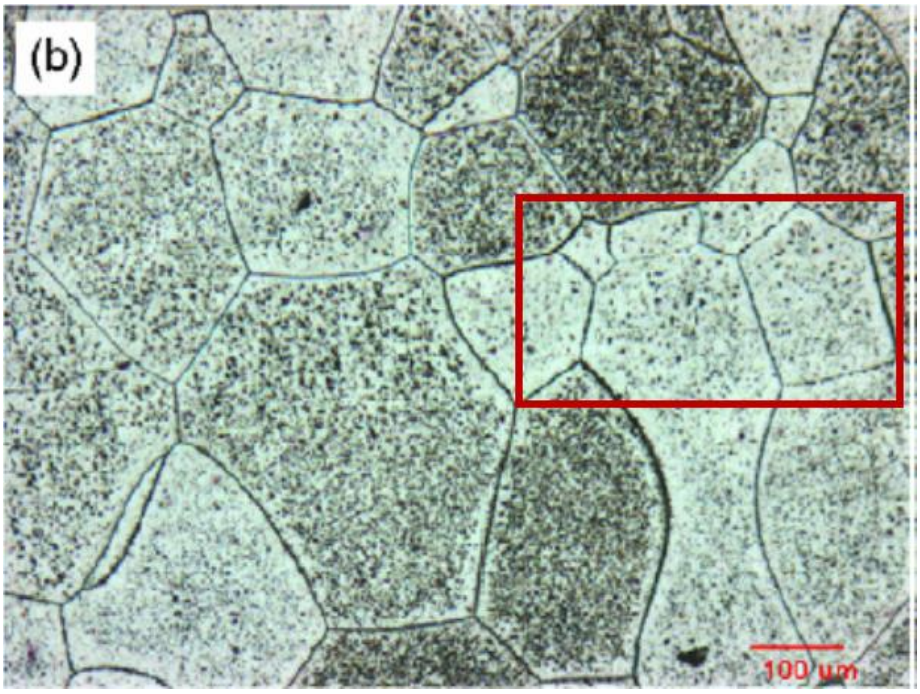

a) original BurTi-Ti64 microstructure

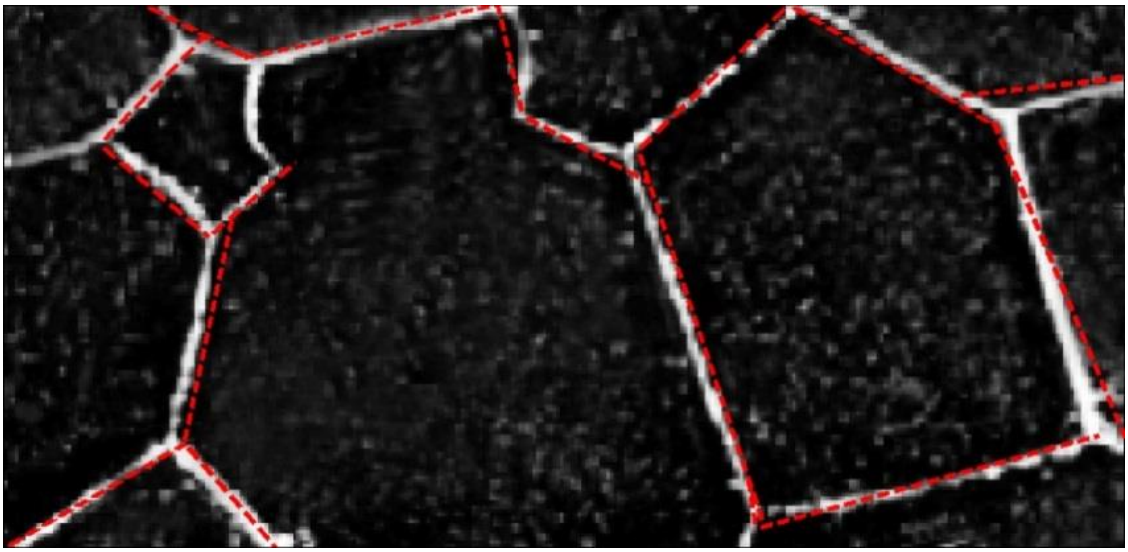

b) Recognized grain boundaries

Figure 25. Surfacelet method results for BurTi-Ti64 composite sample

The results from the line overlay method are shown in Figure 26. Except for one grain boundary in the upper left corner (incorrect angle and too long), the grain boundaries are recognized successfully. Also, an extra boundary was recognized (close to (50, 90)) that is an example of over-representing features. The exception grain boundary resulted from the heuristic used to cluster line segments (use the longest line segment in each cluster), so this is potentially correctable with a better heuristic. After deleting the extra boundary and adjusting the end points of the exception boundary, recognition of entire grains is straight forward, as shown in Figure 26 (b). Due to some missing short grain boundaries, two of the grains are far too large, specifically the blue and the cyan grains.

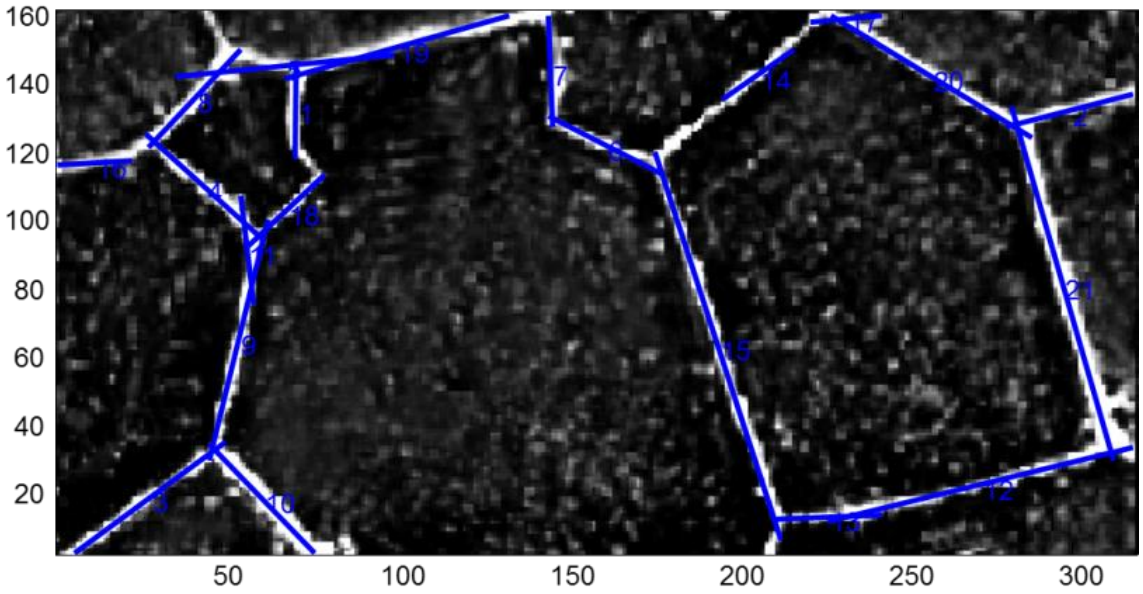

a) Recognized grain boundaries.

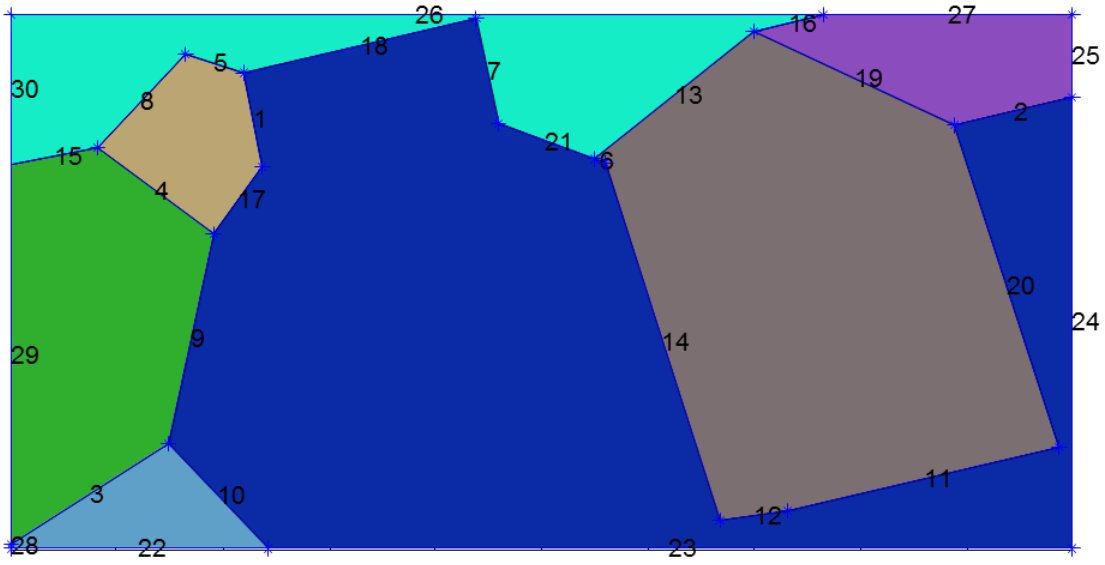

b) Recognized grains.

Figure 26. Line overlay results for the BurTi-Ti64 example

6.4 Summary

This chapter shows three different examples to demonstrate capability of the surfacelet based method regarding extraction of the 2D linear microstructure features. A calcium-Phosphate fiber example represents very simple linear features. A butterfly wing method is applied to the image and all fibers are recognized. Two different approaches, the butterfly wing method and the line overlaying method, are applied to a metal alloy example and a Titanium alloy example. Two approaches yield the same results on the metal alloy example. On the other hand, the line overlaying method shows remarkable results on the Titanium alloy example, while the butterfly wing method shows the result with couple of unrecognized line segments. Therefore, this chapter answers a research question1, proving hypothesis 1a.

> ***Research question 1: "Can an entire geometric feature in the microstructure image be extracted as an explicit geometric model using the surfacelet method?"***
>
> Hypothesis 1.a: *"A surfacelet based method that includes the Radon transform can be used to detect linear features using infinite lines, for 2D images, or bounded planes, for 3D datasets, and this can provide an explicit geometric model of these microstructure features."*

The hypothesis of this research question is validated in this chapter by showing the process by which the line segments constructed to the microstructure model using the proposed 2D Surfacelet based method. The 2D Surfacelet based method can be successfully used to recognize 2D linear features with explicit form, which is the same representation system that current CAD systems use.

This chapter contributes step A in Figure 2, which is extracting geometric features and constructing a microstructure model for linear features. Unlike other known method, it provides

explicit geometric information so that can be integrated current CAD system easily. This step allows to complete a reverse engineering of material process.

CHAPTER 7
SENSITIVITY OF BUTTERFLY WING METHOD

Recognized geometric features construct grain boundaries shown in example above. However, even though the geometric features are recognized nicely, the result still has small un-matched geometric features compare to an input image. The errors are occurred by the overlapped butterfly wings due to the complexity of the image. In this section, a sensitivity of butterfly wing method will be analyzed depending on how one chooses a point in the 2D Radon transform domain. Terminologies are already given in section 5.1.3.1.

- Alpha (α): angle parameter, x-axis on the Radon transform domain
- Angle step (Δα): distance between the peak point and edge of the butterfly wing
- B index (b): distance parameter, y-axis on the Radon transform domain
- Segment parameter (Δb): number of pixels that searches the cross points of the butterfly wing. Vertically arrayed pixels at Δα. The segment parameter is aligned at α ± Δα and it searches edge of the butterfly wing.

Investigation of different factors, which affect sensitivity of the butterfly wing method, is presented in section 7.1, 7.2, 7.3 and 7.4. In addition to that, effects of different factors with a simple synthetic line segment are explored in section 7.5.

7.1 Parameter 1: Angle step parameter (Δα)

This section explains the sensitivity of the butterfly wing method depending on an angle step parameter ($\Delta\alpha$). X-axis represents angle parameter (α) and the angle step parameter ($\Delta\alpha$) shown in Figure 27, indicating distance between a peak point and the cross point of the butterfly wing.

Figure 27 shows a sample peak point from the complicated Radon transform domain. Vertically aligned yellow circles in Figure 27 represent a width of the butterfly wing (Δb). The End points of the yellow circles are corresponded to U, W, Q, and R shown in Figure 17 and Figure 21.

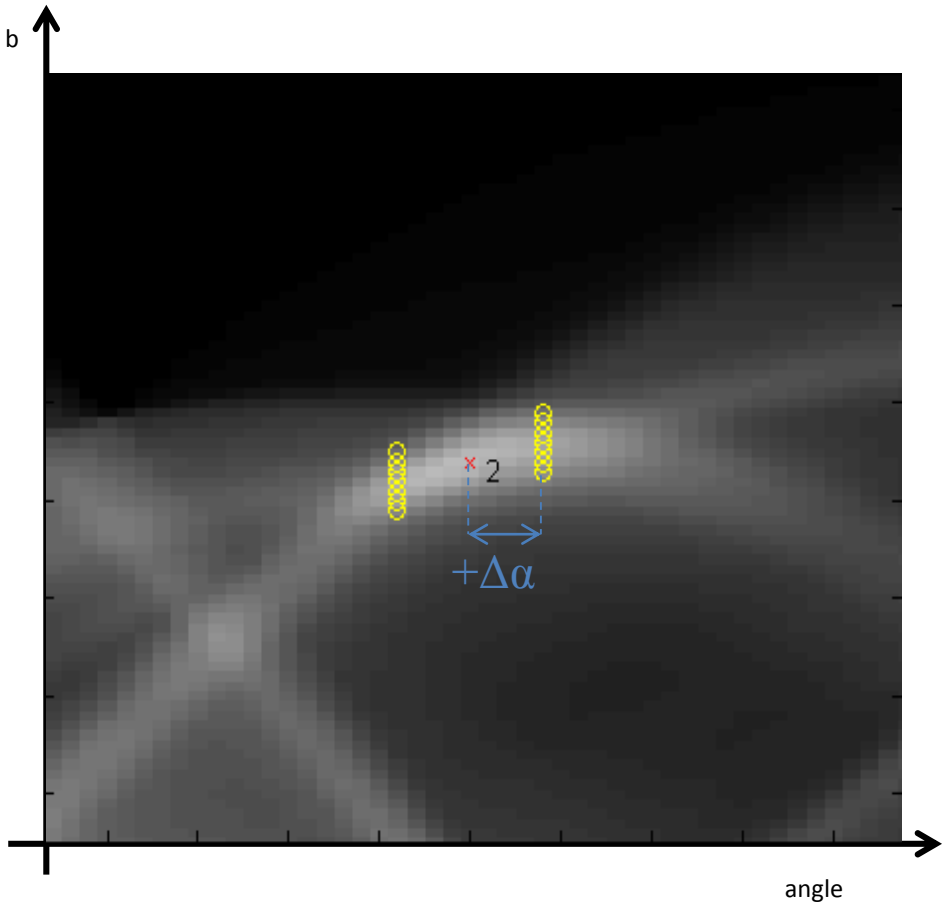

Figure 27. Sample peak point with defined range in Δα distance

In order to examine the sensitivity of angle step parameter (Δα), different angle step parameters are chosen with the same condition, segment parameter of 6 and threshold value of 0.5. By using nine different set of parameters, the reconstructed line segment are calculated. Figure 28 shows defined range with different angel step parameter (Δα) at the same segment parameters (Δb) and threshold (th). As shown in Figure 28 (e) and Figure 28 (f), increment of

angle step parameter ($\Delta\alpha$) does not produce the same defined range. This is because of the overlapped butterfly wings around the peak point. If there is no other overlapped butterfly wing, no matter how large angle step parameter ($\Delta\alpha$) are chosen, the defined range (starts/end at the cross point of the butterfly wing) will be the same.

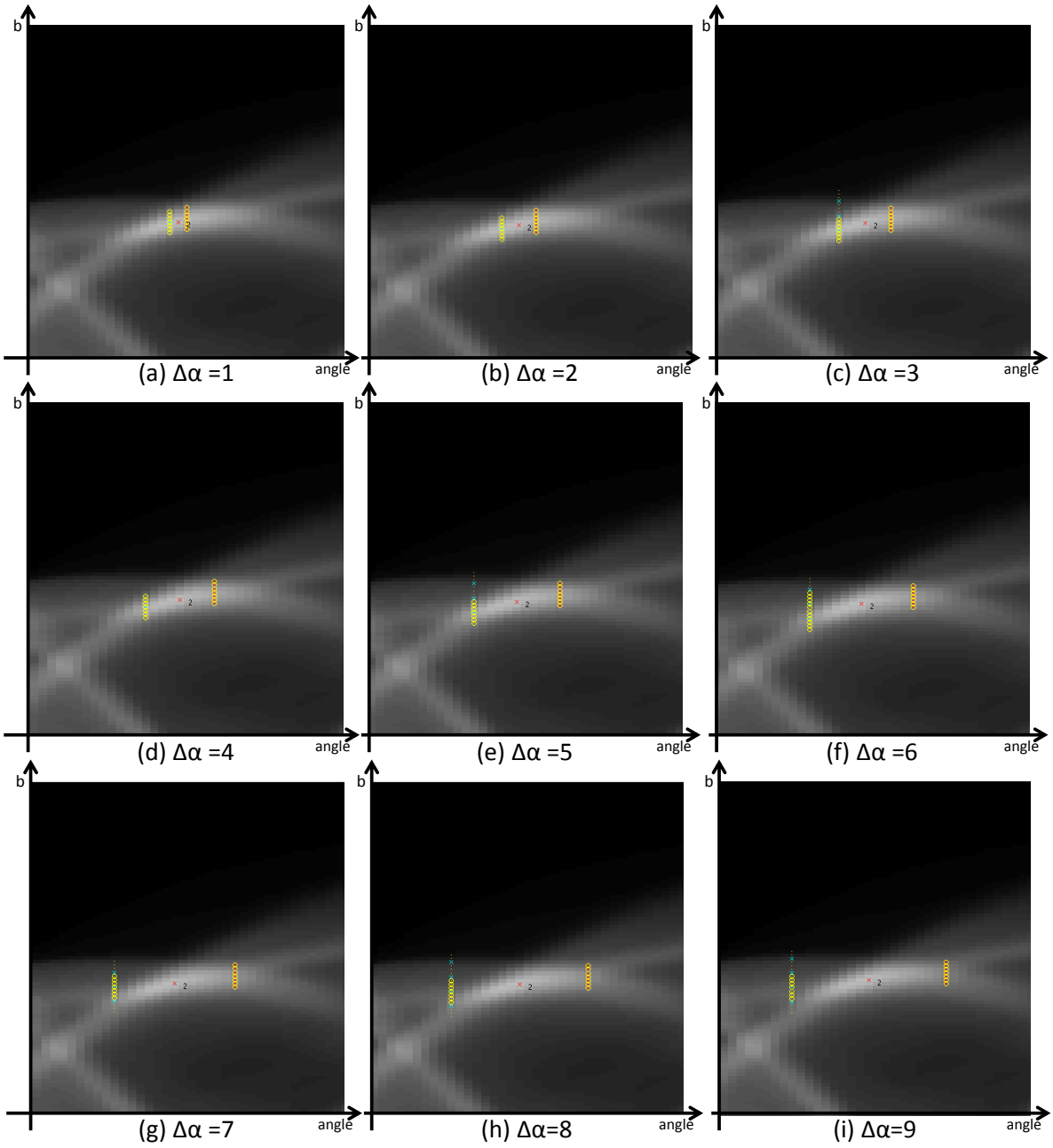

Figure 28. Defined range with different angle step parameter at segment parameter of 6 and threshold value of 0.5

Table 4. Reconstructed length of the line segment with different angle step parameter

angle step	1	2	3	4	5	6	7	8	9
Length of line seg.	343.77	171.89	114.59	85.94	68.75	57.30	49.11	42.97	38.20

Depending on the angle step parameter ($\Delta\alpha$), the reconstructed lengths of the line segment are shown in Table 4. A 'known length' is defined by comparing the reconstructed length and the length of line segment in the original image. If a length of reconstructed line segment is the same as the original length of in the image, the length can be called 'known length'. The known length is used for calculating the sensitivity analysis. By using the reconstructed length, the sensitivity analysis of angle step parameter ($\Delta\alpha$) is calculated. The sensitivity is calculated both ways. The one is to find the difference between a current step and a previous step and the other is to find the difference between a current step and the middle step. The former one is called local sensitivity and the letter one is called global sensitivity. Equation (16) shows the local sensitivity where x_i represents the current angel step and x_{i-1} represents the previous angle step while equation (17) indicates the global sensitivity where x_{middle} represents middle step among the entire angle step.

$$Local\ Sensitivity = \frac{length\ at\ x_i - length\ at\ x_{i-1}}{\Delta\alpha\ at\ x_i - \ \Delta\alpha\ at\ x_{i-1}} \qquad (16)$$

$$Global\ Sensitivity = \frac{length\ at\ x_i - length\ at\ x_{middle}}{\Delta\alpha\ at\ x_i - \ \Delta\alpha\ at\ x_{middle}} \qquad (17)$$

Figure 29 shows the local sensitivity of angle steps, indicating the sensitivity decreases when the angle step parameter ($\Delta\alpha$) increases. When angle steps parameter ($\Delta\alpha$) increase, the reconstructed lengths decrease. Also, decreasing rate of the reconstructed length decreases,

shown in Figure 29. The global sensitivity of the angle steps parameter ($\Delta\alpha$) shows similar trends as the local sensitivity does, shown in Figure 30. Since the global sensitivity is calculated using the middle point, in this case angle step of 5, the result at the global sensitivity at $\Delta\alpha$ =5 is always zero, shown in Figure 30.

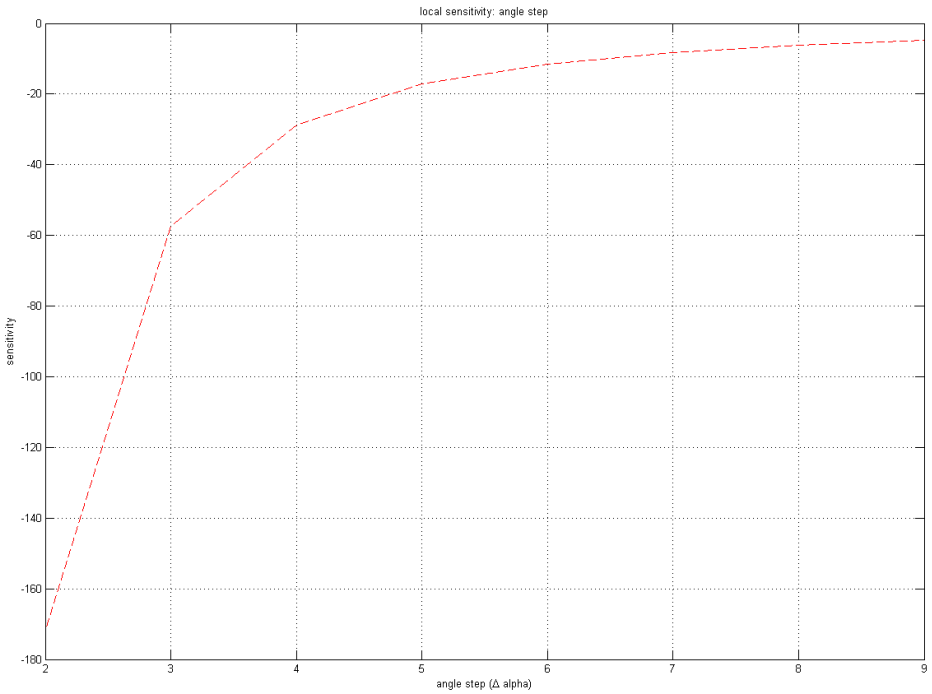

Figure 29. Local sensitivity of angle steps

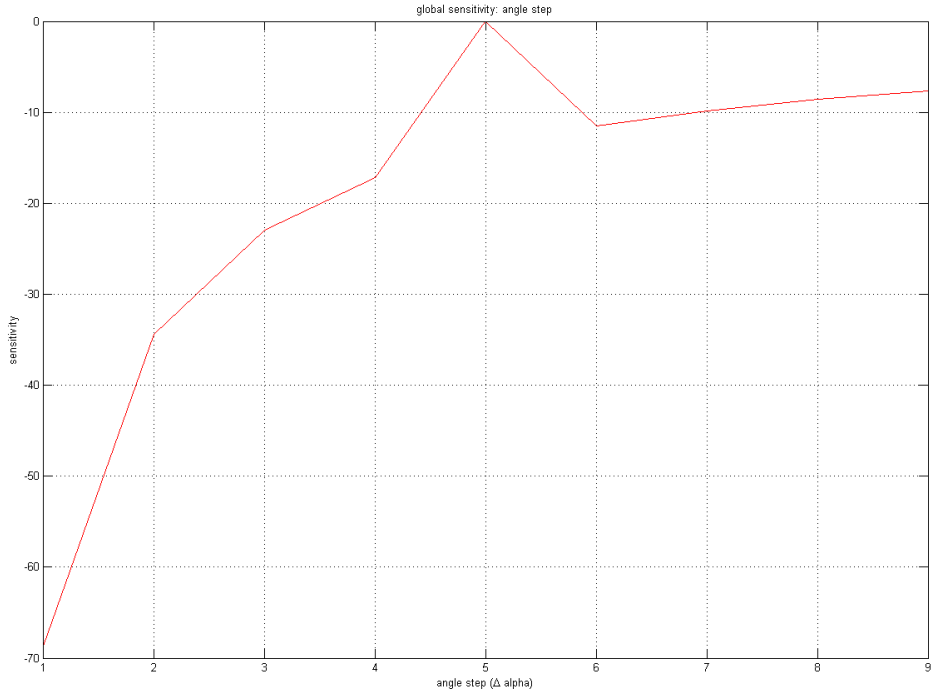

Figure 30. Global sensitivity of angle steps

When the large angle step parameter ($\Delta\alpha$) is used, the cross points of the butterfly wing are less affected than when the small angle step is used. This is because of the butterfly wing shape consisted with sinusoidal curves. The slopes of the butterfly wing are non-linear in α direction, as shown in Figure 31. Two different angle steps, $\Delta\alpha_1$, $\Delta\alpha_2$, and its corresponding cross points (green, blue dots) are shown in Figure 31. As mentioned in equation (13), the reconstructed length depends on the slope of the butterfly wing. Therefore, two different slopes (green line and blue lines) in Figure 31 mean the different reconstructed lengths. Green line shows a slope with angle step of $\Delta\alpha_1$ while blue line shows a slope with angle step of $\Delta\alpha_2$. Green slope is steeper than blue one indicating that a reconstructed length of line segment with angle step parameter of $\Delta\alpha_1$ is larger than one with angle step parameter $\Delta\alpha_2$. Even though those slopes

are found in the same butterfly wing, the curved shape of the butterfly wing is a reason for having different reconstructed lengths with different angle steps.

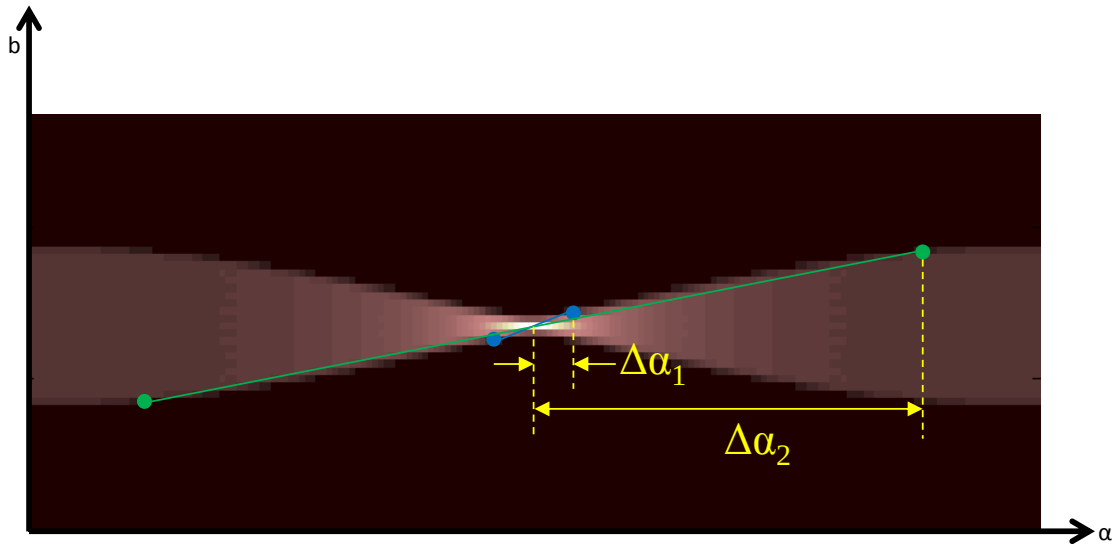

Figure 31. Two different angle steps in the same butterfly wing

In order to see how the angle step parameter ($\Delta\alpha$) affects to find the defined range, three angle steps parameters ($\Delta\alpha$) are compared. Figure 32 shows three different angle step parameters ($\Delta\alpha$) at the same butterfly wing. The known length of the linear feature is found at angle step of 4 shown in Figure 32 (b). The defined range is slightly shifted on the right wing at $\Delta\alpha = 3$ as shown in Figure 32 (a). Even though it is only one pixel off, the result increases 32.7%. At angle step $\Delta\alpha = 5$, left wing of the defined range is found slightly shifted and also this causes 20% decrease of the reconstructed length.

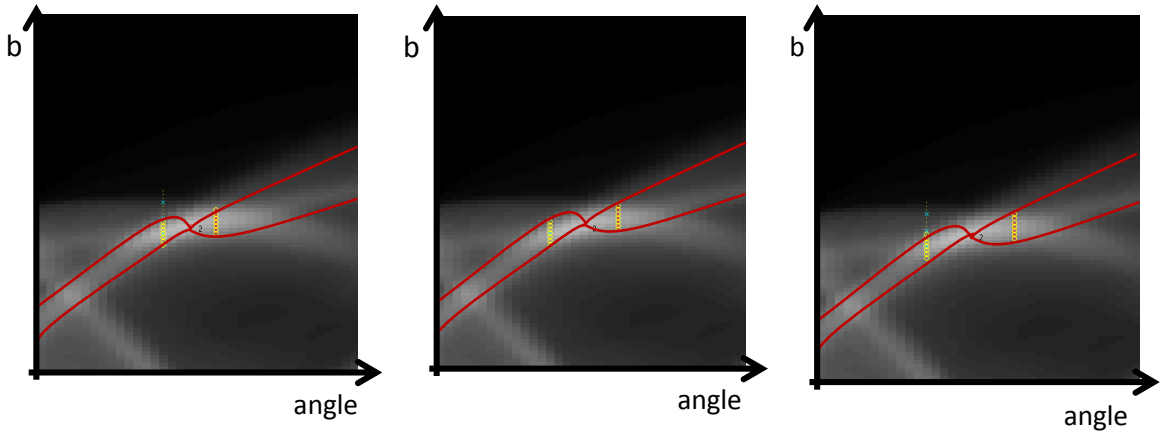

(a) Angle step Δ α=3 (b) Angle step Δ α=4 (c) Angle step Δ α=5

Figure 32. Butterfly wing (red curve) and the defined range at angle step 3,4 and 5

7.2 Parameter 2: Segment parameter (Δb)

When the line segment is reconstructed a segment parameter (Δb) is importantly used like angle step parameter (Δα). A segment parameter (Δb) is finite number of pixels consecutively stacked from offset value shown in Figure 33. An angle step parameter (Δα) is taken from the peak value (α, b) in x axis direction. By using an angle step, offset value (α+Δα, b) is found. Then a segment parameter (Δb) is used to narrow down the range to find the cross point of the butterfly wing. Vertically aligned yellow circles in Figure 33 indicate segment parameter (Δb), which is piled from offset value to both up and down directions.

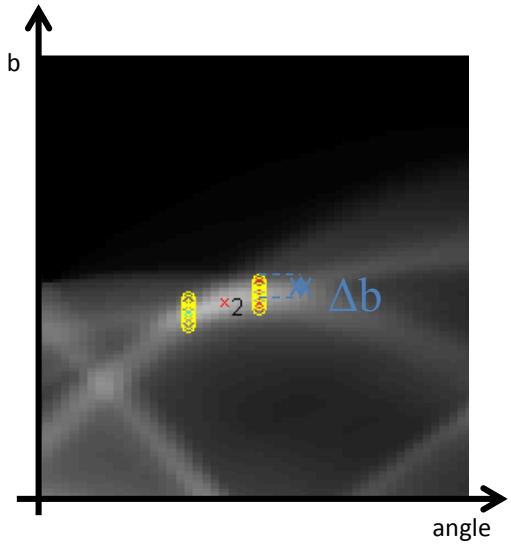

Figure 33. The Defined range (yellow circles) Δb apart from peak value (red cross)

Yellow circles in Figure 34 show the defined range of the butterfly wings with the different segment parameter (Δb), when angle step parameter (Δα) is 4 and threshold value is 0.5. The known length is found at segment parameter (Δb) is 6, shown in Figure 34 (f). By increasing of segment parameter (Δb), a reconstructed length also increases. As mentioned section 5.3.3.2, the cross points of the butterfly wing are selected in reduced range defined by a segment parameter (Δb). Therefore, incremental of the segment parameter produces a large defined range. The large defined range indicates a long reconstructed length shown in

Table 5.

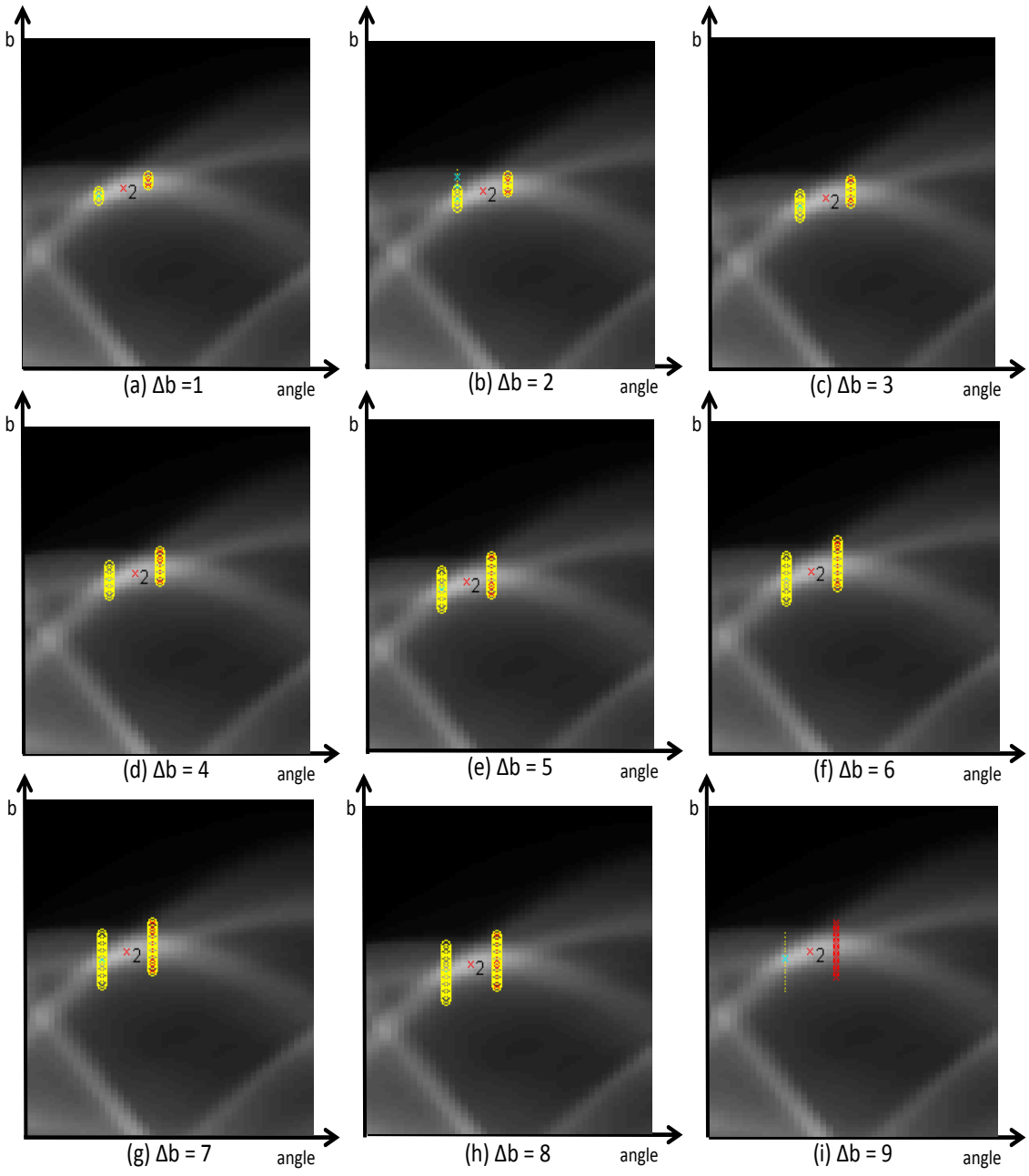

Figure 34. The Defined range with different segment parameter at angle step parameter of 4 and threshold value of 0.5

Table 5. Reconstructed length of the line segment with different segment parameter

segment parameter	1	2	3	4	5	6	7	8	9
length of line seg.	28.65	57.30	85.94	114.59	128.92	143.24	143.24	143.24	N/A

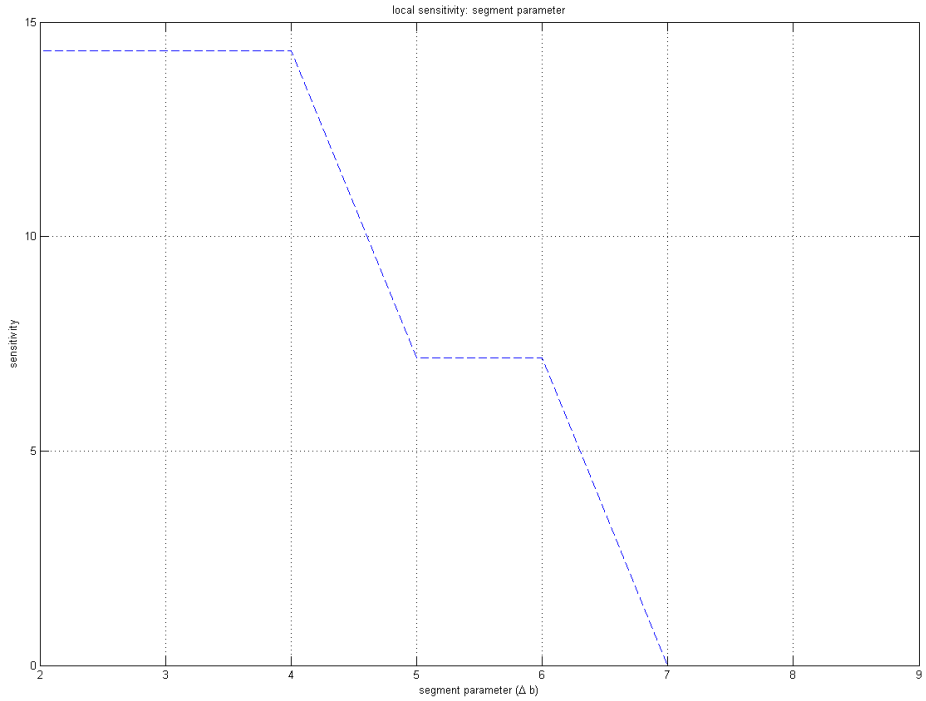

Figure 35. Local sensitivity of segment parameter

The local sensitivity of the segment parameter (Δb) is shown in Figure 35, showing decreasing pattern with increasing of segment parameter (Δb). Since the local sensitivity is calculated using equation (16), it shows step shape. Flat lines between segment parameter (Δb) of 2 and 4, and segment parameter (Δb) of 5 and 6, indicate constant reconstructed length of the line segment.

The butterfly wing is consisting with pixels, which is square shape. In order to represent sinusoidal shape of the butterfly wing with square shaped pixel, stair shape is used shown in

Figure 36 (c). A stair shape, representing the curved edge, indicates that the intensity values of the butterfly wing are discretized. Therefore as shown in Figure 35 (f), (g), and (h), the same cross points of the butterfly wing are found even though a segment parameter (Δb) is increased. This is why the local sensitivity has flat line at segment parameter (Δb) of 7, 8, and 9.

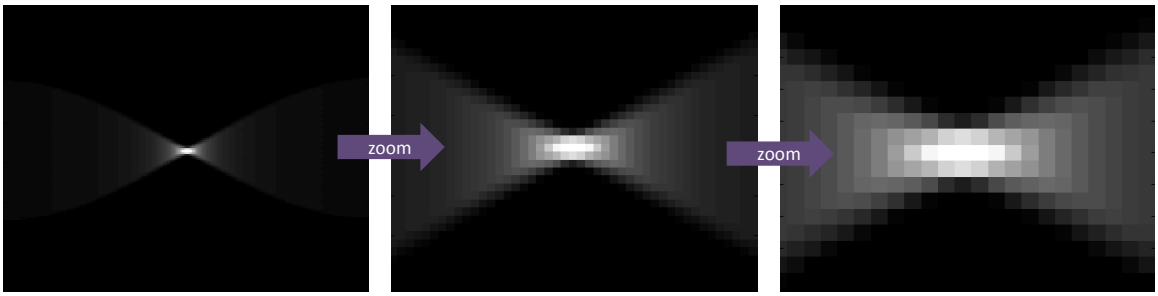

Figure 36. Stair shape of the butterfly wing

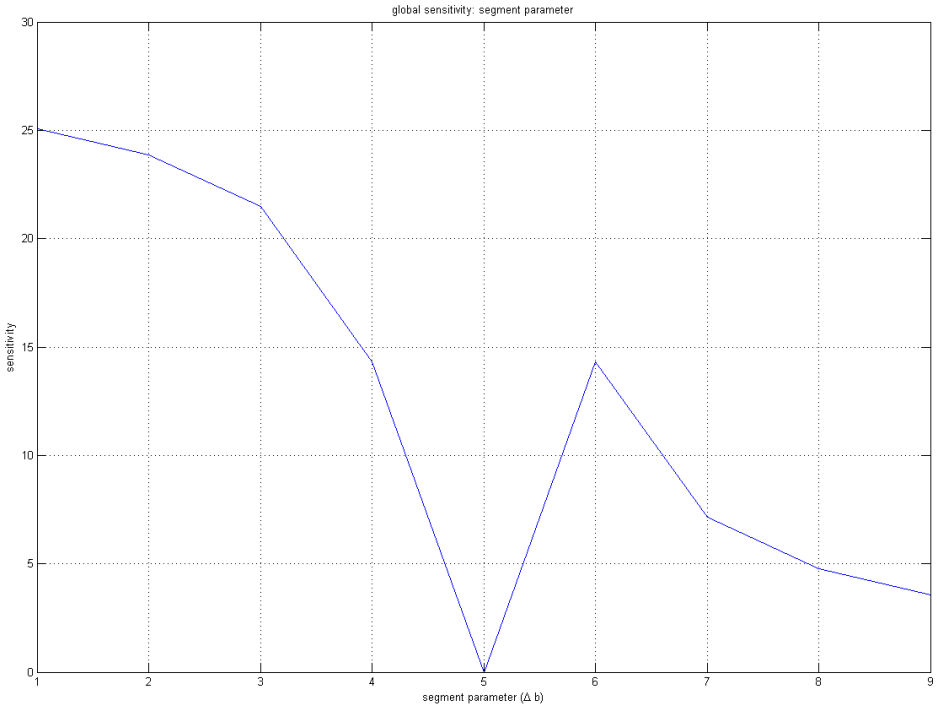

Figure 37. Global sensitivity of segment parameter

On the other hand, the global sensitivity shows a smoothly decreasing pattern as shown Figure 37. As mentioned in equation (17), the global sensitivity is calculated using the middle point, in this case segment parameter (Δb) of 5. Therefore, the sensitivity at segment parameter (Δb) of 5 is always zero. Other than segment parameter (Δb) of 5, the sensitivity of segment parameter decreases with increasing of segment parameter (Δb). This means the reconstructed lengths of the line segment increase with incremental of segment parameter (Δb), which is consistent with

Table 5.

7.3 Parameter 3: Threshold value

A threshold value is one of the important parameter for reconstructing linear feature. Threshold value is used to find the defined range. Figure 38 shows the defined range of the butterfly wings with different threshold values when the angle parameter ($\Delta\alpha$) is 4, and segment parameter is (Δb) 6. From Figure 38 (a) to Figure 38 (i), threshold value increases with 0.1 steps. As shown in

Table 6, the known length is found at Figure 38 (a), (b), (c), (d), (e) and (f), indicating until threshold value is 0.5 the defined range has enough pixels to extract reconstruction information. If a threshold value is greater than 0.5, the lengths of the line segments decrease. This is because only small number of pixels are satisfied the threshold value.

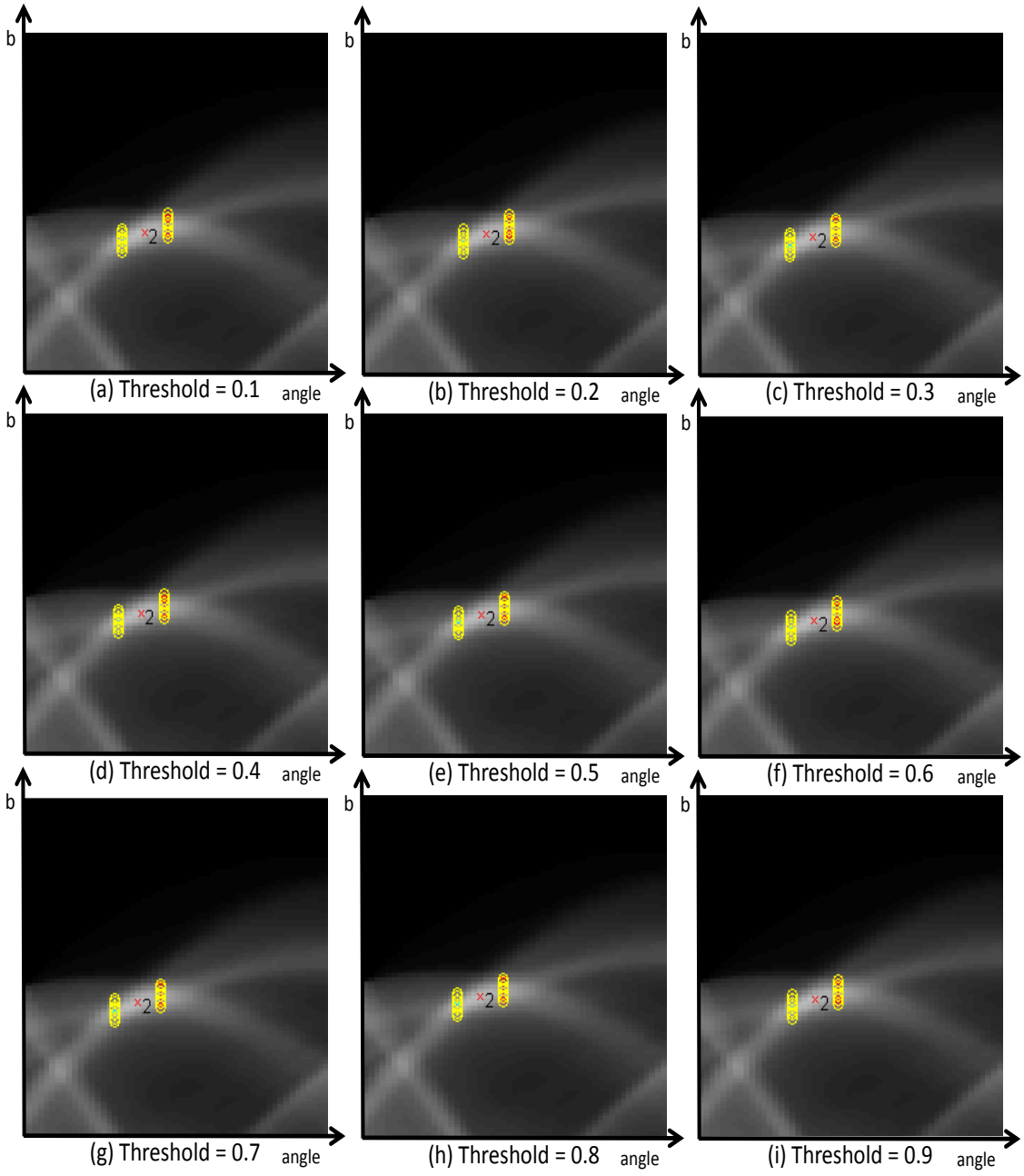

Figure 38. The Defined range with different threshold value at angle step of 4 and segment parameter of 6

Table 6. Reconstructed length of the line segment with different threshold value

threshold	0.1	0.2	0.3	0.4	0.5	0.6	0.7	0.8	0.9
length of line segment	85.94	85.94	85.94	85.94	85.94	85.94	71.62	57.30	42.97

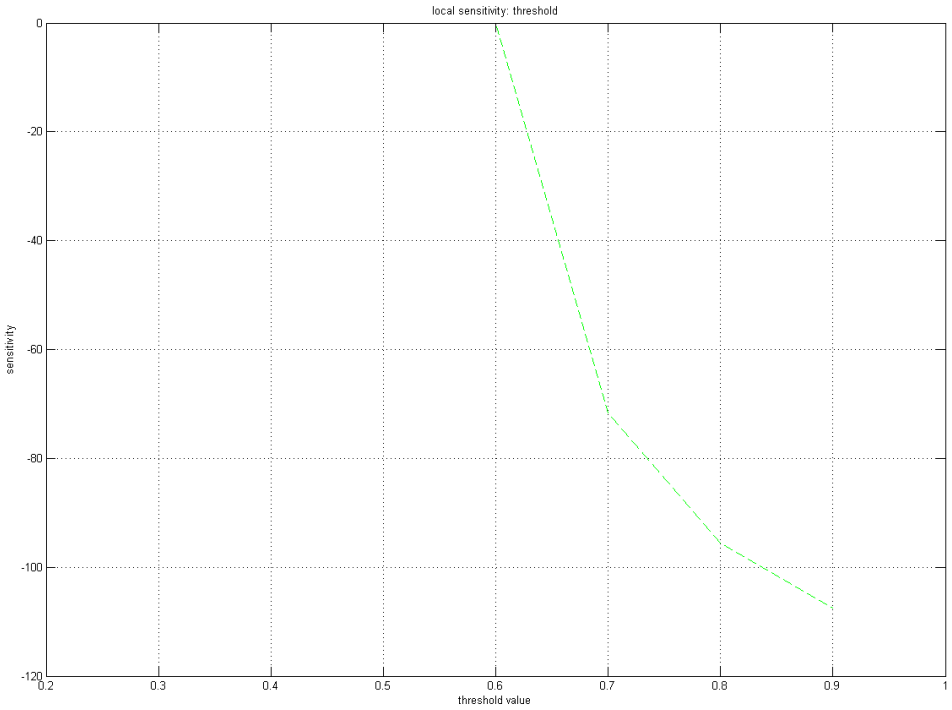

Figure 39. Local sensitivity of threshold value

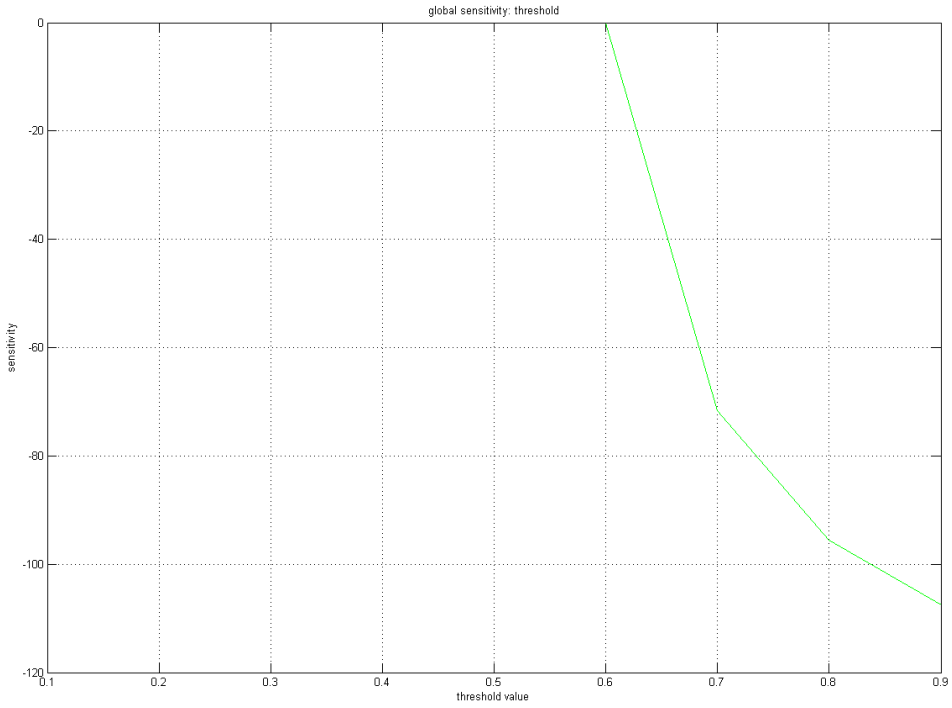

Figure 40. Global sensitivity of threshold value

Figure 39 represents the local sensitivity of the threshold value while Figure 40 represents the global sensitivity of the threshold value. Two different sensitivities show the same trends because of discretized pixel values in the Radon transform domain. In order to determine the defined range, pixels with a magnitude greater than the threshold value of the maximum of 2x Δb are used. Because of this process, the cross points of the butterfly wing are found identically even though the threshold value increases. Also the large threshold value extracts only a few numbers of pixels, producing a short length of the reconstructed line segment.

7.4 Overlapped butterfly wing

Since a real microstructure image contains irregular linear features, the butterfly wings of linear features are overlapped in the Radon transform domain. A peak value is overlapped by several

butterfly wings, and this allows surroundings of the peak value brighter than single butterfly wing. This is the reason why the length of reconstructed line segment has non-linear pattern.

The overlapped butterfly wings can be identified one by one as shown in Figure 41. Figure 41 (a) shows plentiful overlapped butterfly wings around peak 2. Figure 41 (b) is zoomed in figure of the butterfly wing around peak 2. As Figure 41 (b) shows, there are 3 sets of butterfly wings around the area. Figure 41 (e) is the butterfly wing which corresponds to the peak number 2. Figure 41 (c) and (d) show butterfly wings overlapped to the correct butterfly wing. The overlapped butterfly wings as shown in Figure 41 (c) and (d) cause the non-linearity of reconstructed linear feature.

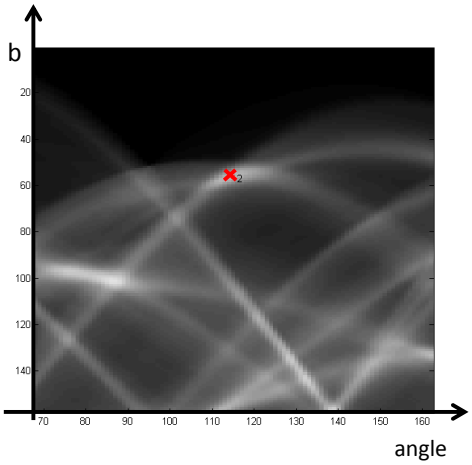

(a)Radon transform domain

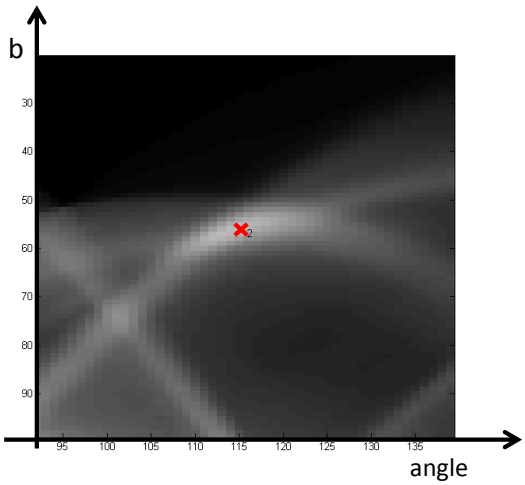

(b) Zoomed in butterfly wing

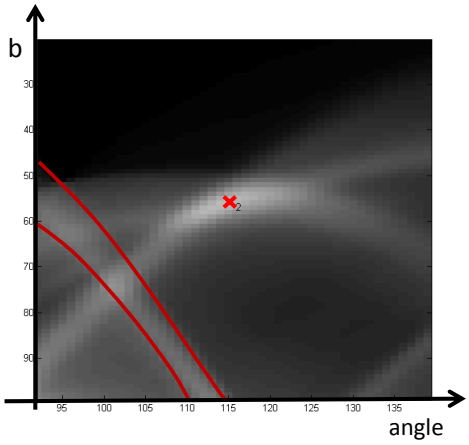

(c) Overlapped butterfly wing around peak value

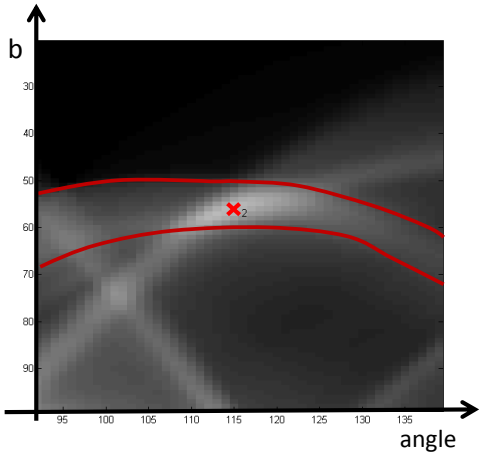

(d) Overlapped butterfly wing around peak value

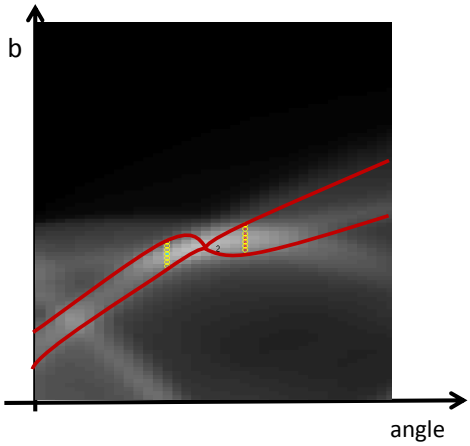

(e) Butterfly wing with detected Range 2

Figure 41. Overlapped butterfly wing around peak value area

7.5 Sensitivity of synthetic line segment

7.5.1 Parameter 1: Angle step

In order to see the effect of the overlapped butterfly wings, a single synthetic line segment is investigated. Figure 42 (a) shows an image with 70 pixels long and 3 pixels thick line segment in 100 by 100 pixels of an image domain. When the Radon transform is applied to the linear feature, a set of non-deformed butterfly wing is generated as shown in Figure 42(b). Different angle step parameters on a set of butterfly wing are shown in Figure 43 with segment parameter of 4 and threshold value of 0.5. A peak point is in the middle of the Radon transform domain and the butterfly wing is placed horizontally. This case is a simple case, meaning a butterfly wing is not overlapped or interrupted by the other butterfly wings. The defined range in the butterfly wings is found symmetrically as shown in Figure 43. However, the reconstructed lengths of the line segment are varies. Digital images consist of pixels so it shows limits to represent accurate feature. When we zoom in the butterfly wings, diagonal lines are represented as a stair shape. Due to the limited resolution of the digital image, the defined range in each angle step is found one pixel shifted in Figure 43 (c), (f), (g), and (h). This is the reason why the reconstructed line segments are not constant even though the butterfly wing is not interrupted by any other factors.

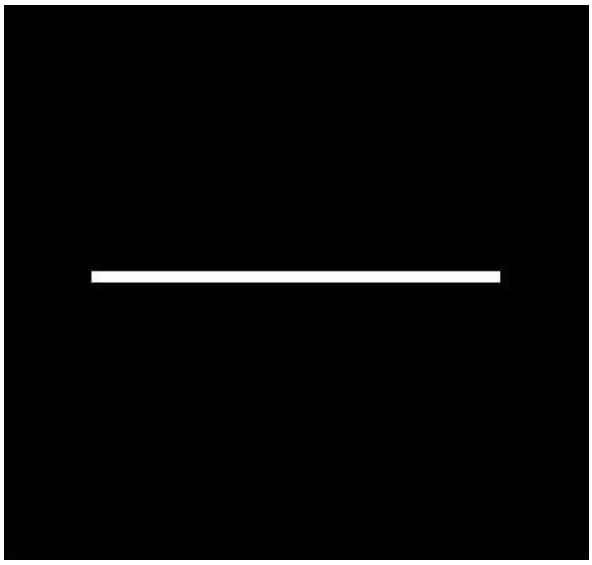

(a) Synthetic linear feature in the image domain

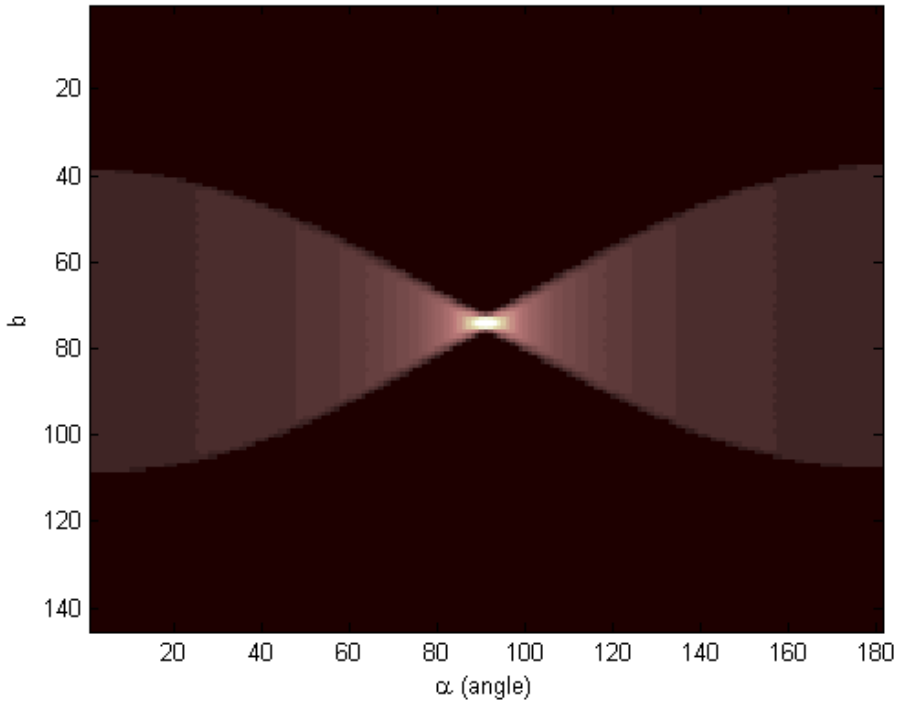

(b) A butterfly wings in the Radon transform domain

Figure 42. Simple line segment and its Radon transform

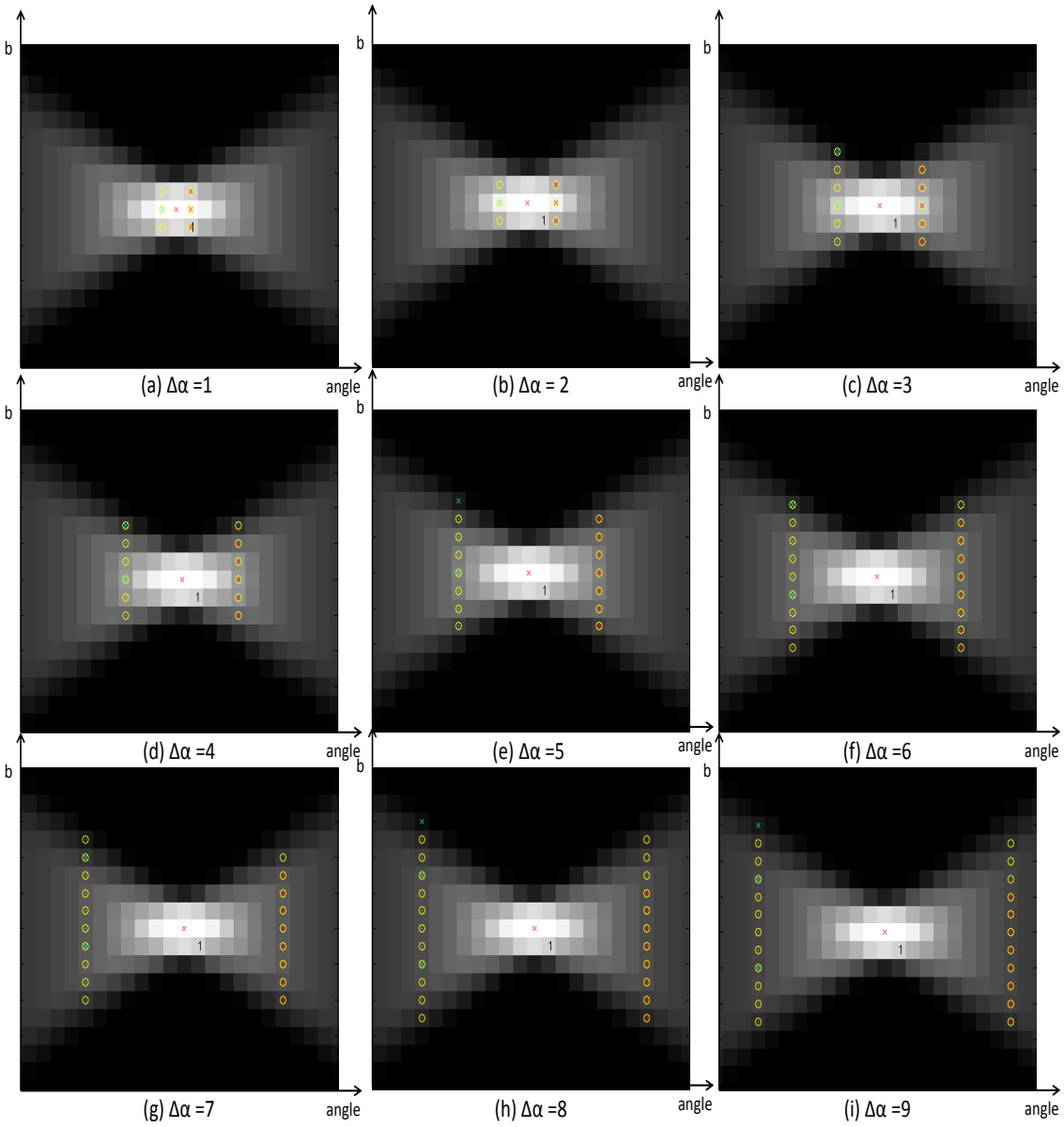

Figure 43. The Defined range with different angle step parameter in simple line case

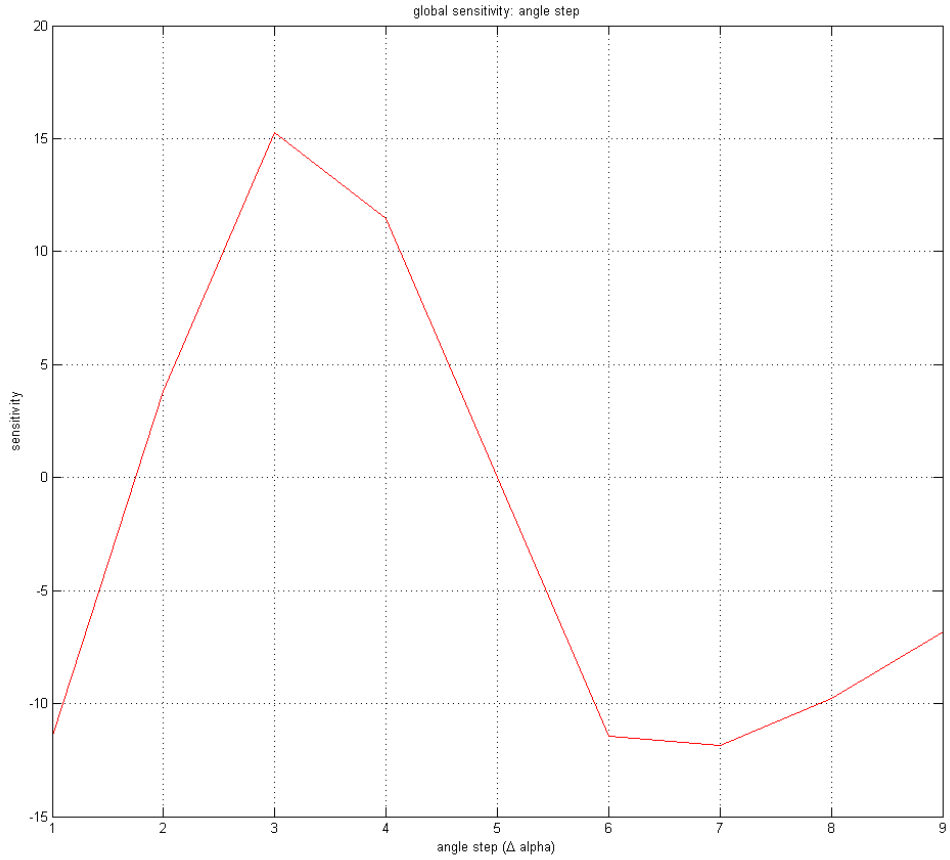

Figure 44. Global sensitivity of angle step in the simple line case

Figure 44 shows the sensitivity of angle step parameter in the simple line case. Even though there are no overlapped butterfly wings, it shows no trends. This is because that the gradient of the intensity of the pixels around the peak area are non-linear. If three parameters ($\Delta\alpha$, Δb, and threshold value) are changed together it shows constant trends. This will be explained section 7.5.3 below.

7.5.2 Parameter 2: Segment parameter

Figure 45 shows the Radon transform of a synthetic line segment with different segment parameters when $\Delta\alpha$ is 5 and the threshold value is 0.5. The same synthetic line segment is used as shown in Figure 42(a). A small size of the defined range is detected as shown in Figure

45 (a), (b), (c) since the segment parameters are too small to find the appropriate cross points of the butterfly wing. Once the segment parameter increases (from $\Delta b=4$ to $\Delta b=9$) to select the cross points of the butterfly wing, the reconstructed lengths are the same shown in

Table 7.

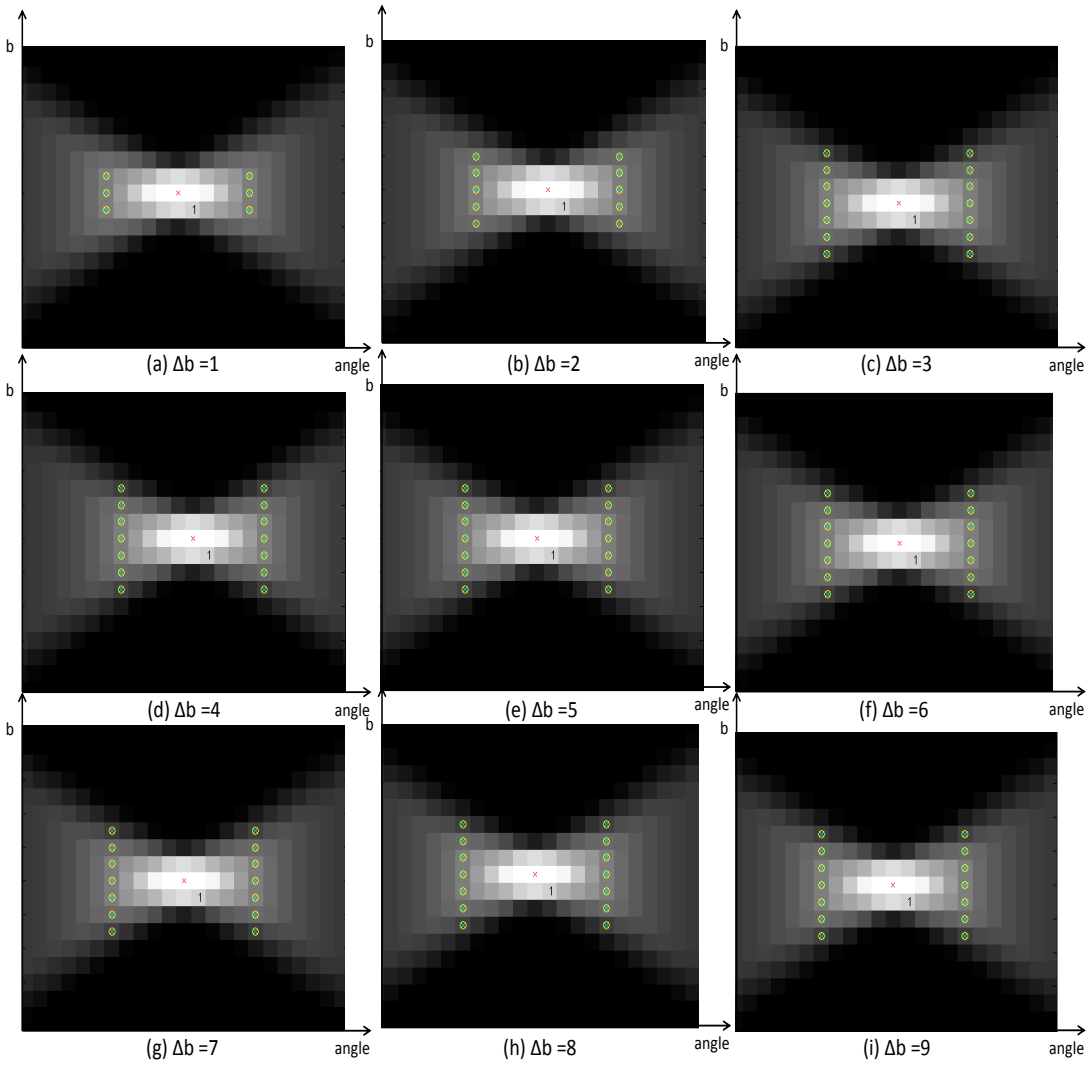

Figure 45 Detected Range 2 with different segment parameter in simple line case

Table 7. The reconstructed line segment with different segment parameter in simple line case

Segment parameter	1	2	3	4	5	6	7	8	9
length of line segment	22.92	45.84	68.75	68.75	68.75	68.75	68.75	68.75	68.75

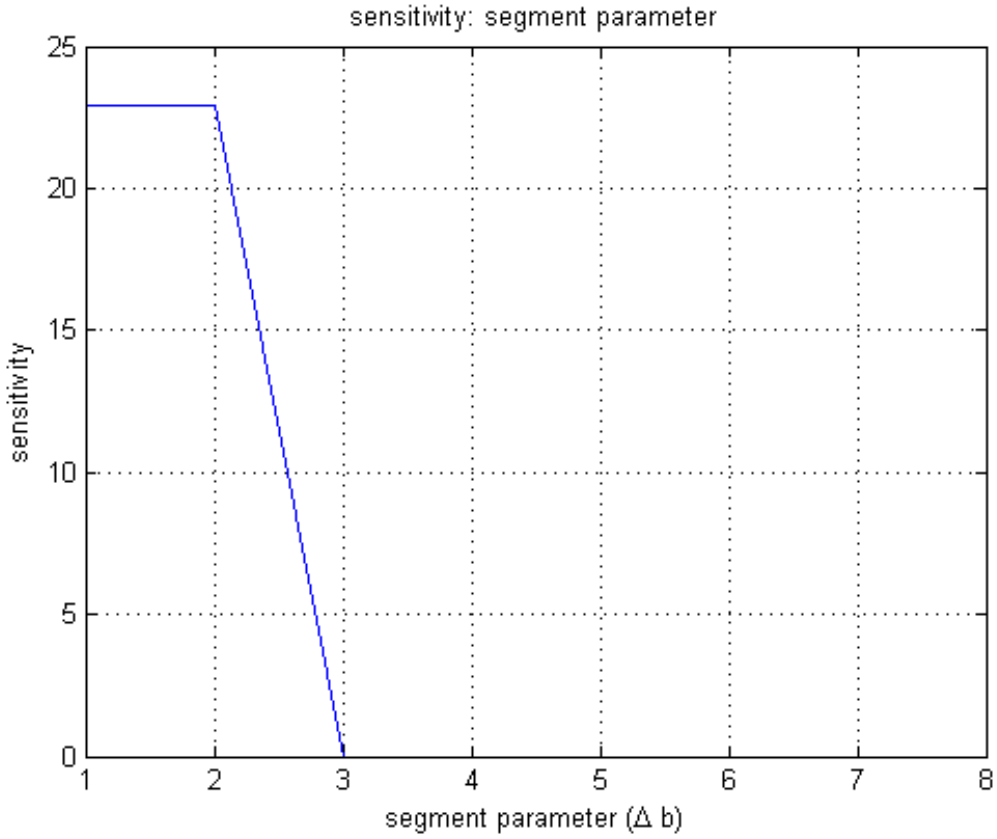

Figure 46. Global sensitivity of segment parameter in simple line case

Figure 46 shows the sensitivity of the segment parameter. Compare to the sensitivity of the angle step parameter, it is stable. Especially, from the segment parameter of 3, the reconstructed line segment shows constant length. Since this is the simple case, the butterfly wing does not interrupted by the others. This can produce constant and stable result with the

different segment parameter. When the segment parameter is 1 or 2, size of the segment parameter is not enough to cover width of the butterfly wing, therefore it generates short reconstructed line segment.

7.5.3 Parameter 3: Threshold value

Figure 47 shows the defined range in a single butterfly wing with the different threshold values when $\Delta\alpha$ is 5 and Δb is 4. The defined range at the threshold values of 0.3, 0.4, and 0.5 generate the same length of the linear feature shown in Figure 47 (c), (d), and (e). When the threshold value is small (e.g., 0.1 and 0.2), the defined range includes redundant pixels, it causes long reconstructed line segment. Table 8 shows the reconstructed lengths of the linear feature with the different threshold values. The larger threshold value is used, the shorter length of linear feature is obtained. The large threshold value only includes a few numbers of pixels to extract for selecting the cross points of the butterfly wing. This is because why the reconstructed length decreases when the threshold value increases.

Table 8. The reconstructed length with different threshold value in simple line case

threshold	0.1	0.2	0.3	0.4	0.5	0.6	0.7	0.8	0.9
length of line segment	91.67	74.48	68.75	68.75	68.75	45.84	45.84	45.84	22.92

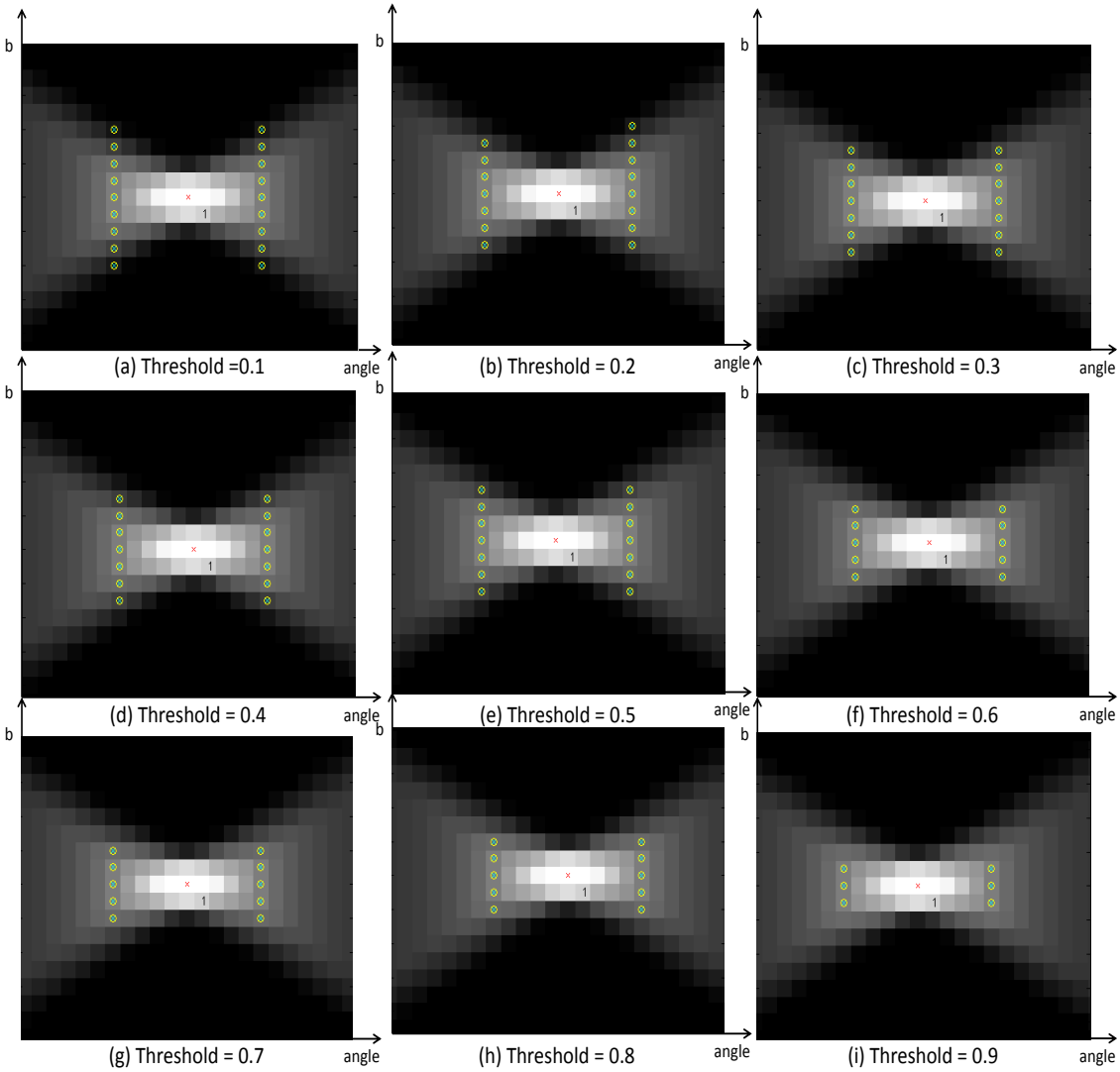

Figure 47. The Defined Range with threshold value in simple line case

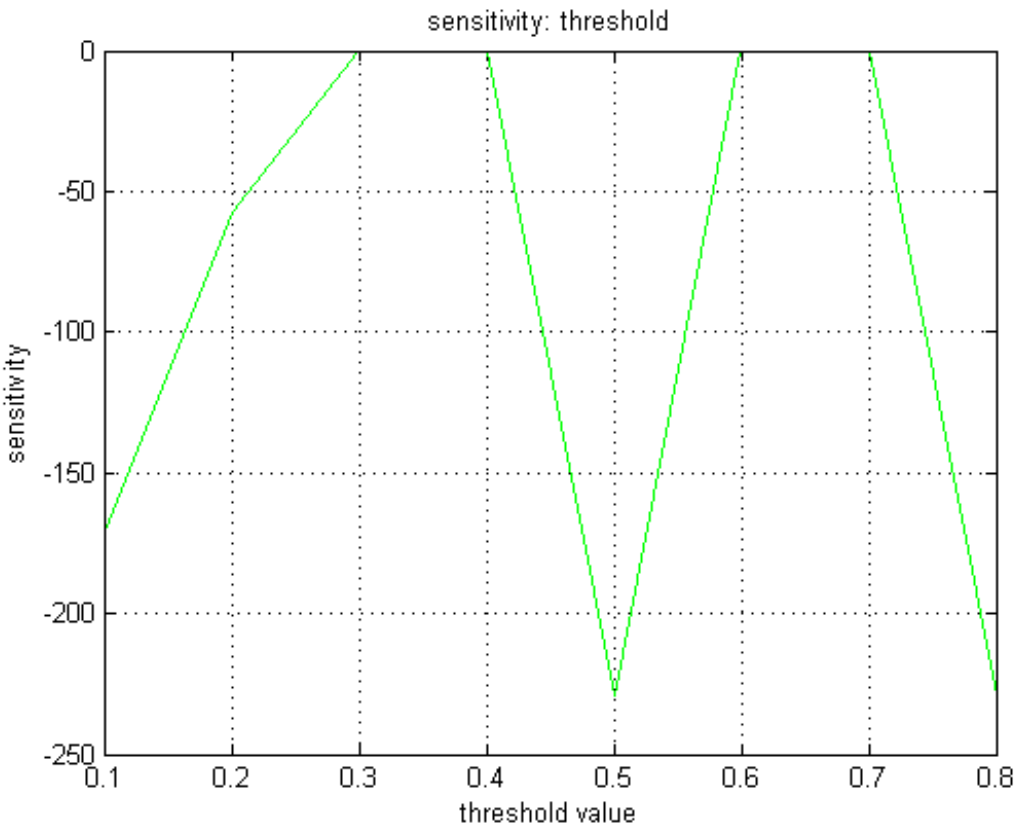

Figure 48. Global sensitivity of threshold value in simple line case

As shown in Table 8, the length of line segment decreases like stair shape when the threshold value increases. When the threshold value increases from 0.2 to 0.3, the reconstructed length decreases, increasing the sensitivity. On the other hand, when threshold value increases from 0.3 to 0.5, the reconstructed length holds the same length (=68.75). This is shown as a flat line in the sensitivity graph in Figure 48. The flat line indicates that there is no length change between two points (threshold value 0.3 and 0.4).

In the butterfly wing, three parameters are engaged in calculation of the length of line segment. The combinations of three parameters produce a trend as shown in Table 9. Since there is no overlapped butterfly wing, the cross points of the butterfly wing are only selected based on the

intensity value of pixels in the Radon transform domain. Followings are patterns among those three parameters regarding to the reconstructed length.

1. A large angle step does not guarantee longer length. As shown in Table 9 (a), (b), and (c), threshold value is the same when the angle step is increased. The reconstructed length increases between (a) and (b), and it decreases between (b) and (c). This is because the gradient of the butterfly wing decreases non-linearly.

2. When the segment parameter increases, the reconstructed length increases until the segment parameter of 3. (But, when $\Delta\alpha$ is 6, the reconstructed length increases until the segment parameter of 4) This means, it is important to use appropriate size of the segment parameter in order to cover width of the butterfly wing. If the segment parameter longer than the width of the butterfly wing, it drops redundant pixels in the segment parameter. This is why the reconstructed length increases only in the segment parameter of 1, 2 and 3.

3. As shown in Table 8, when the threshold value increases the length of the line segment decreases like stair shape. This pattern shows at the small angle step with the large threshold value and the large angle step with the small threshold value.

Table 9. Comparison of reconstructed length among three parameters (Δα, Δb, and threshold value)

Δα=4, threshold = 0.4			
Δb	1	2	3
length	28.65	57.30	57.30
Δb	4	5	6
length	57.30	57.30	57.30
Δb	7	8	9
length	57.30	57.30	57.30

(a)

Δα=5, threshold = 0.4			
Δb	1	2	3
length	22.92	45.84	68.75
Δb	4	5	6
length	68.75	68.75	68.75
Δb	7	8	9
length	68.75	68.75	68.75

(b)

Δα=6, threshold = 0.4			
Δb	1	2	3
Length	19.10	38.20	52.52
Δb	4	5	6
Length	62.07	66.85	66.85
Δb	7	8	9
Length	66.85	66.85	66.85

(c)

Δα=4, threshold = 0.5			
Δb	1	2	3
length	28.65	57.30	57.30
Δb	4	5	6
length	57.30	57.30	57.30
Δb	7	8	9
length	57.30	57.30	57.30

(d)

Δα=5, threshold = 0.5			
Δb	1	2	3
length	22.92	45.84	68.75
Δb	4	5	6
length	68.75	68.75	68.75
Δb	7	8	9
length	68.75	68.75	68.75

(e)

Δα=6, threshold = 0.5			
Δb	1	2	3
length	19.10	38.20	47.75
Δb	4	5	6
length	57.30	57.30	57.30
Δb	7	8	9
length	57.30	57.30	57.30

(f)

Δα=4, threshold = 0.6			
Δb	1	2	3
length	28.65	57.30	57.30
Δb	4	5	6
length	57.30	57.30	57.30
Δb	7	8	9
length	57.30	57.30	57.30

(g)

Δα=5, threshold = 0.6			
Δb	1	2	3
length	22.92	45.84	45.84
Δb	4	5	6
length	45.84	45.84	45.84
Δb	7	8	9
length	45.84	45.84	45.84

(h)

Δα=6, threshold = 0.6			
Δb	1	2	3
length	19.10	38.20	47.75
Δb	4	5	6
length	57.30	57.30	57.30
Δb	7	8	9
length	57.30	57.30	57.30

(i)

7.6 Summary

This chapter investigates the sensitivity of the butterfly wing method. The cross points of the butterfly wing are the important parts to achieve accurate reconstructed line segments. In the Radon transform domain, three parameters are the factors, three parameters, the angle step parameter ($\Delta\alpha$), the segment parameter (Δb) and the threshold value (th), to identify the cross points. The sensitivity of three parameters is explained in this chapter. In order to explore the sensitivity of the butterfly wing for a complicated image, three parameters are tested and investigated under the controlled scenarios. An extensive analysis of the butterfly wing method would help to understand the errors occurred during the recognition process.

If a butterfly wing exists in the Radon transform domain, it can be easy to control to select the cross point to calculate the linear features. Other than three parameters, the overlapped butterfly wings also affect the process of selecting the cross points in the butterfly wing. The effect of the overlapped butterfly wings is also explored and compared.

CHAPTER 8
RESEARCH QUESTION 1A: 3D LINEAR FEATURE EXTRACTION

This chapter will explain an approach for extracting 3D linear features in the microstructure voxel data set. As was the case for 2D linear geometric features, a 3D surfacelet based method will be used. In order to define grain boundaries, a plane overlaying method will be applied on the result of the 3D Radon transform.

The first research question aims to extract geometric features. In this chapter 3D linear geometric features are the focus.

8.1 Feature Recognition method for 3D linear: 3D Surfacelet based method

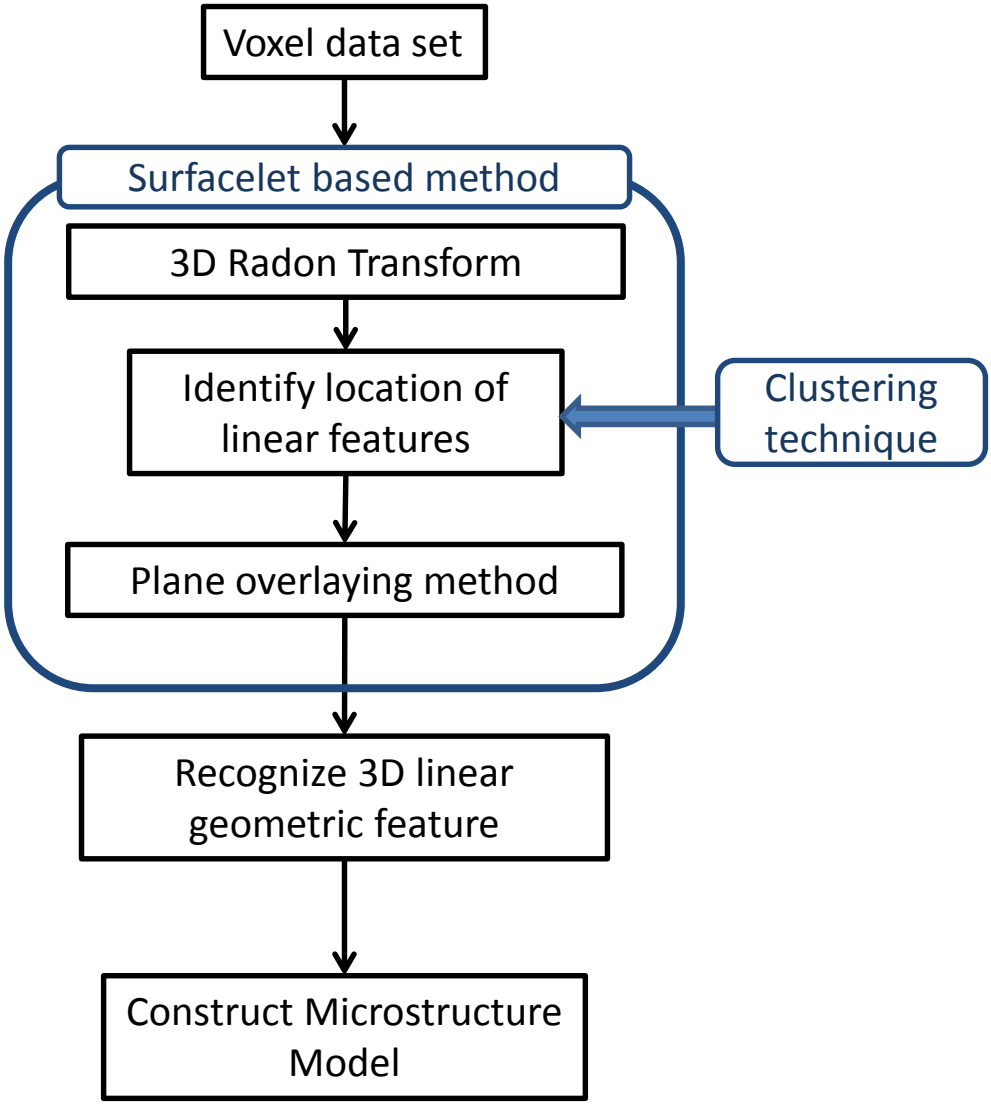

Figure 49. Feature recognition method for 3D linear geometric features

A surfacelet based method consists of the 3D Radon transform and the plane overlying method. Similar to the 2D feature recognition method mentioned in chapter 4, Figure 49 shows the process of recognizing 3D linear features from the voxel data sets.

A pre-processing step, calculating the gradient of the voxel data set, is performed in a process similar to the 2D linear recognition method. The gradient of the 3D voxel data set aims to

highlight grain boundaries in the complicated voxel data set. The gradient of a scalar function is denoted ∇f where ∇ denotes the vector differential operator del. In the three-dimensional Cartesian coordinate system, the gradient is

$$\nabla \mathrm{f} = \frac{\partial f}{\partial x} i + \frac{\partial f}{\partial y} j + \frac{\partial f}{\partial z} k$$

where *i, j* and *k* are the standard unit vectors. Since each grain has the same intensity value for all of its voxels, the gradient of the inside of the grain is zero. When this gradient is calculated between two grains, it gives a non-zero value. By calculating this gradient, an input voxel data set is converted to a binary data set, which highlights grain boundaries. In this way, grain boundaries can be recognized the 3D surfacelet based method.

In order to find the locations of linear features in the voxel data set, the 3D Radon transform is applied to the binary voxel data set, producing a 3D coefficient set. The 3D coefficient set provides a three-dimension-matrix, which is used to locate linear features in the voxel data set. By applying the clustering technique onto the 3D coefficient set, the locations of linear features are identified. Then, the plane overlaying method is applied to the input voxel data set using information from the previous step. The plane overlaying method recognizes the size of linear features. After determining the locations and sizes of the 3D linear features, the 3D microstructure model will be constructed. The following sections will explain in detail the 3D Radon transform and plane overlaying method.

8.2 3D Radon transform

In this section, the 3D Radon transform will be explained. The 3D surfacelet based method for 3D linear geometric features represents plane singularities and is defined as

$$y_{a,b,\alpha,\beta}(r) = a^{-1/2} y(a^{-1}(cos\beta cos\alpha \cdot x + cos\beta sin\alpha \cdot y + sin\beta \cdot z - b)) \qquad (8)$$

where α is rotation about the Z axis, $\beta \in [0,\pi]$ is a new angular parameter about the local X axis, and *b* is a translation along the local Y-axis, as shown in Figure 50. α, β, and b are the main components of the 3D Radon transform. In order to extract 3D linear geometric features, the 3D Radon transform is mainly used in this research. The 3D Radon transform uses a plane, which is the fundamental shape in 3D space while the 2D Radon transform uses the lines to search linear features in the 2D image domain.

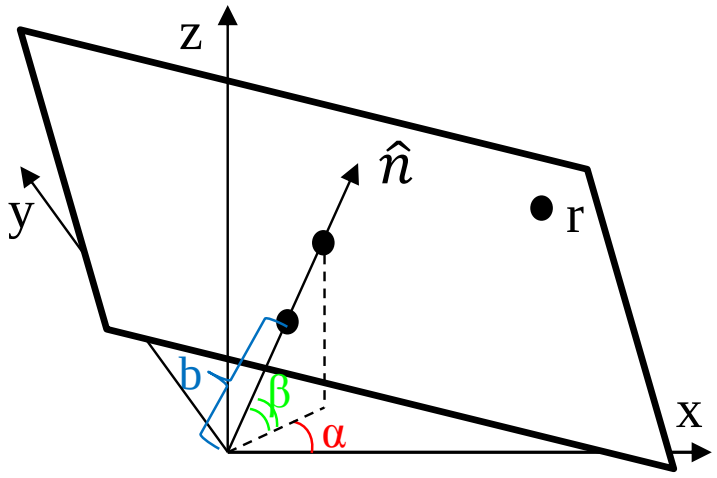

Figure 50. 3D Radon plane and its transformations

As shown in Figure 50, the 3D Radon transform is designed for recognizing 3D linear features. The fundamental feature, a plane, searches linear features in the voxel data set using three transformations. As shown in Figure 51, if a plane is at the x-z plane, the first rotation is about the global Z axis (α) followed by rotation about the local x axis (β). Then the last translation is along the local y axis (b). The complete transformation matrices are shown in Equation (18)[24].

$$R_Z * R_x * T_y = \begin{bmatrix} cos\alpha & -sin\alpha & 0 & 0 \\ sin\alpha & cos\alpha & 0 & 0 \\ 0 & 0 & 1 & 0 \\ 0 & 0 & 0 & 1 \end{bmatrix} * \begin{bmatrix} 1 & 0 & 0 & 0 \\ 0 & cos\beta & -sin\beta & 0 \\ 0 & sin\beta & cos\beta & 0 \\ 0 & 0 & 0 & 1 \end{bmatrix} * \begin{bmatrix} 1 & 0 & 0 & 0 \\ 0 & 1 & 0 & b \\ 0 & 0 & 1 & 0 \\ 0 & 0 & 0 & 1 \end{bmatrix} \quad (18)$$

where $\alpha \in [0,\pi]$,$\beta \in [0,\pi]$ $b \in [1$, edge length of voxel data set]. Figure 51 graphically shows each step of 3 transformations in the 3D Radon transform. We assume that the Radon plane starts at x-z plane and that it is at the middle of the voxel data set as shown in Figure 51 (a). Then the Radon plane rotates 30 degrees about the global Z axis (α) as shown in Figure 51 (b), followed by 90 degrees rotation about the local x axis (β) as shown in Figure 51 (c). The last transformation is translation along the local y axis (b). As shown in Figure 51 (d), the plane translates a distance of 10 units from its location as represented Figure 51 (c). The Radon plane moves with a combination of α, β, and b and searches linear geometric features (plane) in the entire voxel data set.

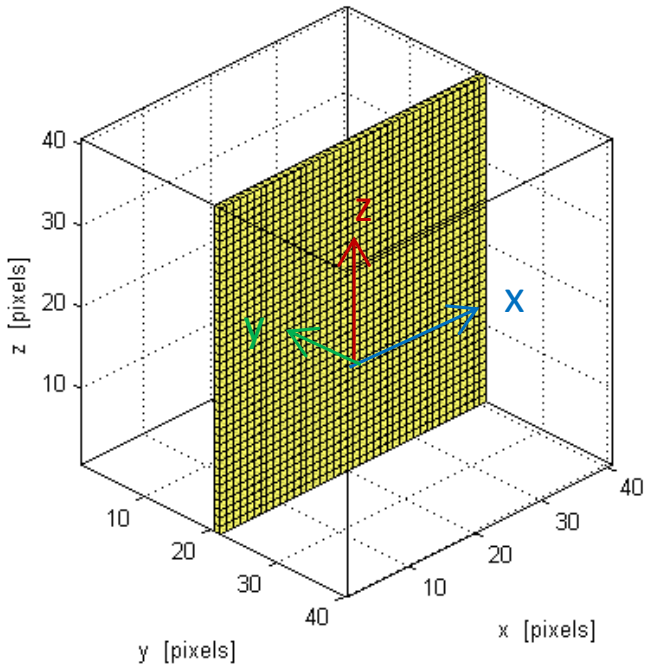

(a) A x-z plane at the middle of the voxel data set

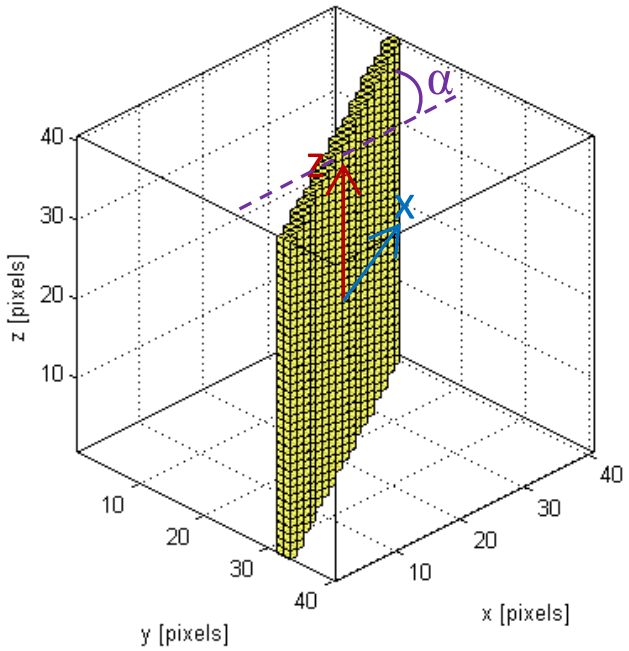

(b) Rotation 30 degree about global Z axis (α)

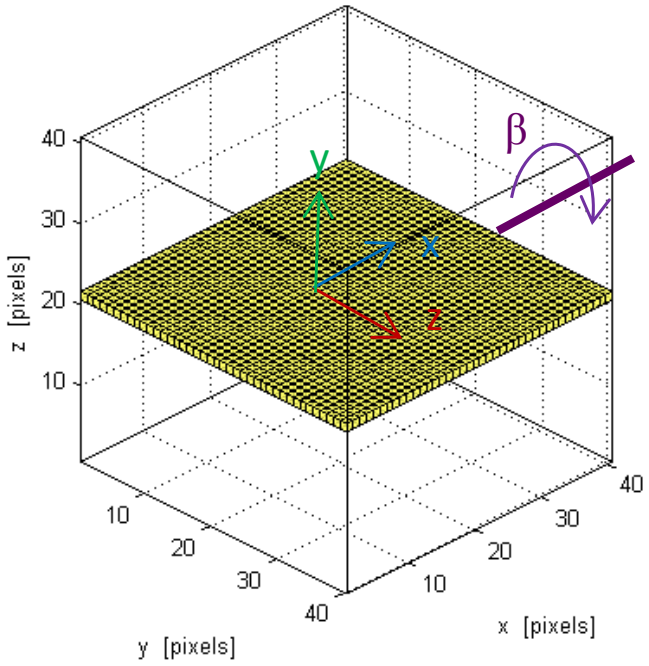

(c) Rotation 90 degree about local x axis (β)

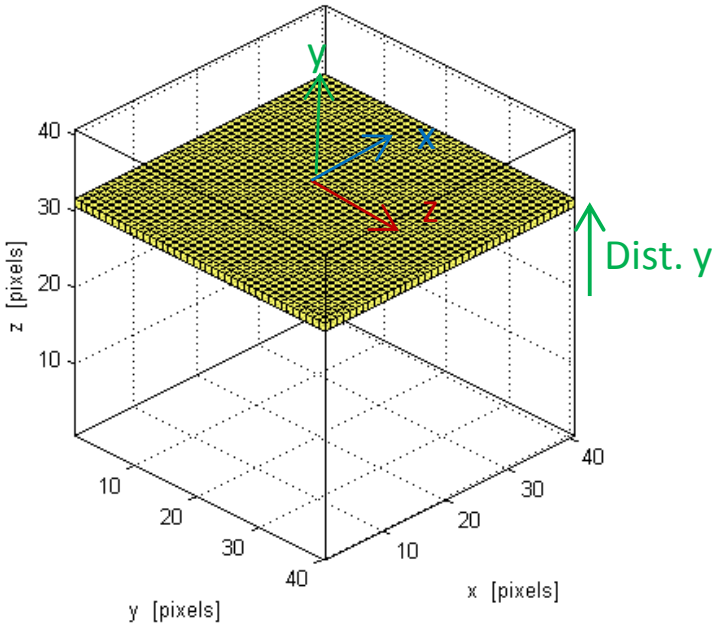

(d) Translate 10 unit along local y axis (b)

Figure 51. Three transformations in 3D Ridgelet (starting from x-z plane)

By searching linear geometric features, the 3D surfacelet generates 3D coefficient sets, which have 3 dimensions, α, β and b. If a linear feature is located at angle of α, β, and distance of b, it can be found by the Radon plane, which moves entire voxel data sets using a combination of α, β, and b. The Radon plane in the 3D surfacelet identifies linear feature in the voxel data set at (α, β, b) and converts the number of identified voxels to the 3D coefficient Radon transform domain. The integral equation of the 3D Radon transform is

$$\mathrm{R}(\alpha, \beta, \mathrm{b}) = \int_{\alpha=0}^{\alpha=\pi} \int_{\beta=0}^{\beta=\pi} \int_{b=1}^{b=b} y_{a,b,\alpha,\beta}(\mathbf{r})\, dr \qquad (19)$$

where **r** =(x,y,z) is the location in the domain Ω in the Euclidean space. The integrated value is interpreted as an intensity value.

When the Radon plane finishes searching the entire voxel data set, the size of the 3D coefficient matrix is α x β x b, which is 180x180x edge length of the voxel data set. Each element in the matrix has an intensity value that corresponds to the number of overlapped voxels between the Radon plane and the microstructure voxel data sets. If the Radon plane perfectly fits to a linear feature, the 3D surfacelet identifies the largest number of overlapped voxels in that feature and that can be converted as the highest intensity value at α, β and b in the 3D Radon transform coefficient set.

8.3 Recognize peak value: Clustering

The highest intensity value in 3D coefficient matrix is represented as a bright spot, and this is called the 'peak value.' In order to identify the peak value from the complicated 3D coefficient matrix, the clustering technique is used. Clustering is one of the techniques mentioned in section 5.2.2. If several peak values are located near one another in the 3D coefficient matrix, they can often be considered to represent one linear feature. These peak values will be clustered together using a k-means clustering method based on pair-wise distances between peaks. Among the peak values in the cluster, I take the largest value in the clustering area. Since a three dimensional matrix is used, the clustering technique is applied on each dimension to recognize peak values. By using clustering for the 3D coefficient set, the peak values that represent the 3D linear features can be chosen. Selected peak values represent α, β, and b, which correspond to a location where the linear feature is placed in the microstructure voxel data sets. These peak values can be used for next step, which is a plane overlaying method to find size of the 3D linear features.

8.4 Method of 3D Linear Feature extraction: Plane overlaying method

In order to recognize the location and size of 3D linear features, a plane overlaying method is proposed. This method is similar to the line overlaying method explained in section 5.4. The concept of the plane overlaying method is to superimpose a plane of voxels on the original voxel data set while the line overlaying method uses a line of pixels to superimpose on the original image.

In this research, a binary 3D voxel data set is used due to computational limitations. When the 3D surfacelet identifies the location of the peak value (α_{high}, β_{high}, b_{high}) in the 3D Radon transform domain, a plane is superimposed onto the microstructure binary voxel dataset at the location of α_{high}, β_{high} and b_{high}. To be specific, the superimposed plane is also in the voxel data set that is the same size as the microstructure voxel data set. This voxel data set is binary, with one plane intensity value of 1 and the other vales are 0. This voxel data set with superimposed plane is multiplied by the microstructure binary voxel data sets. Figure 52(a) represents the microstructure binary voxel data set, while Figure 52(b) shows a binary voxel data set for a plane located at peak value (α_{high}, β_{high}, b_{high}). When those two voxel data sets are superimposed, any voxel from the microstructure voxel data set that lies on the plane at (α_{high}, β_{high}, b_{high}) is extracted as shown in Figure 52(c). By using several peak values and repeating the plane overlaying method, linear features represented as blue regions shown in Figure 52(c) can be recognized.

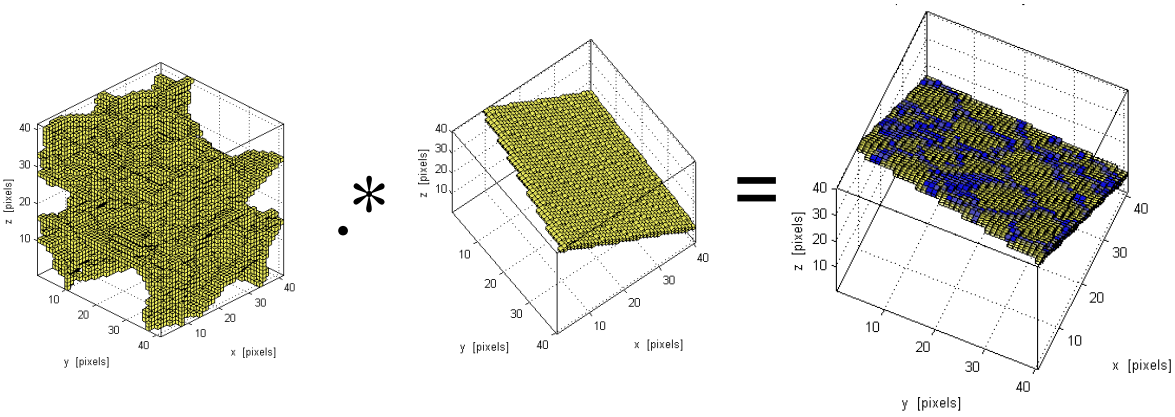

(a) The original voxel data set

(b) A plane located at peak value (α_{high}, β_{high}, b_{high}) in a voxel data set

(c) Extracted plane from the original voxel data set using superimposing step

Figure 52.The original binary voxel data set multiplied by a plane located at peak value (α_{high}, β_{high}, b_{high})

After inserting a plane, the result obtained by using the plane overlaying method is analyzed. The plane overlaying method inserts a plane, and this plane flatten onto the 2D domain as

shown in Figure 53. It is important to identify where the large region starts and ends (blue pixels in the red circle in Figure 53). Each pixel is analyzed in the flattened plane using 3x3 or 5x5 patches. In this way, cross sections of other linear feature (green circle in Figure 53) can be separated from the large area (red circle in Figure 53). In order to determine the large blue region, a scoring system is applied on the patch. A subject pixel is placed at the center of the patch and neighbor pixels are tested. In the patch, edge connections between pixels are counted. Depending on the number of neighbor pixels, a center pixel gets points. Figure 54 shows how the scoring system works on an image domain. The 2D binary image domain shown in Figure 54 (a) is tested with a 3x3 patch. The score is plotted with different colors as shown in Figure 54(b). If a pixel is surrounded by other pixels, forming a large region, that pixel gets a high score and is represented as red color, while low-score pixels get blue or cyan color as shown in Figure 54(b). By using this scoring system, large regions (red circle area in Figure 53) and cross sections of other linear features (green circle area in Figure 53) can be separated. After calculating the score of each pixel, the connectivity of each pixel in the large area is checked. By doing that, the found large area can be mapped to the 3D voxel data set. While the connectivity of each pixel is being checked, the minimum area tolerance is applied so that small areas can be eliminated. Figure 55 shows the process of finding linear features after the plane overlaying method has been applied.

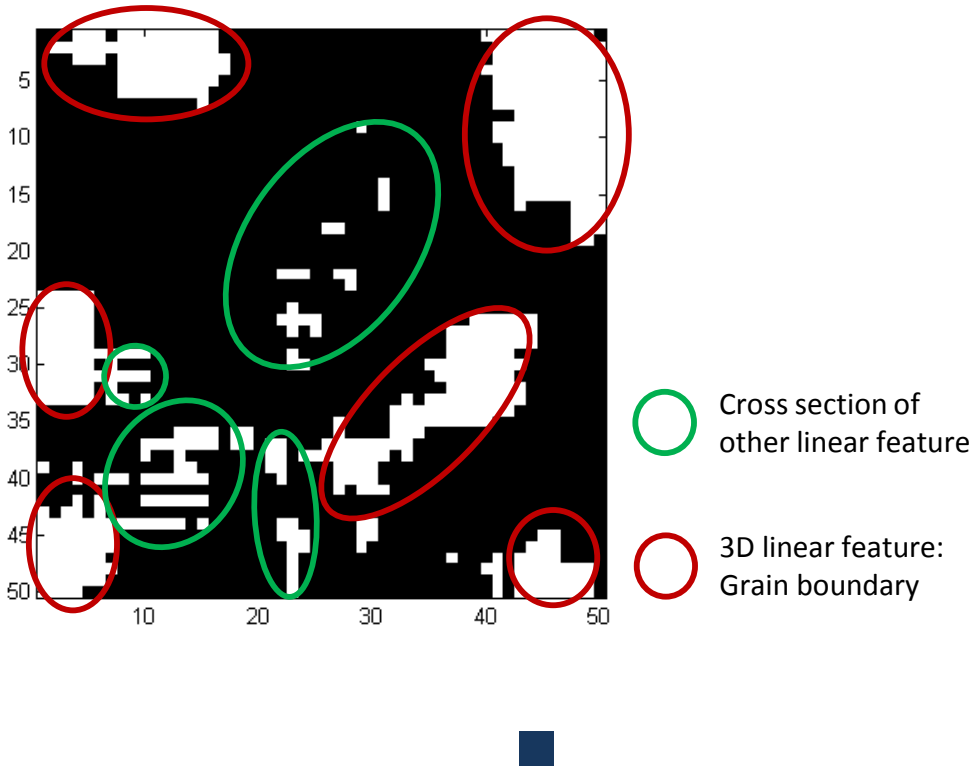

Figure 53. Synthetic flatten plane onto 2D image domain

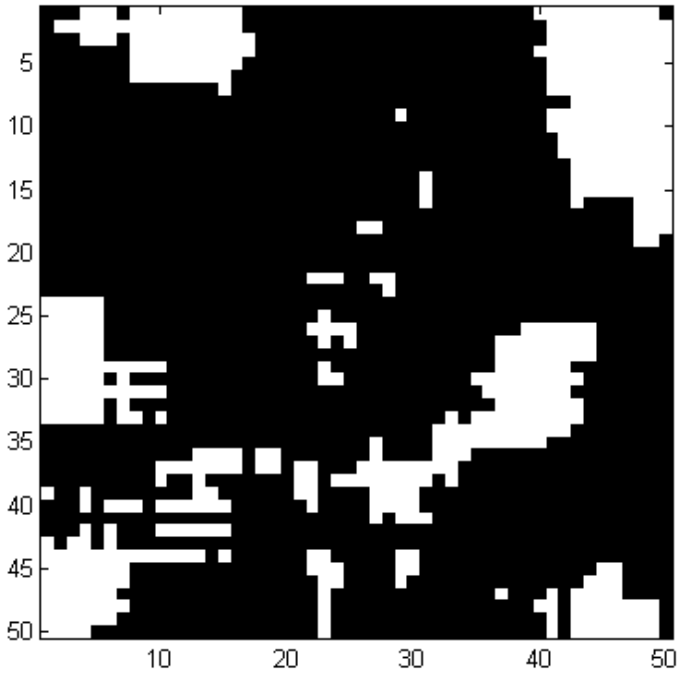

(a) Synthetic image on 2D domain

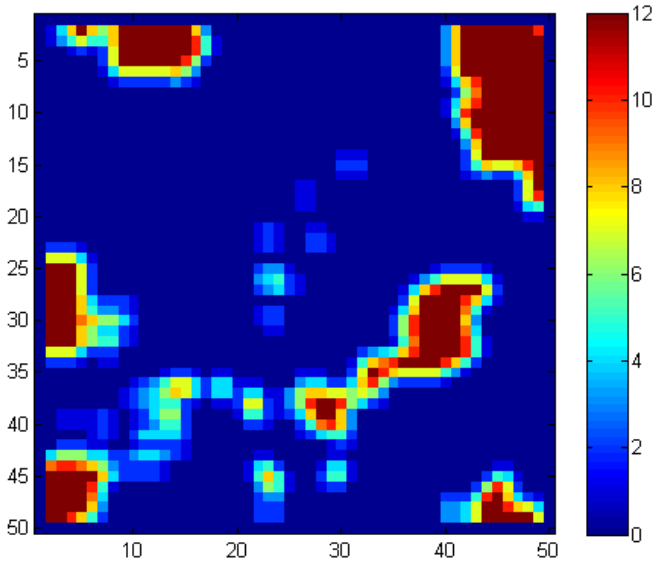

(b) Result of score system of synthetic 2D domain

Figure 54. Result of score system of 2D domain image

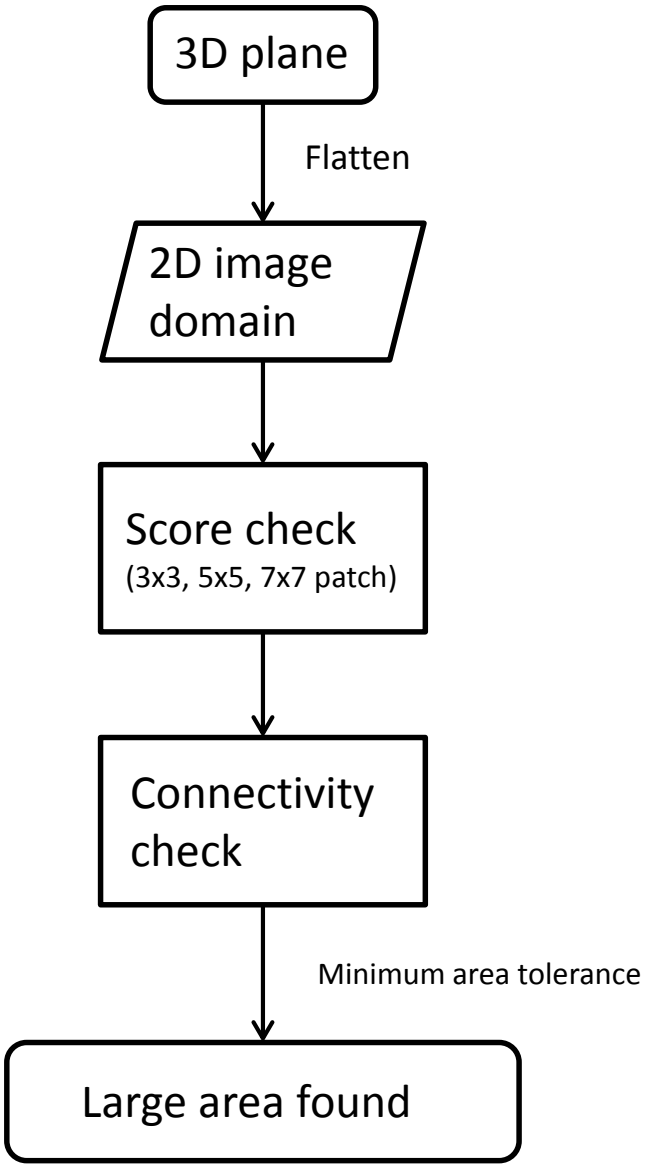

Figure 55. Process of finding linear feature

Once large areas have been found, 3D microstructure grain boundaries are constructed. When two or more linear features share a line of voxels, these are used to determine the adjacency of linear features. In the 3D microstructure voxel data set, linear features mean grain boundaries. By finding several adjacent linear features, which are grain boundaries, it is possible to form a grain in 3D microstructure voxel data set.

8.5 Examples and Results

8.5.1 4-plane example

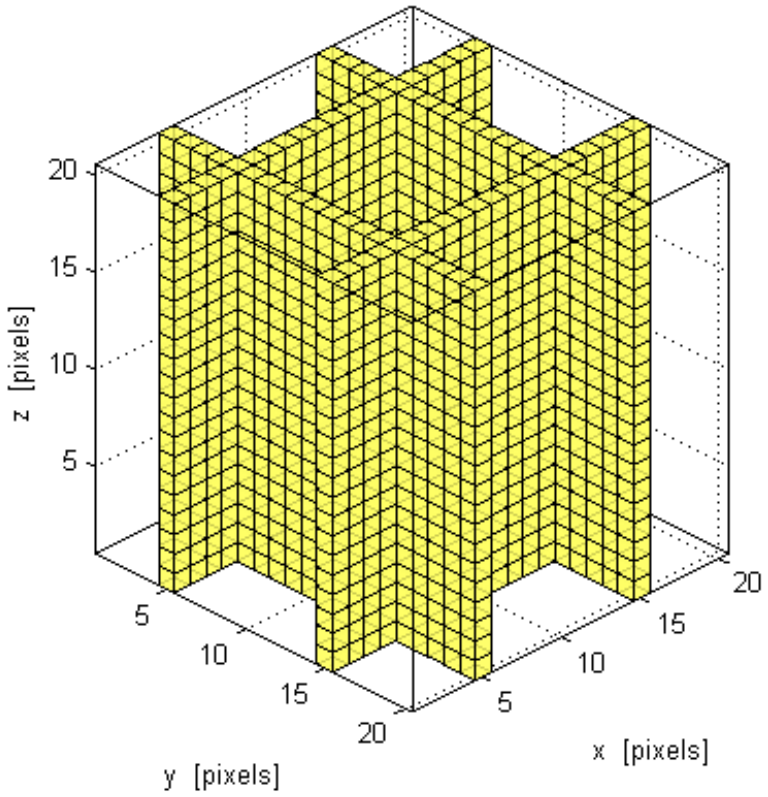

Figure 56. 4-Plane voxel data set

4 planes are spaced 10 units apart. The 3D surfacelet based method is applied to the simple voxel data set. The angles of the four planes from Figure 56 are identified in the Radon transform coefficient domain by finding the peak values. Table 10 shows the expected results and actual results of this example. The α, and β values correspond to the angles of 0 and 180 degrees, while the b values correspond to the translation of the Radon plane along the global Y-axis. Using the 3D surfacelet based method, it is possible to recognize planes in the voxel data set shown. Blue planes are the recognized planes using 3D surfacelet based method in Figure 57.

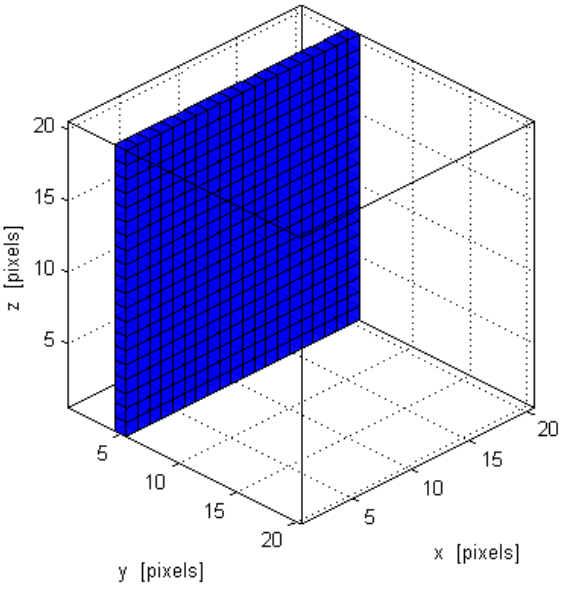

Plane 1

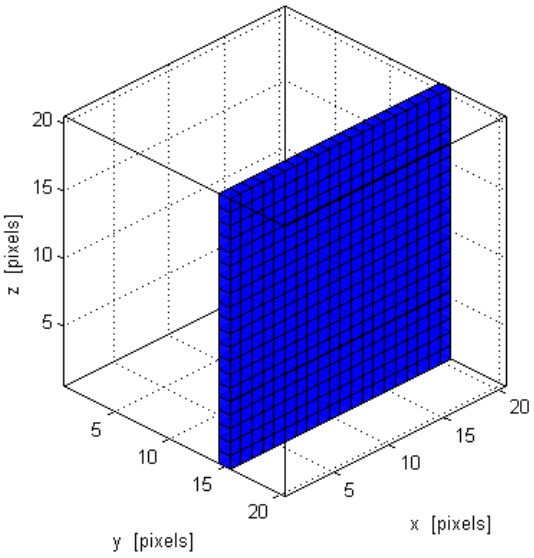

Plane 2

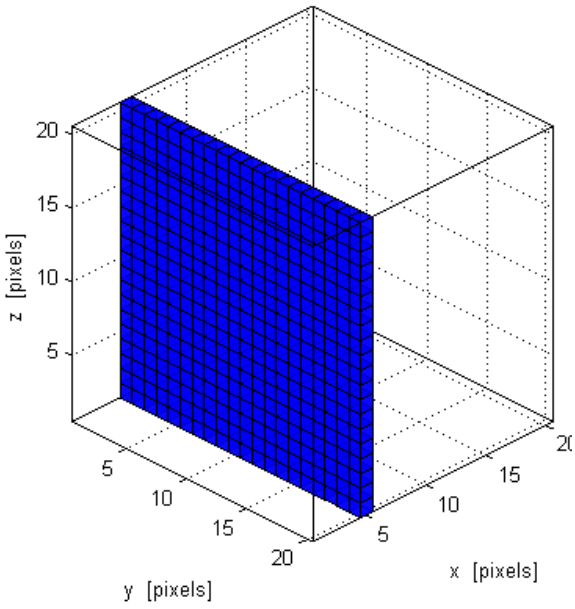

Plane 3

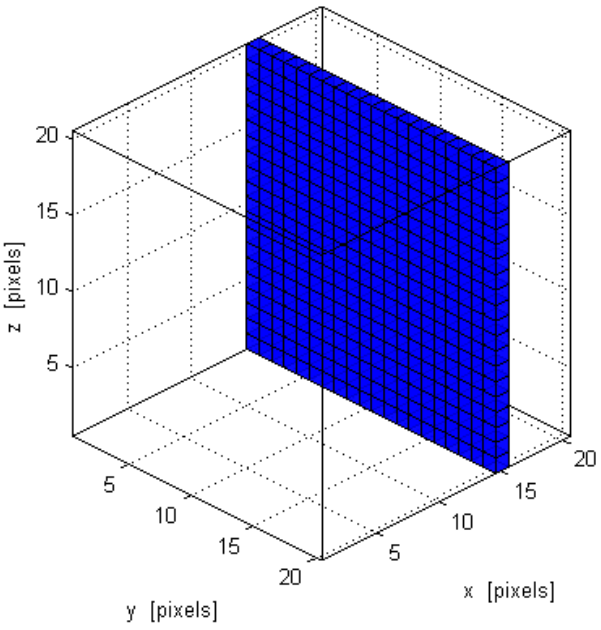

Plane 4

Figure 57. Recognized 4 planes

Table 10. Expected result and actual result of 4-plane example

	Expected result (α, β, b)	Actual result (α, β, b)
Plane 1	(0, 0, 5)	(0, 0, 5)
Plane 2	(0, 0, 15)	(0, 0, 15)
Plane 3	(90, 0, 5)	(90, 0, 5)
Plane 4	(90, 0, 15)	(90, 0, 15)

8.5.2 Cubic example

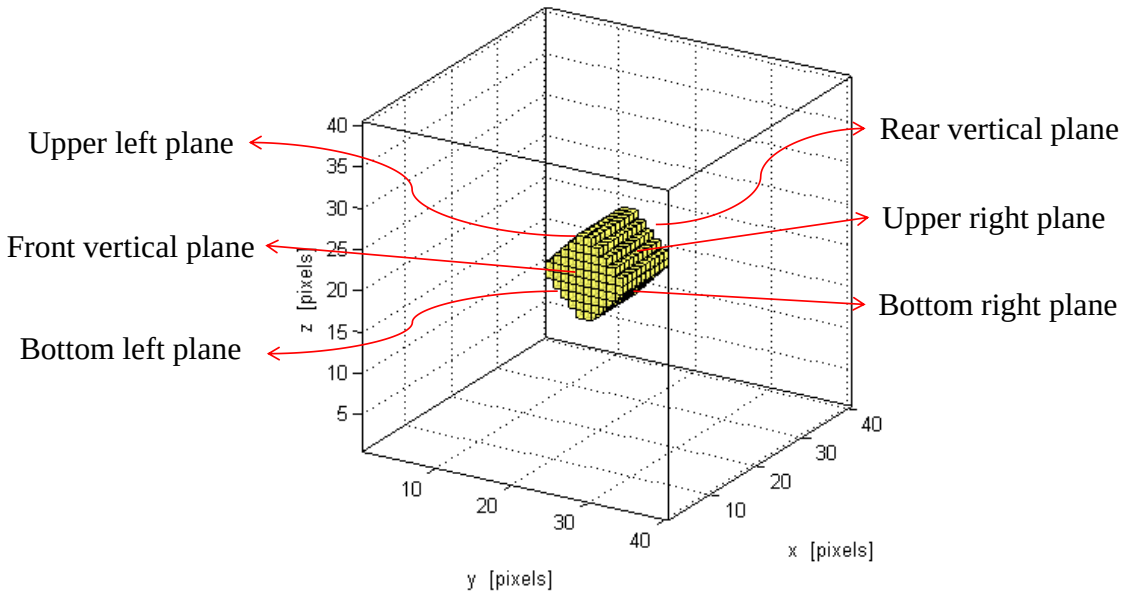

Figure 58. Cubic example

As a second example, a synthetic cubic-shaped voxel data set is used. All 6 planes are 5*5 square and the cube is rotated 45° about the global X-axis, as shown in Figure 58. Since this example is synthetic, each plane is created with specific α, β and b values. By using the 3D surfacelet based

method, 6 planes can be found. In order to find the size of the linear 3D geometric features, the plane overlaying method is used after applying the 3D Radon transform.

When peak values are provided by the 3D Radon transform, the plane overlaying method is applied to the microstructure voxel data set. By using this for entire peak values, 3D linear features can be recognized. Figure 60 shows the result obtained by processing this cubic example. A small blue region on the second column in Figure 60 represents recognized linear features while yellow planes represent a superimposed Radon plane in the microstructure voxel data set.

Table 11. Expected result and actual result of cubic example

	Expected value ($\alpha°$, $\beta°$, b)	Actual value ($\alpha°$, $\beta°$, b)	Differences
Plane 1 (upper left)	(0, 135, 23)	(175, 137, 23)	(5, 2, 0)
Plane 2 (upper right)	(0, 45, 23)	(6, 45, 23)	(6, 0, 0)
Plane 3 (bottom left)	(0, 45, 16)	(1, 45, 16)	(1, 0, 0)
Plane 4 (bottom right)	(0, 135, 16)	(179, 135, 16)	(1, 0, 0)
Plane 5 (front vertical)	(90, 0, 23)	(93, 3, 23)	(3, 3, 0)
Plane 6 (rear vertical)	(90, 0, 16)	(93, 176, 15)	(3, 4, 1)

Table 11 shows a comparison of expected value and obtained values from the 3D surfacelet based method. Planes 3 and 4 have only $1°$ difference in the value of angle α, while planes 1 and 2 show $5°$ and $6°$ difference, respectively. Also, only plane 1 has $2°$ difference on the value of angle β. Those oblique planes (plane 1, 2, 3, and 4) are obtained without differences in the distance value b. On the other hand, the vertical planes show similar differences. Both of the vertical planes are identified with $3°$ difference on angle α value and $3°$, $4°$ difference on angle β

value. Also, only plane 6 has a 1° difference on distance b value. Even though some planes have differences between expected value and actual value, all 6 planes are recognized.

Figure 59 shows one of the cross sections of the 3D Radon transform, including peak values in red circles. The upper red circle corresponds to plane 3(α =1, β= 45, b=16) while the lower red circle corresponds to plane 2 (α =6, β= 45, b=23).

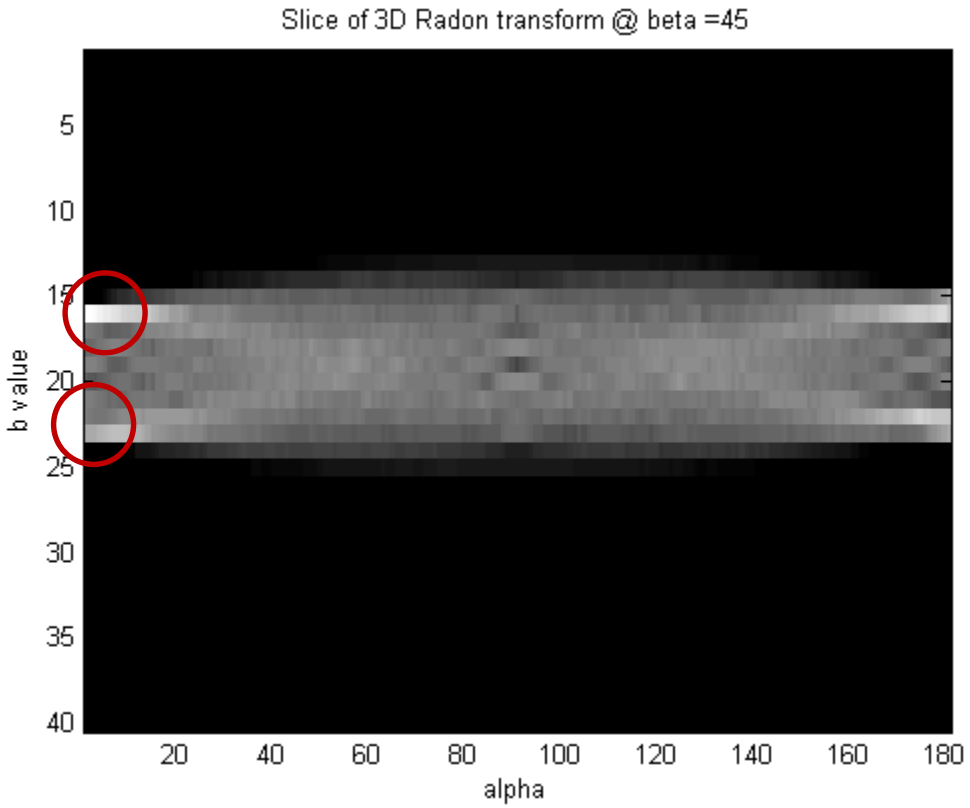

Figure 59. Cross section of 3D Radon transform with peak values (Red circles)

Found peak value with plane overlaying method

Recognized linear feature

Plane 1 (upper left)

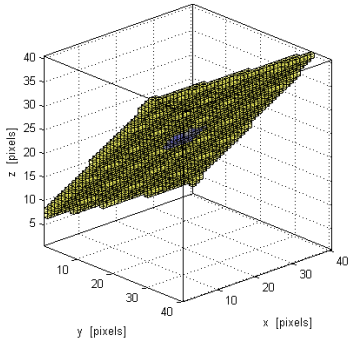

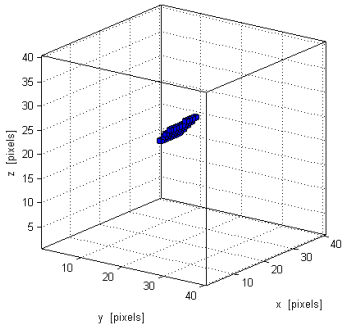

Plane 2 (upper right)

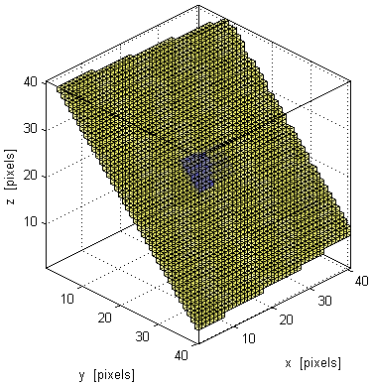

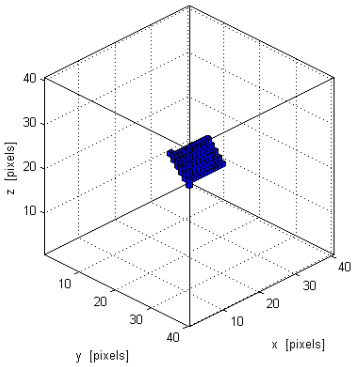

Plane 3 (bottom left)

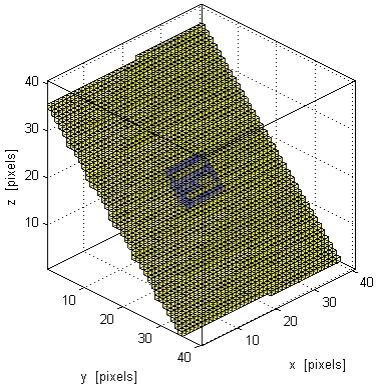

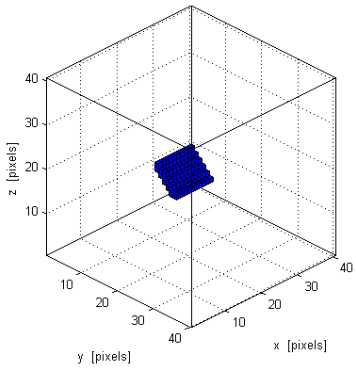

Plane 4 (bottom right)

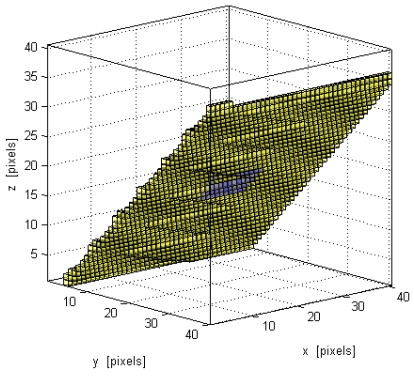

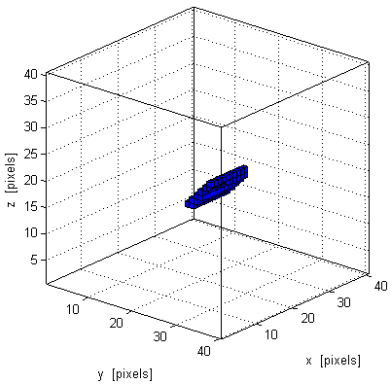

Plane 5 (front vertical)

Plane 6 (rear vertical)

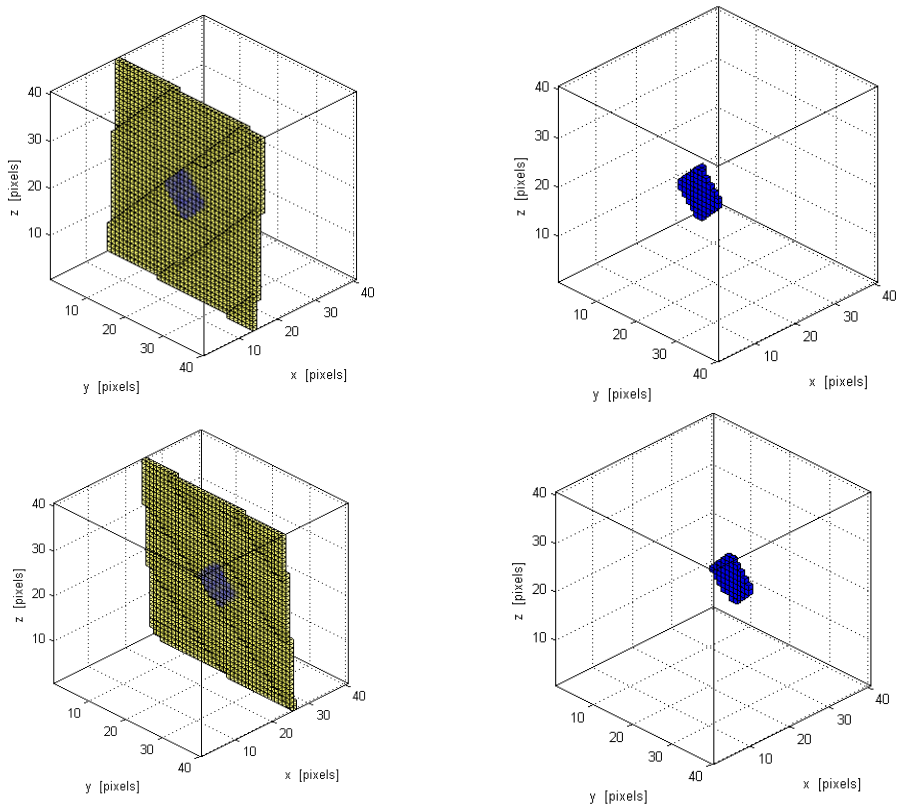

Figure 60. Recognized plane using surfacelet based method for synthetic example

To be specific, the plane overlaying method with score system shows explicitly how regions are recognized as linear features. Figure 61 and Figure 62 show in detail how the 3D plane is flattened onto the 2D image domain and can be recognized as a linear feature. Once large regions are found, common indices between 2 planes are searched to identify shared edges.

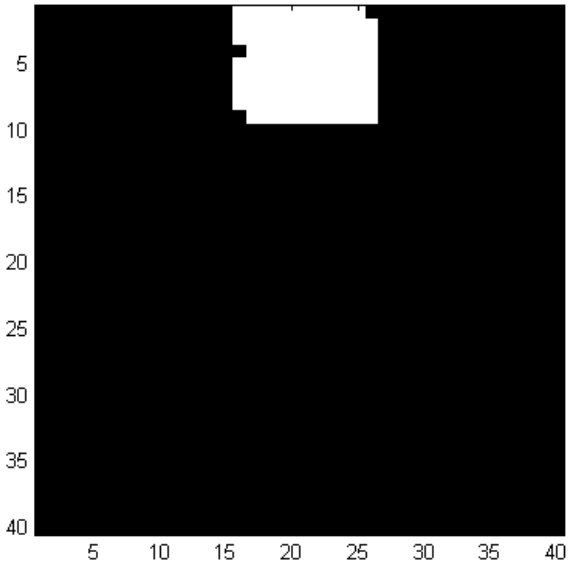

(a) Flatten plane onto 2D image domain (plane 3 in Figure 60)

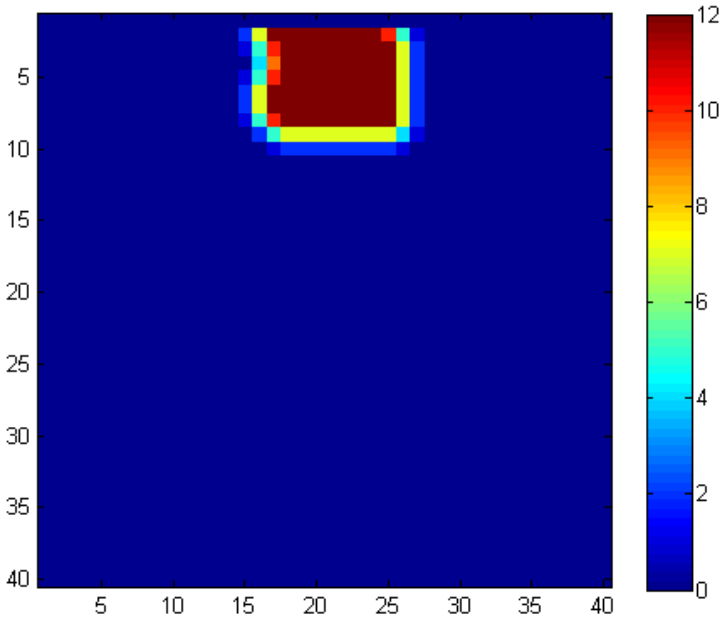

(b) Result of score system (plane 3 in Figure 60)

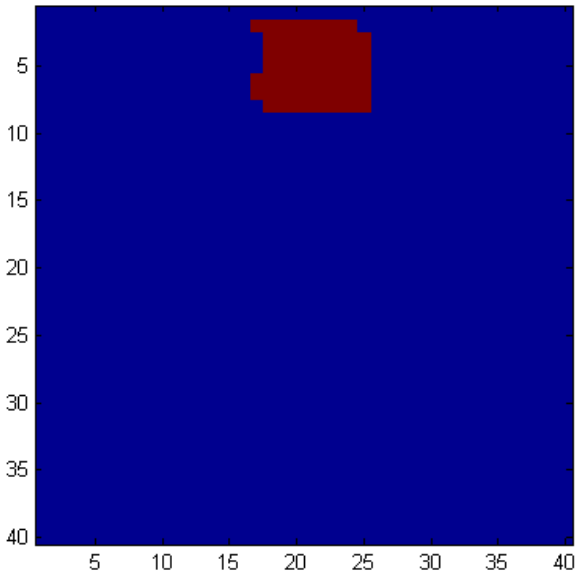

(c) Pixels that have higher score than threshold(=30) in score system result (plane 3 in Figure 60)

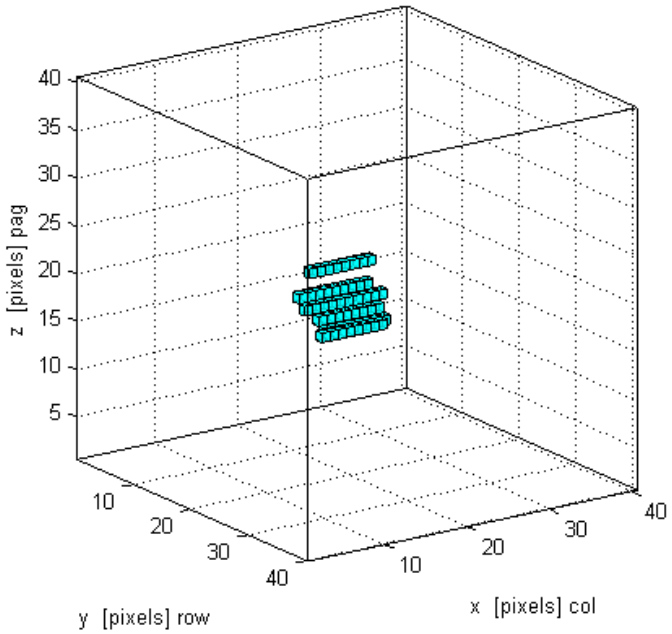

(d) Large regions that are converted into 3D space (pixels are mapped into 3D voxels)

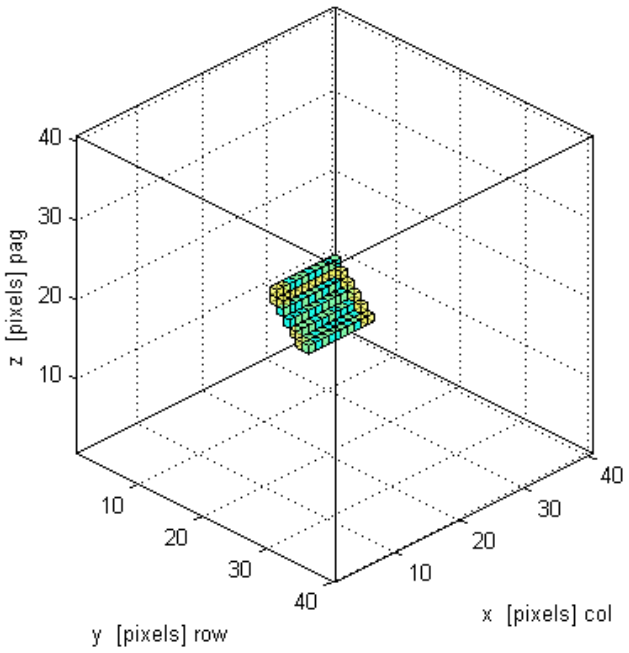

(e) Found large regions in the 3D space with the result of plane overlaying method

Figure 61. Steps of finding large regions in the result of plane overlaying method (plane 3 in Figure 60)

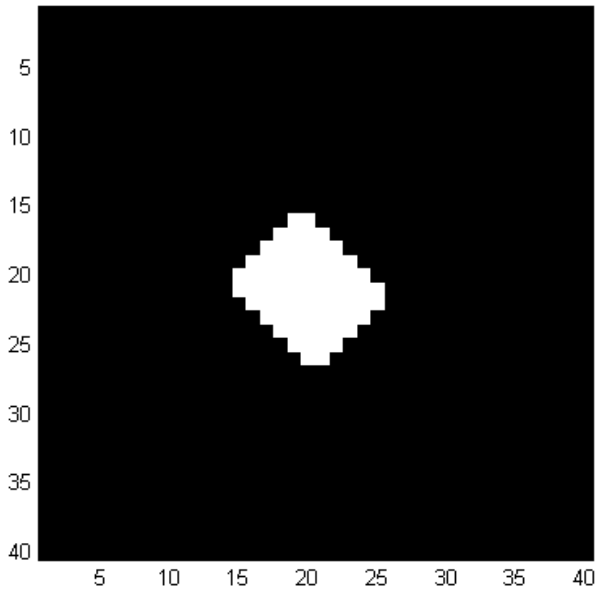

(a) Flatten plane onto 2D image domain (plane 5 in Figure 60)

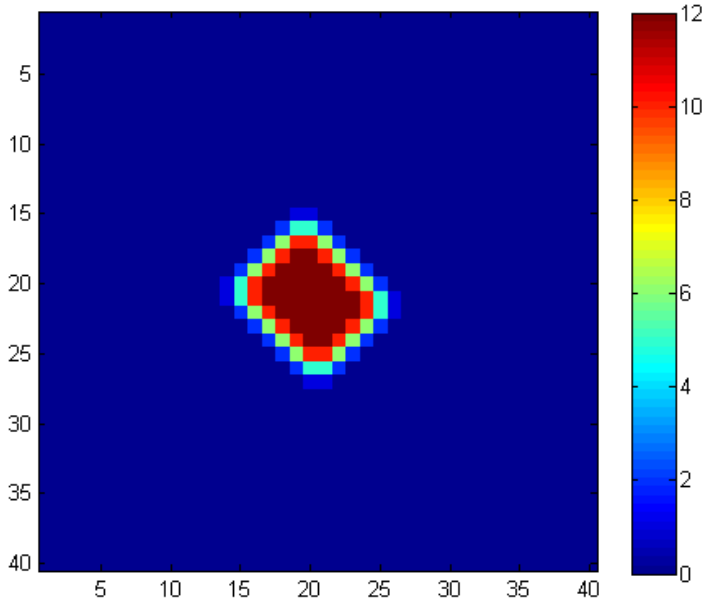

(b) Result of score system (plane 5 in Figure 60)

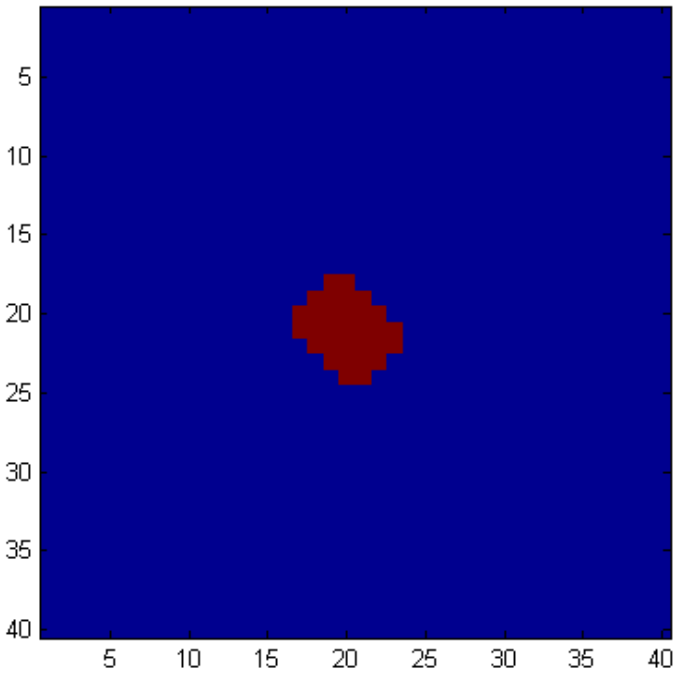

(c) Pixels that have higher score than threshold(=30) in score system result (plane 3 in Figure 60)

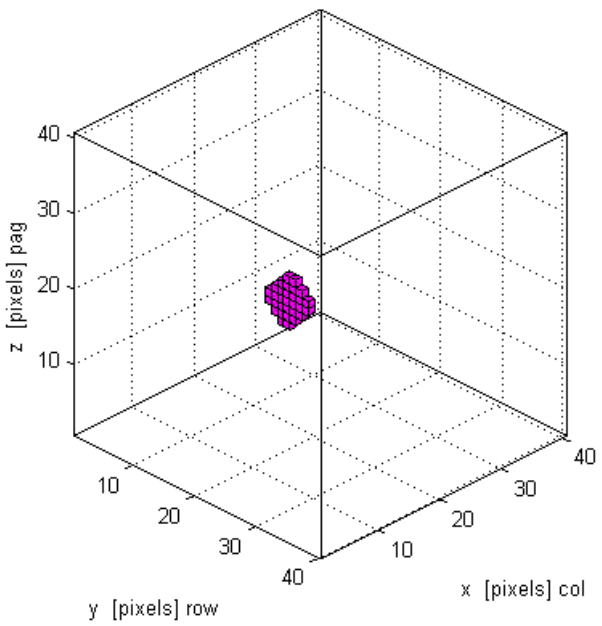

(d) Large regions that are converted into 3D space (pixels are mapped into 3D voxels)

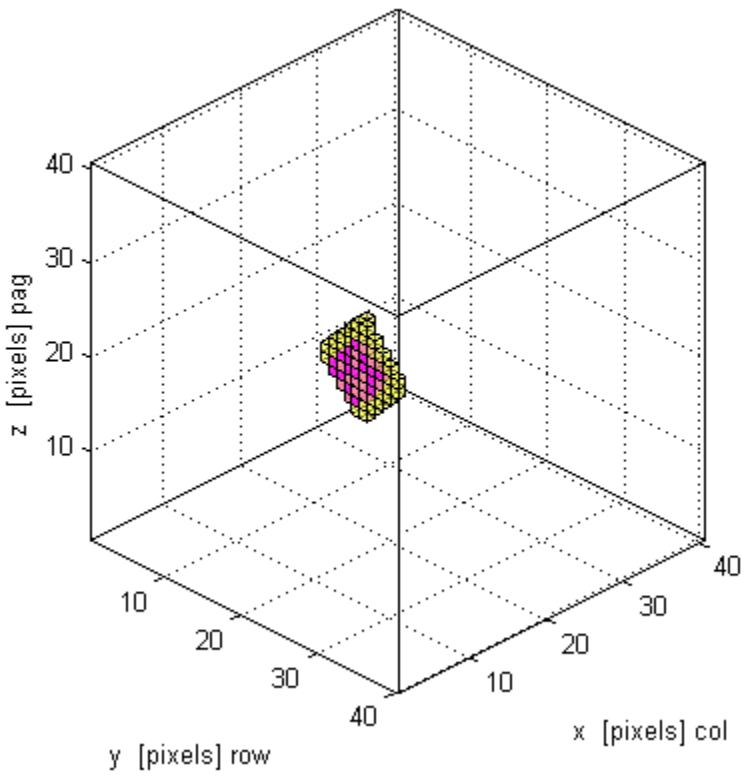

(e) Found large regions in the 3D space with the result of plane overlaying method

Figure 62. Steps of finding large regions in the result of plane overlaying method (plane 5 in Figure 60)

Normally a shared edge between 2 planes can be identified by finding shared voxels, while sometimes this can be identified by finding voxels next to each other at edge of the plane. As shown in Figure 63, there are three voxels that can be considered as a shared edge of plane 3 and plane 5. The shared voxel indices are (16, 17, 19), and (16, 18, 18). Also, 2 voxels are next to each other (16, 19, 17) and (17, 19, 17), and these can be considered as a shared edge. By finding the same indices or neighboring indices, we are enabled to find shared edges in the microstructure linear features in 3D space.

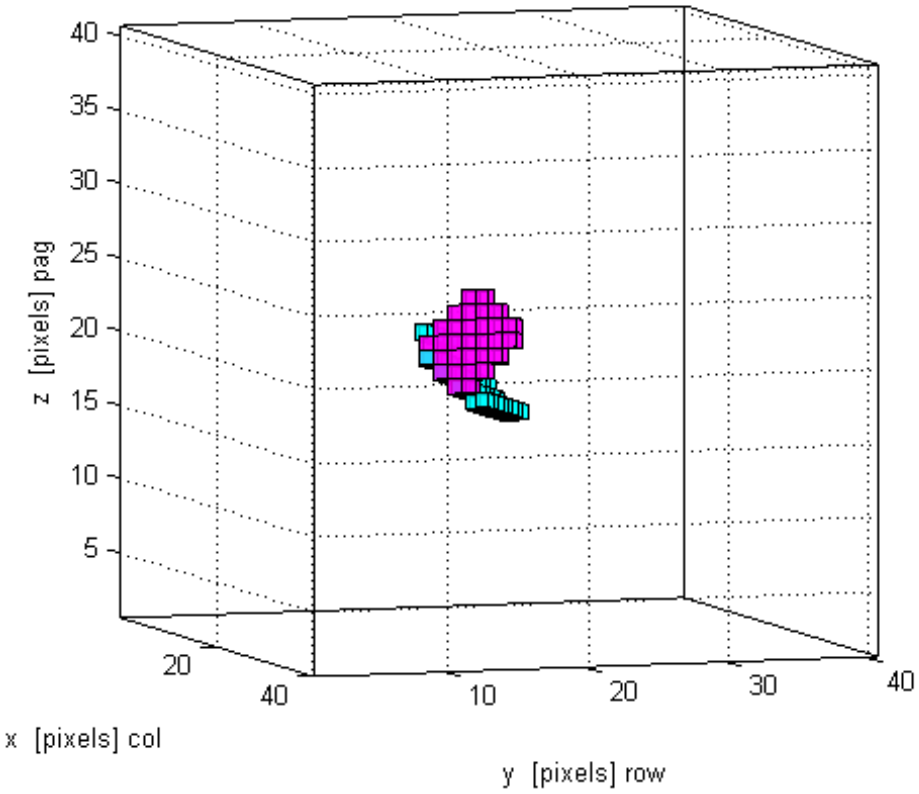

Figure 63. Recognized shared edge between 2 planes

The plane equations of 2 planes are

$$\text{Plane 3: } 18x = 288$$

$$\text{Plane 5: } -3x + 18y + 25z = 757.$$

Therefore mathematically, equation of the shared line between two planes is

$$18y + 25z = 805$$

By substituting indices of shared voxel (16, 17, 19), (16, 18, 18) and (16, 19, 17), the errors are 3.1%, 2.2%, and 1.3%. This indicates that 3D surfacelet based method allows obtaining explicit 3D microstructure model.

8.5.3 *IN100 example*

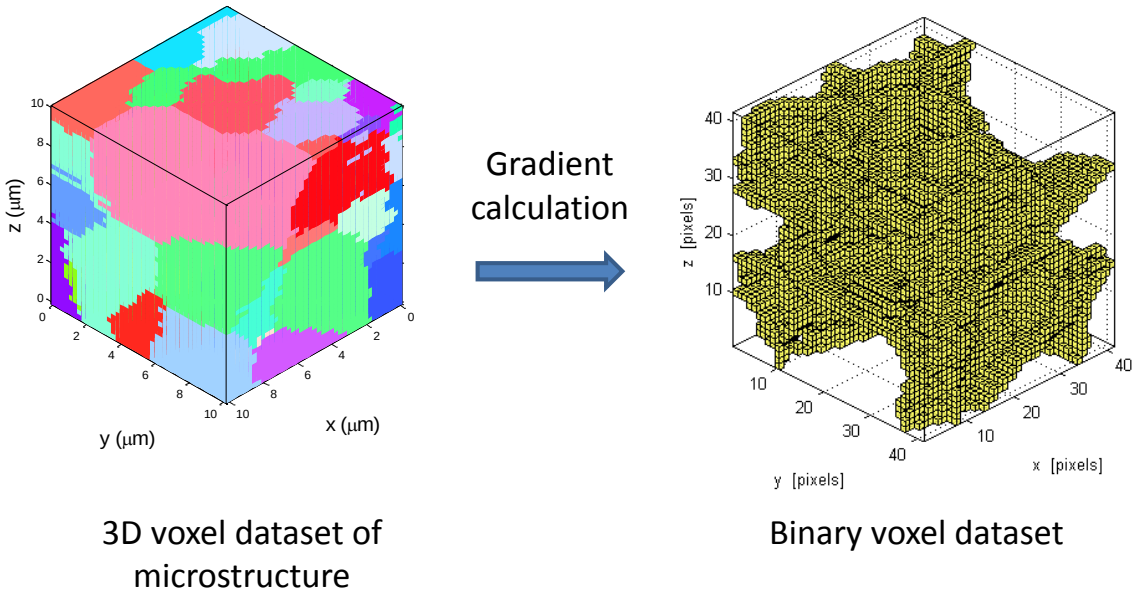

Figure 64. IN100 microstructure voxel data set

3D linear geometric features will be recognized in a dataset obtained from a 10x10x10 μm IN100 nickel-base super-alloy sample, shown in Figure 64 using 3D surfacelet based method [22]. The size of the entire voxel data set is 41x41x41 voxels, and each grain is represented by different colors. Since the voxel data set has abundant information, it is converted to the binary data set using the gradient operator [25]. Since one grain contains the same intensity value, a gradient of inside of a grain is zero. On the other hand, if a gradient is calculated between two different grains, a non-zero value is obtained. By doing that, grain boundaries are highlighted. This process yields a binary voxel data set and helps to reduce computational cost.

Linear grain boundaries can be identified as large regions as shown in Figure 65. Blue regions in the red circles are recognized grain boundaries, while yellow background planes represent superimposed planes during the process of plane overlaying method.

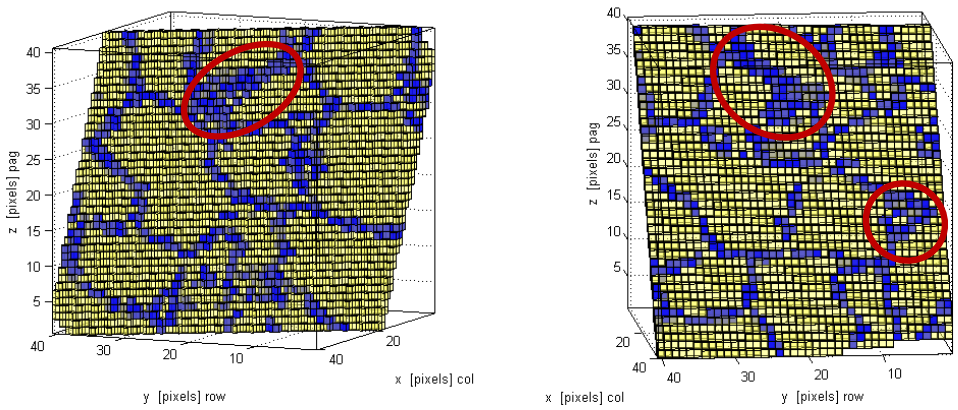

(a) (b)

Figure 65. 3D linear geometric feature (a: Plane 2 in Table 12, b: Plane 1 in Table 12)

In the complicated voxel data set, linear features can be found and can be interpreted as grain boundaries. As an example, one grain in the middle of the voxel data set is found. For one grain, several grain boundaries are recognized, corresponding to several peak values. Table 12 shows α, β and b of several peak values. Different colors (magenta, cyan, blue, green and red) represent different peak values, which have different α, β and b.

Table 12. Peak values correspond to grain boundaries (Fig.62 (a) corresponds to Plane 2, Fig. 62(b) corresponds to Plane 1)

	Alpha	Beta	Y distance
Plane1 (magenta)	56	138	24
Plane2 (cyan)	59	157	19
Plane3 (blue)	0	135	20
Plane4 (green)	173	142	21
Plane5 (red)	95	142	23

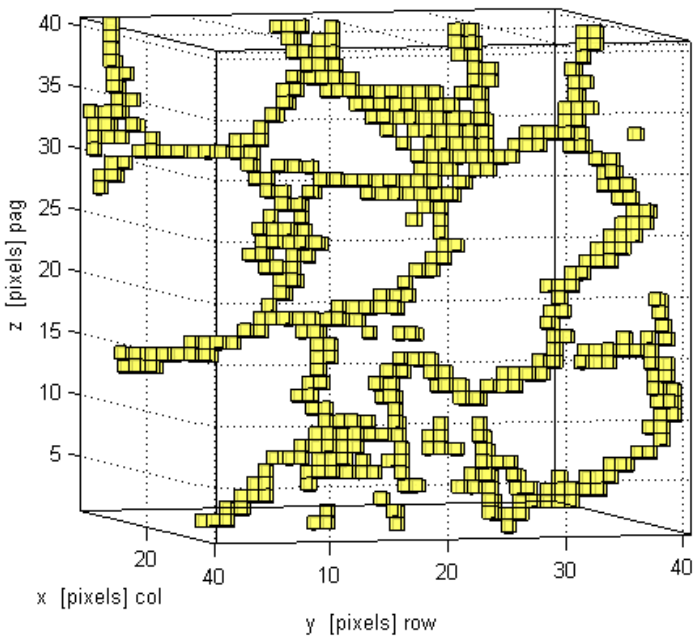

(a) 3D linear geometric feature found by plane overlaying method (plane 1 in Table 12)

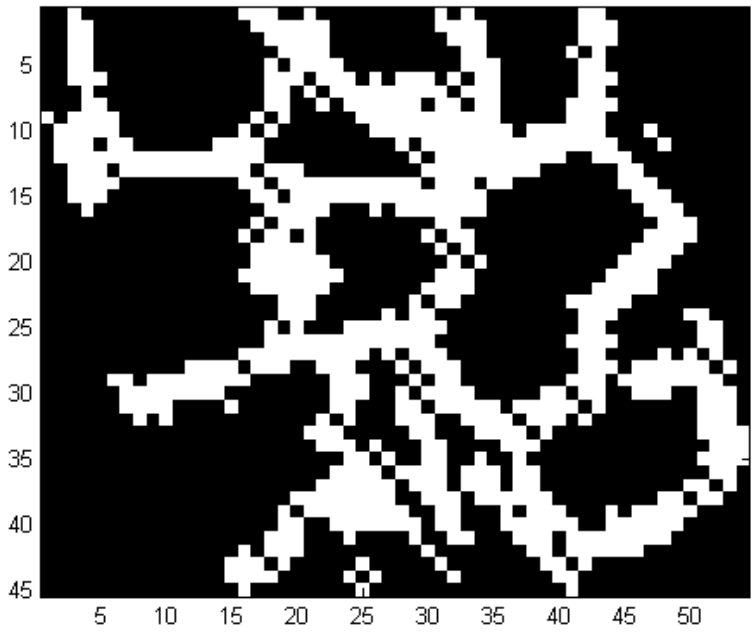

(b) Flatten plane onto 2D image domain (plane 1 in Table 12)

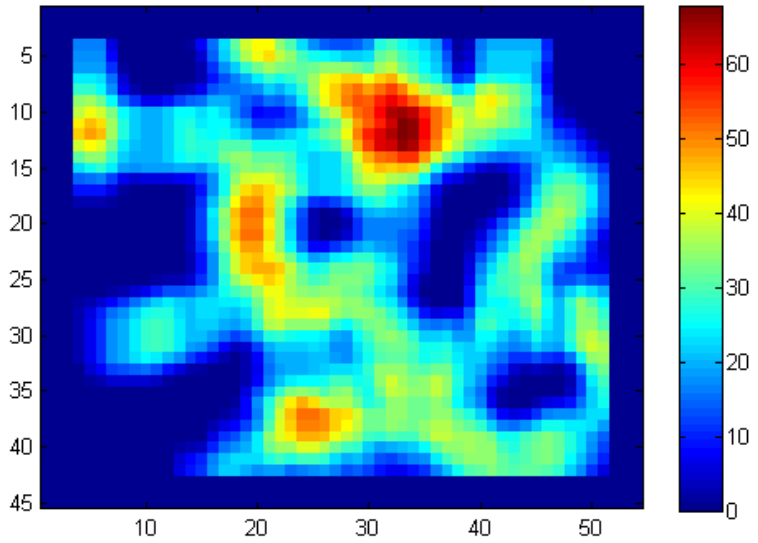

(c) Result of score system (plane 1 in Table 12)

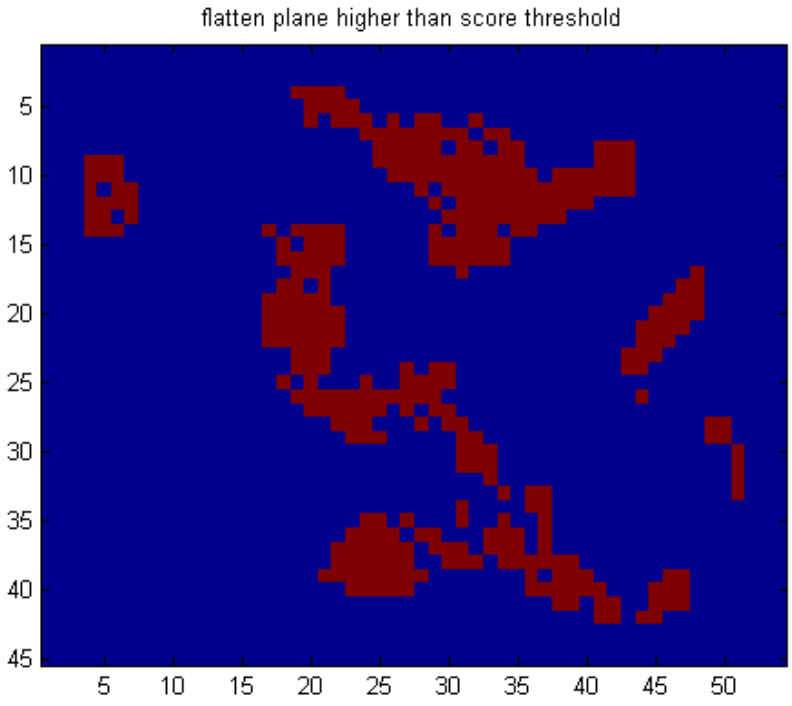

(d) Pixels that have higher score than threshold(=30) in score system result (plane 1 in Table

12)

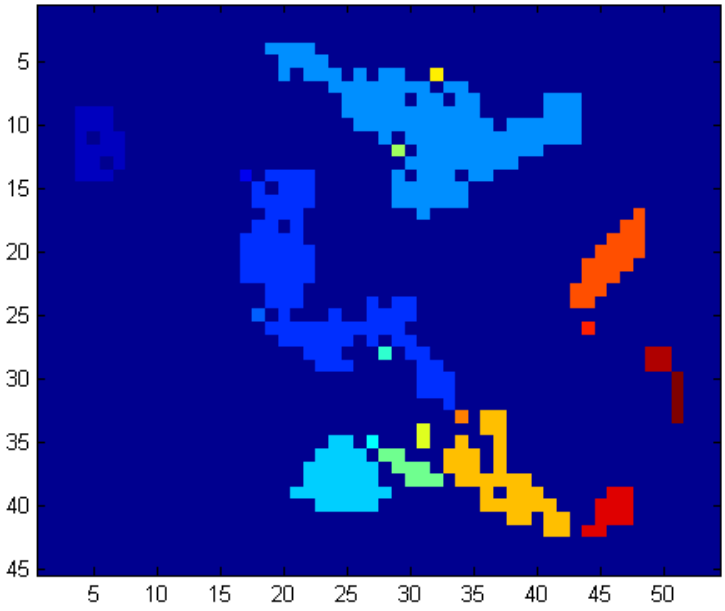

(e) Found large regions by checking connectivity (different color represents different group)

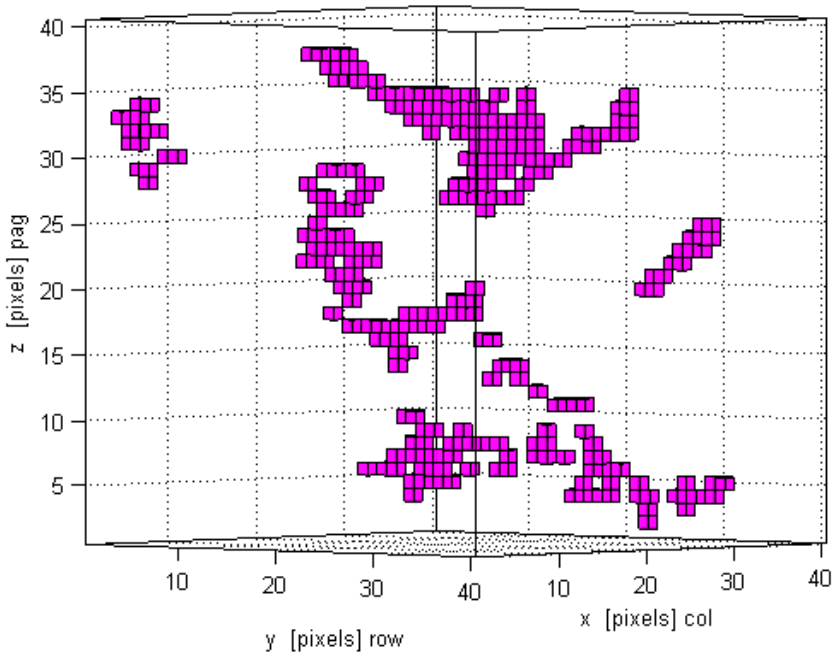

(f) Large regions that are converted into 3D space (pixels are mapped into 3D voxels)

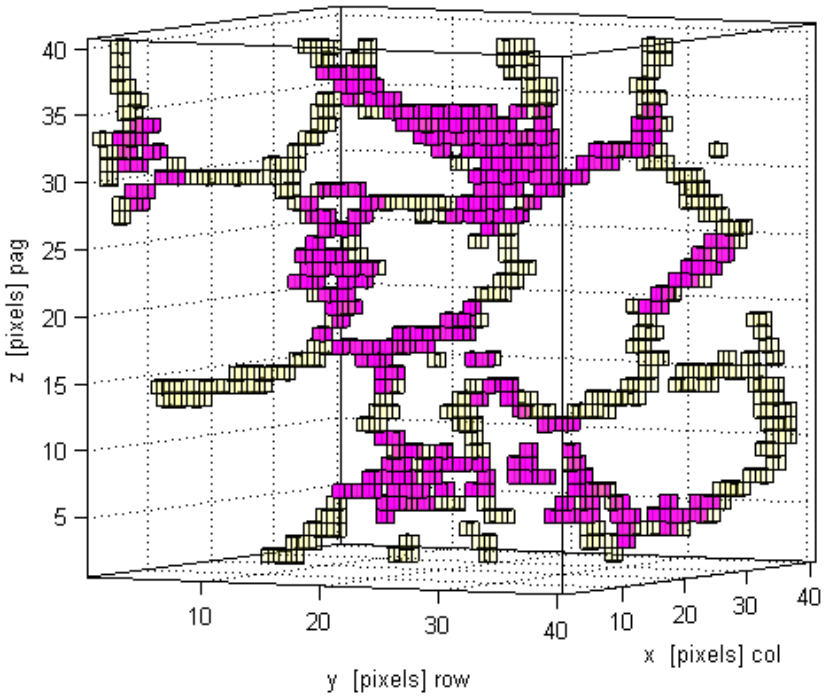

(g) Found large regions in 3D space with the result of plane overlaying method (plane 1 in Table 12)

Figure 66. Steps of finding large regions in the result of plane overlaying method

Figure 66 shows how the large region can be selected in the results obtained with the plane overlaying method. Specifically plane 1 in Table 12 is used as an example. In order to separate a large region from the result of the plane overlaying method, the 3D plane has been flattened, due to the process in Figure 55. The result of the plane overlaying method in 3D space (Figure 66 (a)) is flattened onto the 2D image domain, shown in Figure 66 (b). In the 2D image domain, the score system is applied (Figure 66 (c)). A pixel score is assigned depending on its neighborhood pixels. Then, pixels that have higher scores than the threshold value (in this example, the threshold value is 30) are selected, shown in Figure 66 (d). If selected pixels are connected to its neighboring pixel, large regions can be defined. Determined large regions are represented as different colors in Figure 66 (e). After large regions are determined, the flattened

plane in the 2D image domain is returned to 3D space, shown in Figure 66 (f). The Magenta color voxels in Figure 66 (f) represent found large regions that are in 3D space. Found large regions in 3D space are interpreted as 3D linear features in this research. However, if a large region has less than 5 pixels, it is not considered as a 3D linear feature. Figure 66 (g) shows found large regions (magenta color) mapped onto the result of the plane overlaying method.

Figure 67 shows each flattened plane that corresponds to a peak value shown in Table 12. Those planes form a grain in the voxel data set. 2D image domains (flattened plane), which include several large regions, are shown in Figure 67. Each different color in the 2D domain represents a different large group, which is a different grain boundary in 3D space. These large regions in 2D flattened planes in Figure 67 are returned to 3D space, forming a grain.

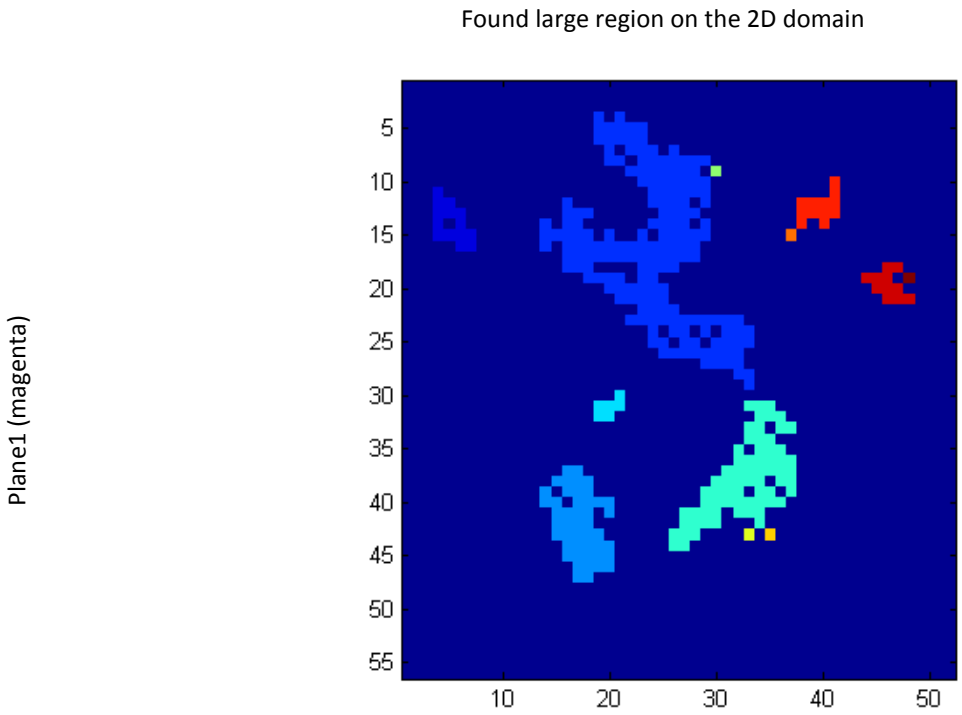

Plane2 (cyan)

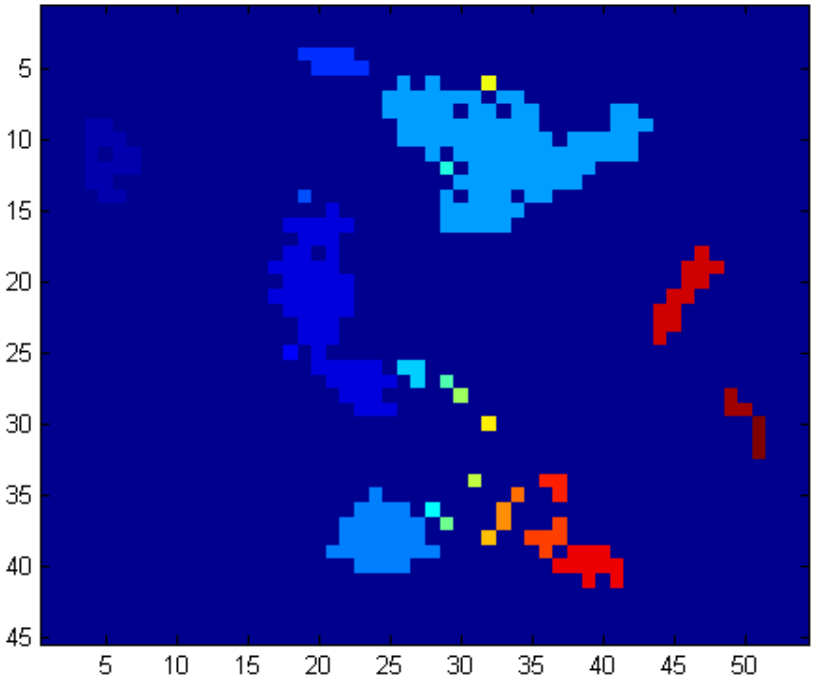

Plane3 (blue)

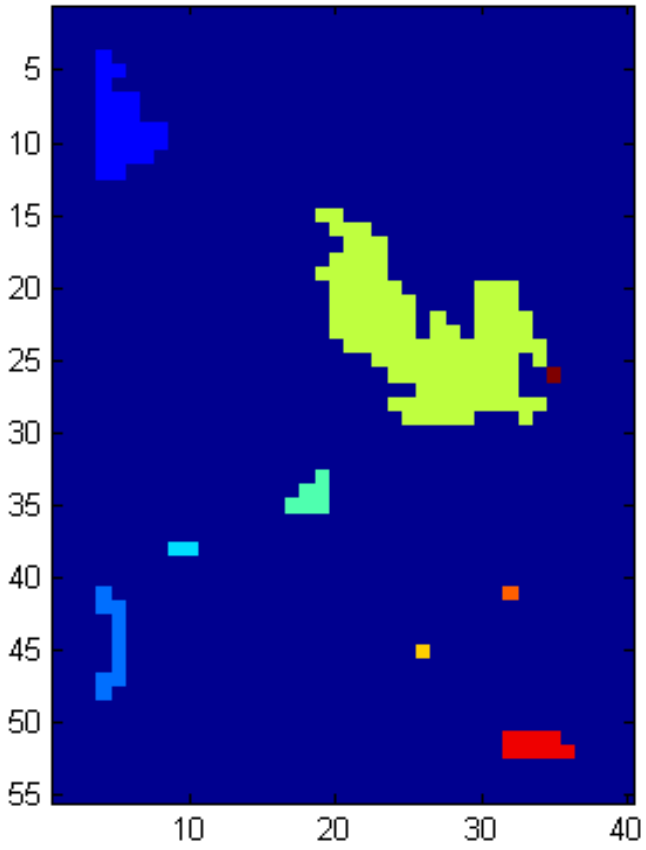

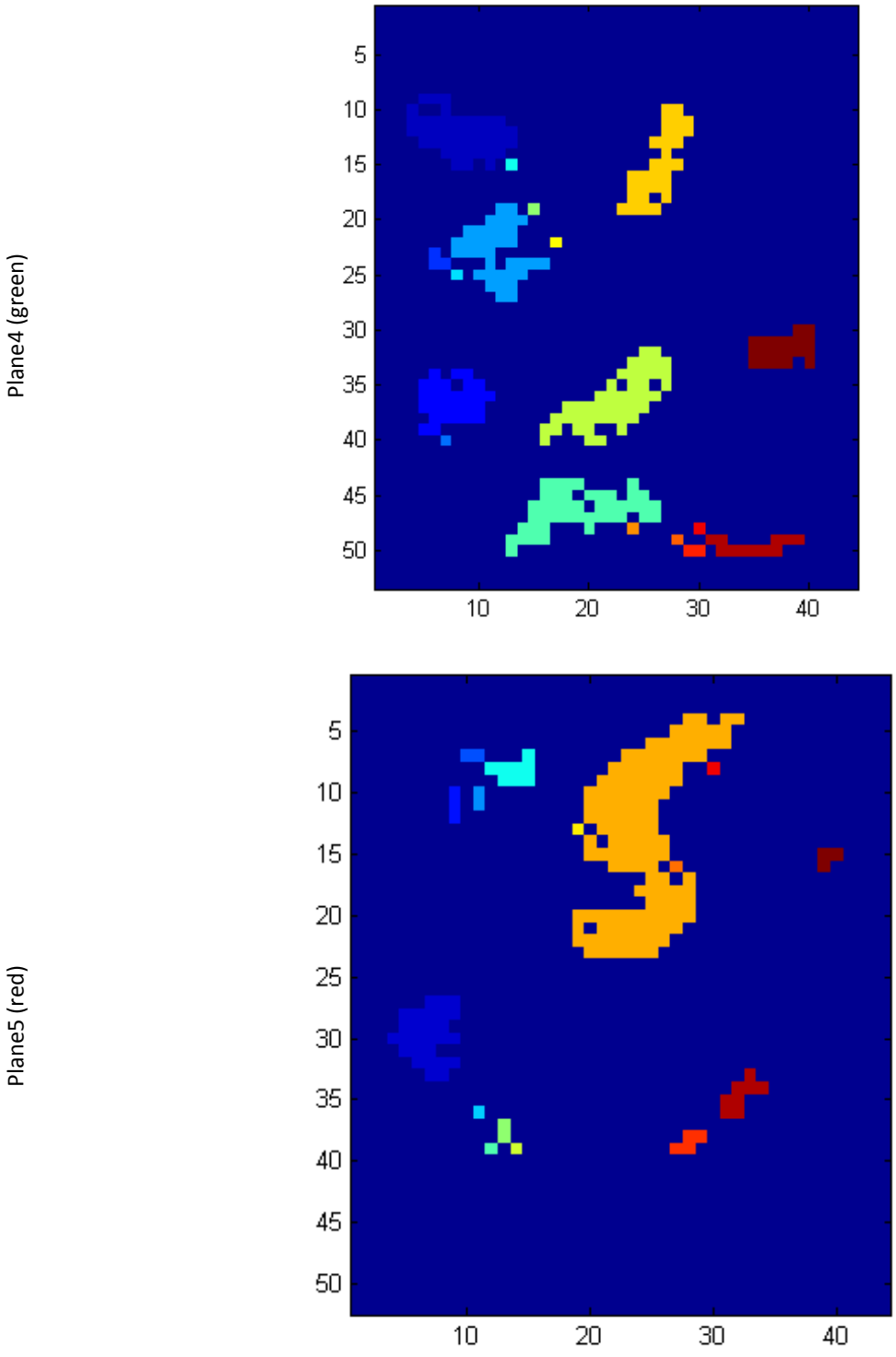

Figure 67. Found peak value corresponded to plane in voxel data set

When several large regions are identified, they form a grain by finding shared sets of voxels between large areas. Figure 68 shows 2 cases of shared voxels between adjacent large regions.

In the top row, plane 2 and plane 3 has large areas that shares a line of voxels; these are shown in the yellow circle in Figure 68. Similar to this, in the bottom row, planes 2 and 5 also have shared voxels, shown in the yellow circle. By finding sets of shared voxels between adjacent large areas, a grain can be formed. Figure 69 shows partially recognized grain boundaries. Each different color indicates different grain boundary and that forms a grain. Even though the result represents partially found grain boundaries for one grain, it is possible to recognize linear feature in the 3D voxel data set using the proposed method.

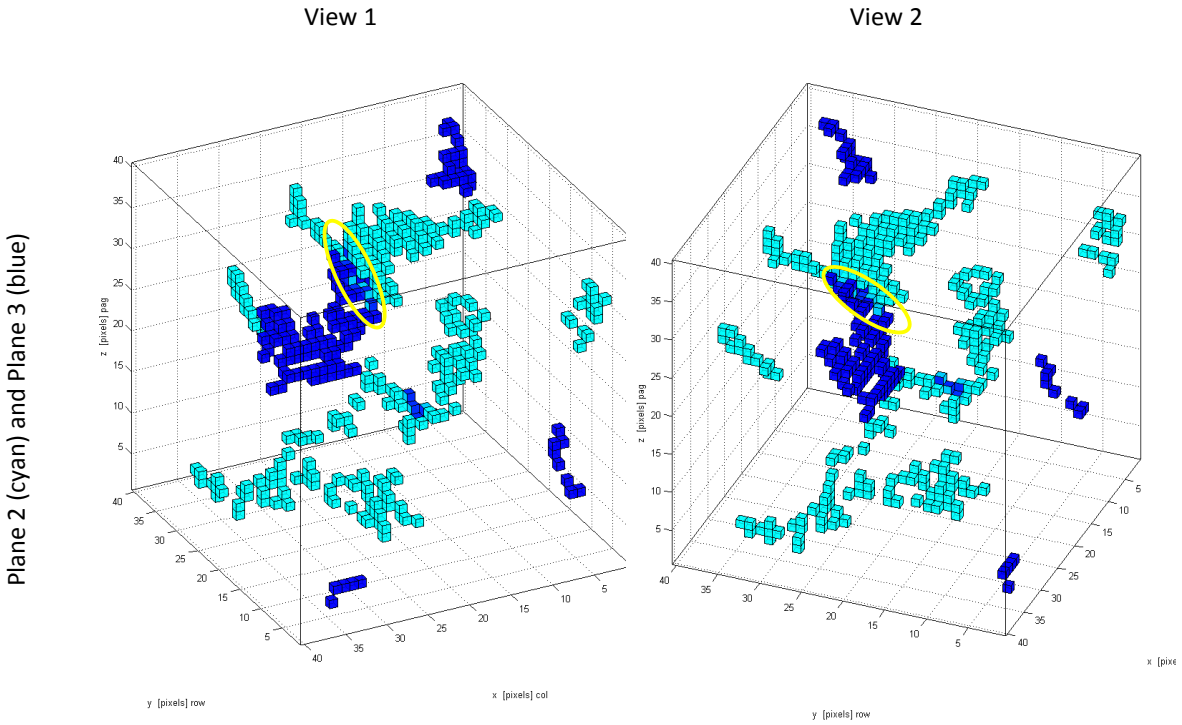

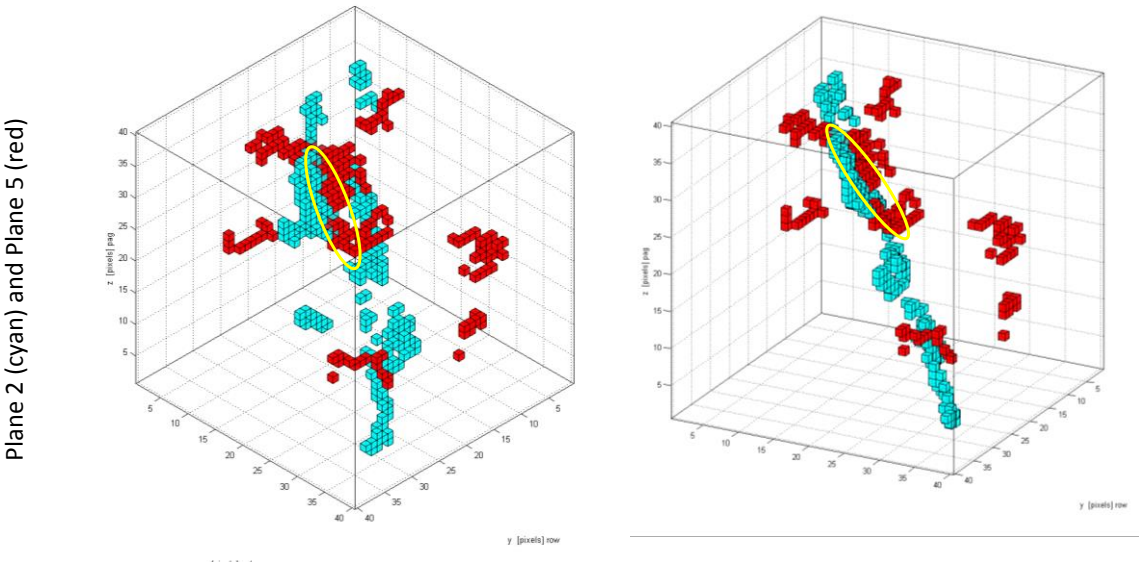

Figure 68. Shared voxel within 2 large areas

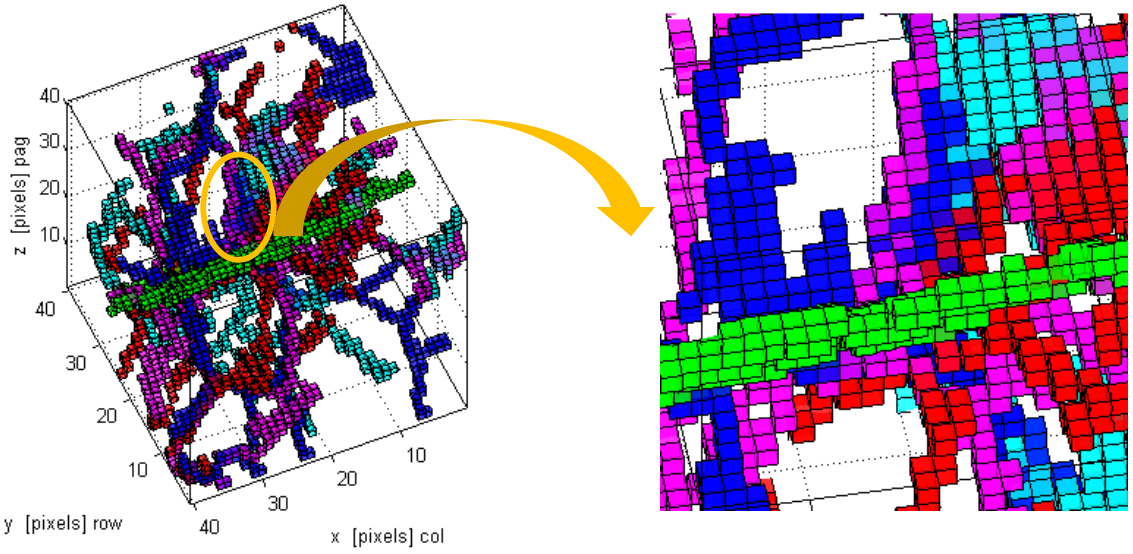

Figure 69. Partially recognized grain boundaries

8.6 Summary

This chapter shows the recognition of 3D linear features in the voxel data set. In order to do that, a 3D Surfacelet based method is used. The 3D Surfacelet based method includes a 3D Radon

transform followed by a plane overlaying method. Each recognized 3D linear feature is used to construct a 3D microstructure. This chapter contributes to answer research question 1 followed by hypothesis 1a.

Research question 1: "Can an entire geometric feature in the microstructure image be extracted as an explicit geometric model using the surfacelet method?"

Hypothesis 1a: "A surfacelet based method that includes the Radon transform can be used to detect linear features using infinite lines, for 2D images, or bounded planes, for 3D datasets, and this can provide an ***explicit geometric model*** *of these microstructure features."*

The hypothesis of this research question is validated in this chapter by showing the process by which the voxel data was constructed microstructure using the proposed method, 3D Surfacelet-based method. 3 examples are demonstrated to show how to select a plane that includes a 3D linear feature in it. Then by testing IN100 voxel data set, the process of constructing the microstructure by using the plane overlaying method is shown. Therefore, the 3D Surfacelet-based method can be successfully used to recognize 3D linear features with **explicit form,** which is the same representation system that current CAD systems use.

This chapter shows how 3D geometric features are recognized and identified by the 3D surfacelet based method, contributing step A in Figure 2. This approach provides explicit voxel indices for each 3D grain so that they can be easily converted microstructure model. By completing this step, a heterogeneous CAD system can be achieved.

CHAPTER 9
RESEARCH QUESTION 1B: NON-LINEAR FEATURE EXTRACTION

In the microstructure image, non-linear geometric features are more common than linear features. A method for recognizing a non-linear feature will be explained in this chapter. Among variety kinds of non-linear features, this research will focus on a circular arc, which is a simple case of a non-linear feature. A Cylinderlet based method will be used to identify circular arcs. A circle overlaying method will be applied on the result of the Cylinderlet in order to specify the length of an arc and start/end points of the arc.

9.1 Feature Recognition method for 2D non-linear feature: 2D Cylinderlet based method

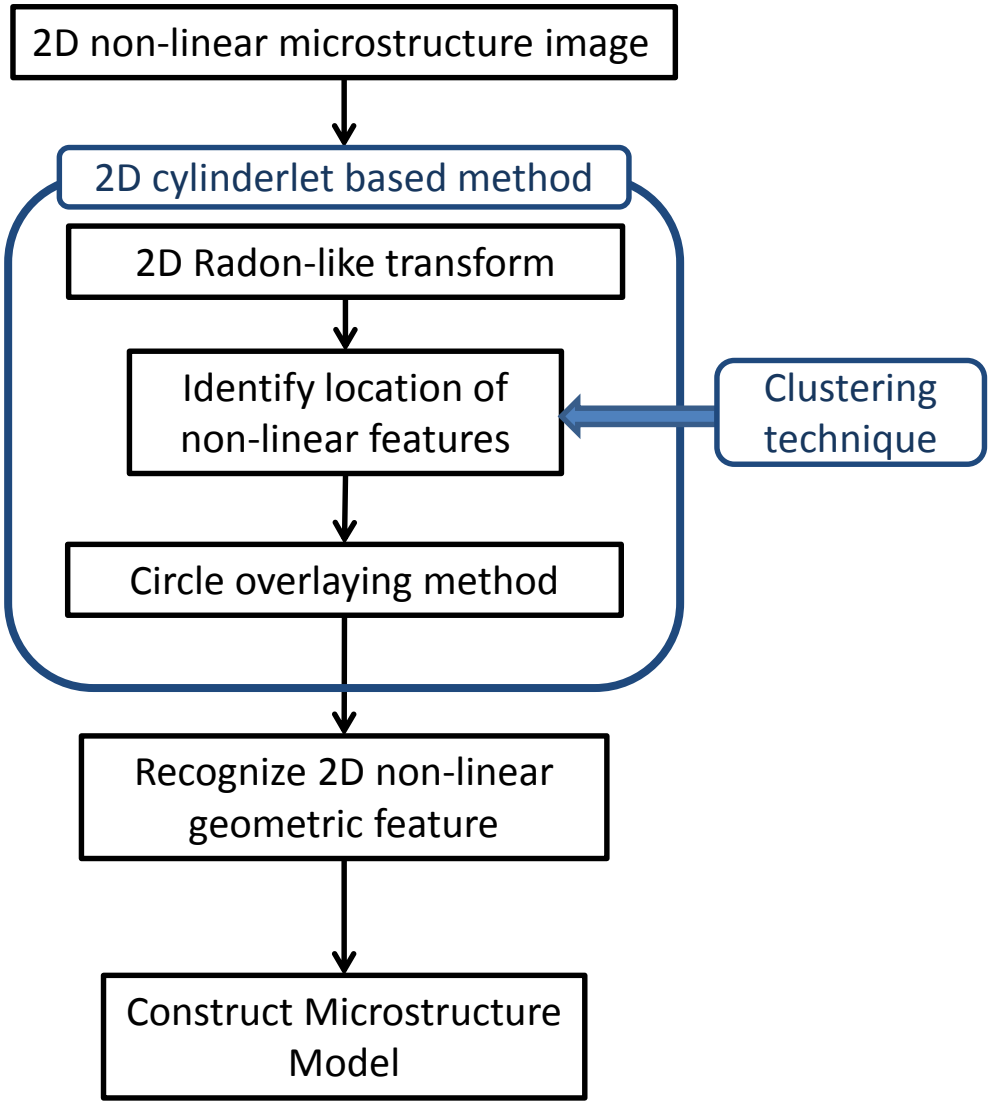

Figure 70. Feature recognition method for 2D non-linear geometric features

Before using the Cylinderlet based method, the gradient of an image is calculated in order to highlight grain boundaries in the image. This step allows us to have the simplified image, emphasizing geometric features and reducing noises in the image. The gradient of a scalar

function is denoted ∇f where ∇ denotes the vector differential operator del. In the two dimensional Cartesian coordinate system, the gradient is

$$\nabla \mathrm{f} = \frac{\partial f}{\partial x} i + \frac{\partial f}{\partial y} j$$

where i, j are the standard unit vectors. Since each grain has the same intensity value for the image, the gradient of the inside of the grain is zero. When the gradient is calculated between two grains, it gives non-zero value. By calculating this gradient of an image, an input image is represented as binary image, which highlights circular geometric features.

A Cylinderlet based method is similar to the surfacelet based method. It includes the circular Radon-like transform followed by the circle overlaying method. The circular Radon-like transform in the Cylinderlet based method is the integral transform consisting of the integral of a function over circles. It searches circular arcs, circles with different diameters and converts to points in the Radon coefficient matrix. If a circular arc in the image domain is matched with a searching pattern (a circle), the circular Radon-like transform counts the matched pixels and converts it into an intensity value in the Radon coefficient domain. If the matched pixels between a circular arc and a searching pattern, it produces a high intensity value, which is bright point in the Radon coefficient domain. A diameter and center coordinate are determined by the circular Radon-like transform. After the circular Radon-like transform is performed, the circle overlaying method is applied to the result of the Radon-like transform in order to find the location of the circular arc. Using a diameter and center coordinate, the circle overlaying method identifies the start/end points of the circular arc. Recognized circular arcs are used to construct an explicit microstructure model in the 2D image domain. Figure 70 shows the process of recognizing a 2D non-linear feature using the proposed method.

9.2 2D circular Radon-like transform

In this section, the circular Radon-like transform in the 2D domain will be explained. The circular Radon-like transform is similar to the 2D Radon transform except it uses the circular pattern instead of the straight line to find the geometric feature in the image domain. Similarly, a surfacelet that represents cylindrical singularities can be defined as

$$y_{\alpha,b,,r_1}(r) = a^{-1/2} y(a^{-1} r[(cos\alpha \cdot x + sin\alpha \cdot y - b)^2 + (-sin\alpha \cdot x + cos\alpha \cdot y)^2]) \quad (20)$$

where an angular element $\alpha \in [0,\pi]$, b explains a translation factor while parameter *r* describes the radius of the circular shape, shown in Figure 71 [26]. Parameters α, b and r are the main components of the circular Radon-like transform. In order to extract the circular arcs in the image domain, different radii of circle patterns are used. A circle pattern of a different radius moves guided by the angular element α and the translation factor b, finding a circular feature in the 2D image domain.

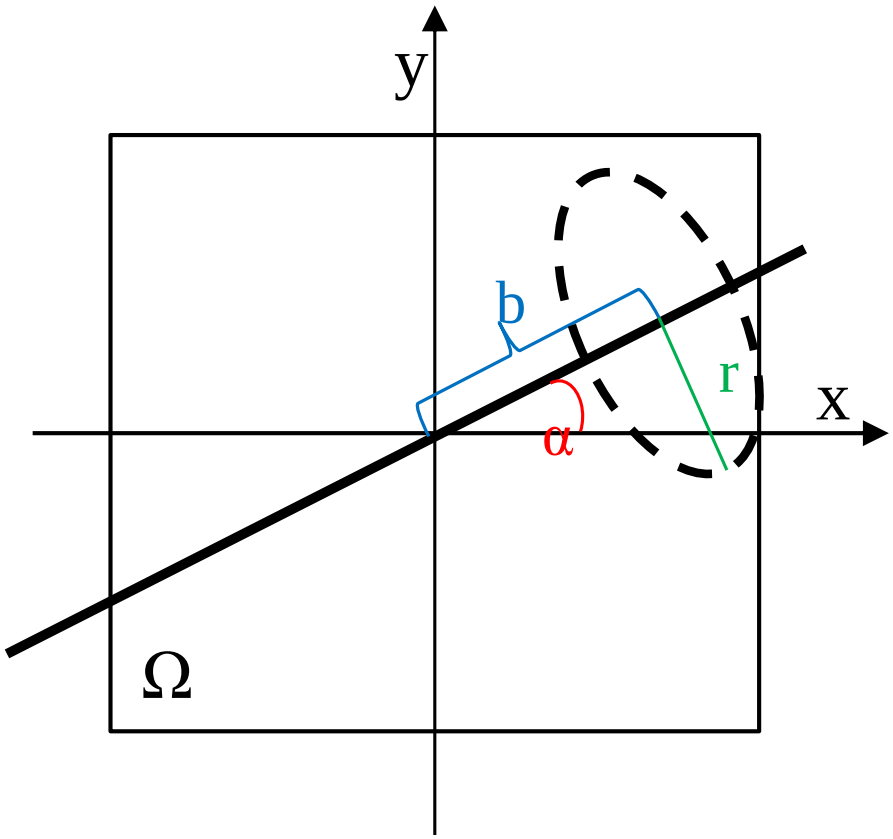

Figure 71. 2D circular pattern and its transformation

By searching the non-linear geometric features, the 2D Cylinderlet generates the 3D coefficient set, which has 3 dimensions, α, b and radius r. If a center of a circular arc is located at (α, b), it can be identified by the circle pattern with radius r. The circle pattern with radius r identifies a circular arc at (α, b, r) in the image domain, converting it to the circular Radon-like transform coefficient domain. The converted value is interpreted as an intensity value in the Radon coefficient domain. If a circular arc in the image domain perfectly matches with a circle pattern in the Radon-like transform, it produces the highest intensity value, represented as the brightest spot in the coefficient domain. The bright spot in the coefficient domain is called 'peak value.' In order to identify the peak value from the complicated coefficient matrix, clustering technique is used. The clustering is one of the techniques mentioned in section 5.2.2. If several peak values

are located near one another in the circular Radon-like transform domain, they can often be considered to represent one circular feature. These peak values will be clustered together using a k-means clustering method based on pair-wise distances between peaks. Among the peak values in the cluster, the largest value will be taken in the clustering area. Since a three dimensional matrix is used, the clustering technique is applied on each dimension to recognize the peak values. By using clustering for the coefficient set, the peak values that represent the 2D non-linear features can be chosen. Selected peak values are represented α, b, and r, corresponding to a location where the circular arc feature is placed at in the microstructure image. These peak values can be used for the next step, the circle overlaying method, in order to find the start and end coordinates of the circular arc.

9.3 Method of 2D non-linear feature extraction: Circle overlaying method

In the previous section 9.2, the peak values including radius and center coordinate of circular arc feature are obtained by using the circular Radon-like transform and clustering technique. The next step is to identify the location of the circular arc. In order to recognize the start and end coordinate of circular arc, the circle overlaying method will be used.

Similar to the line overlaying method, the circle overlaying method superimposes a circle with a given radius from the previous step on the original image at given center coordinate. Pixels of circle can detect the circular arc in the original image and the start and end coordinate of the circular arc feature can be obtained. The steps of the method are as follows:

Given: a peak (α, b, r), a maximum gap (gap_{max}), and a minimum circular arc length (c_{min})

Find: all circular arcs consisting of image pixels along the circle corresponding to (α, b, r) that is at least c_{min} long and that can span gaps of no more than gap_{max} wide.

1. Generate a circle centered at (α, b) with radius r
2. Extract pixel values from the image along those pixel coordinates
3. Find a gap longer than gap_{max} along the circular arc
4. Fill a gap if it is smaller than gap_{max}
5. Keep each circular arc that is at least c_{min} long

9.4 Examples and Results

9.4.1 Example 1: Simple Synthetic arcs

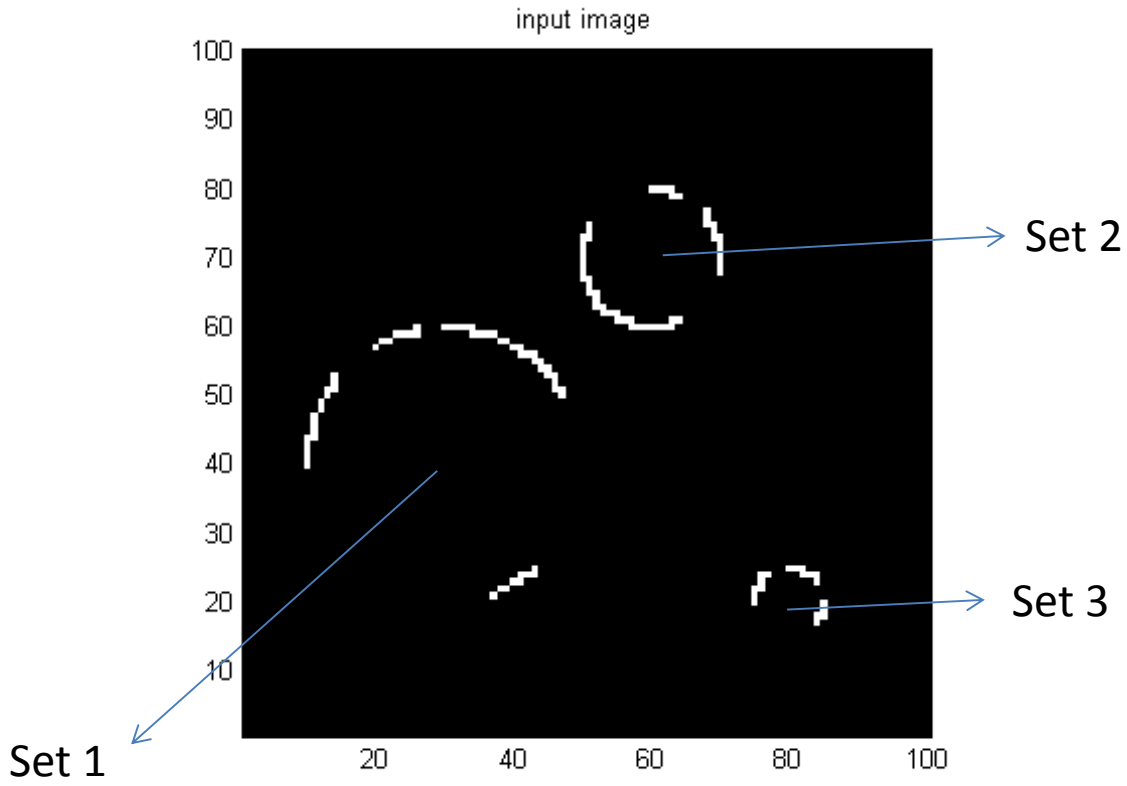

Figure 72. Simple synthetic arcs image

Figure 72 shows the simple synthetic arcs in the 100* 100 pixel 2D image domain. Sets of arcs have gaps needed to be connected. The 2D Cylinderlet based method is applied to the simple

synthetic arcs. Radii of each arc and center coordinates are identified using the circular Radon-like transform coefficient domain by finding the peak values. Table 13 shows the expected results and the actual results of each set of arcs. The circular Radon-like transform only identifies the center coordinates and radii of sets of arcs. In order to recognize start and end points of the arc, the circle overlaying method is used. The circle overlaying method detects gaps between arcs. If a gap is less than a tolerance, two arcs are considered as one arc and the circle overlaying method connects them. A gap between two arcs is calculated as linear line because of size of the gap is relatively small compare to size of the arc.

Table 13. Expected result and actual result of simple synthetic example

	Expected center coordinates and radius	Found center coordinates and radius
Set 1	(30, 40), $r_1 = 20$	(30.2, 39.7), $r_1 = 20$
Set 2	(60, 70), $r_2 = 10$	(60.6, 71.2), $r_2 = 10$
Set 3	(80, 20), $r_3 = 5$	(81.4, 20.6), $r_3 = 5$

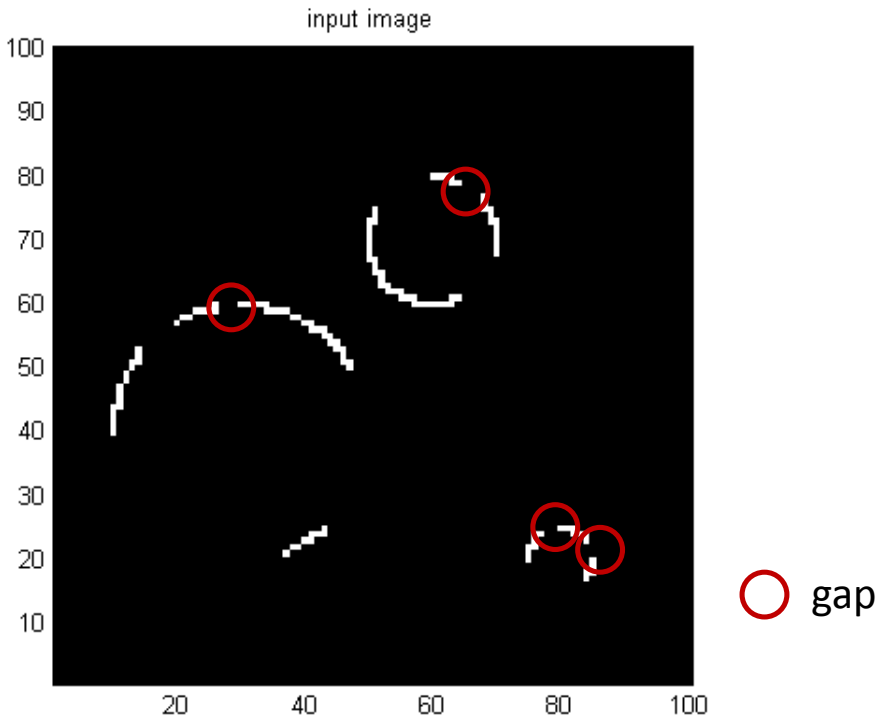

Figure 73. Simple synthetic arc (Red circles represent gaps)

Set 1

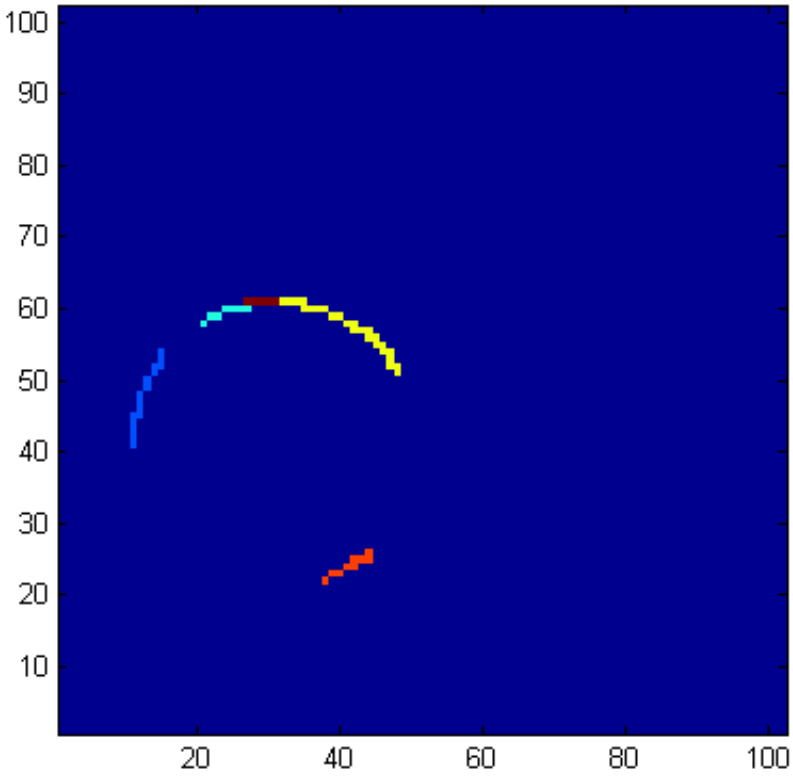
100
90
80
70
60
50
40
30
20
10
20
40
60
80
100

Set 2

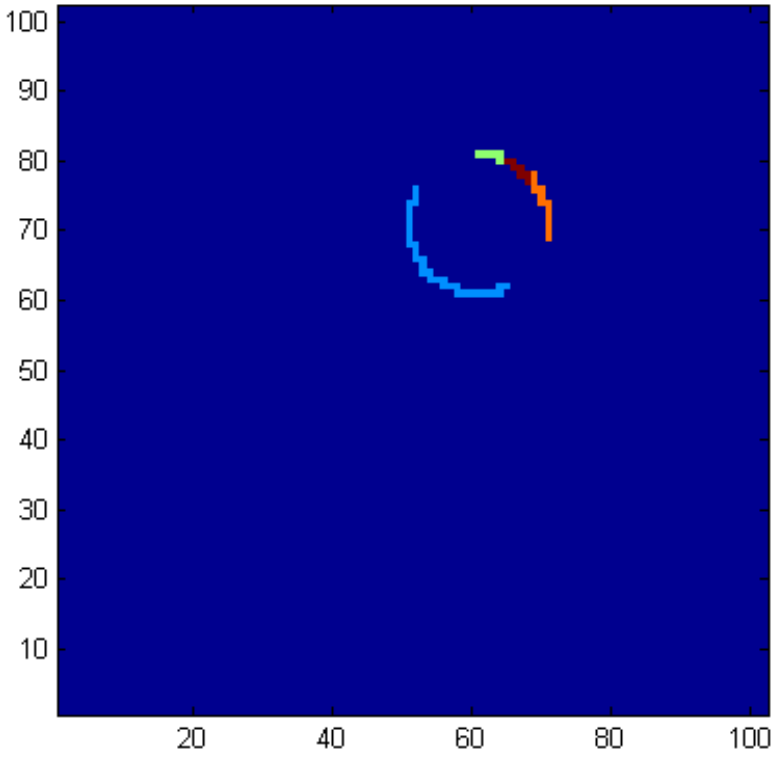
100
90
80
70
60
50
40
30
20
10
20
40
60
80
100

Set 3

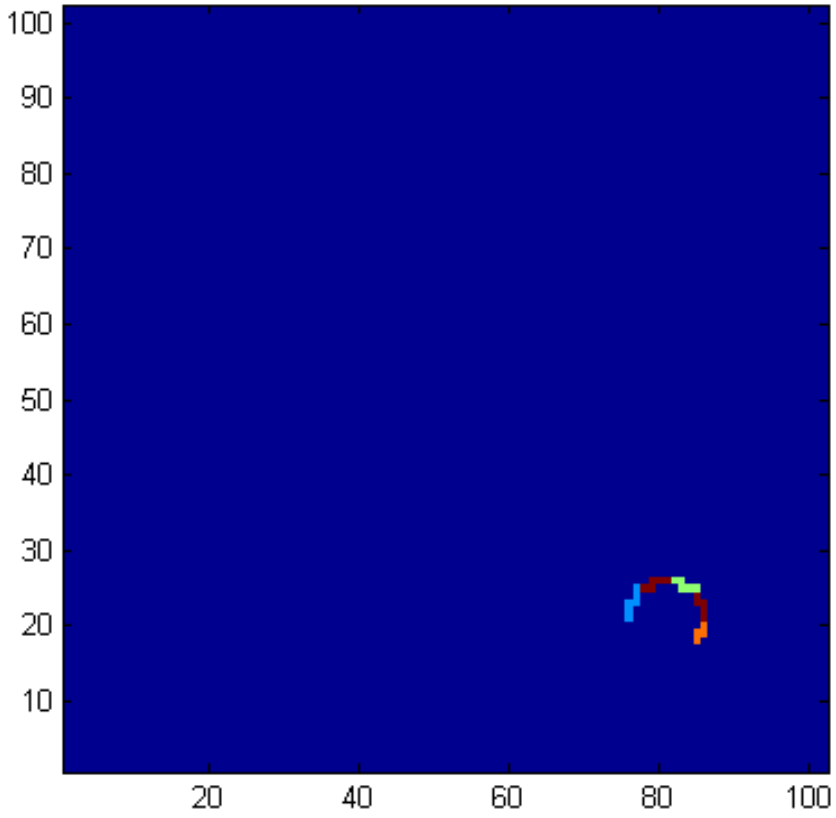

Figure 74. Recognized arcs in the set (red color represents gaps which connects arcs)

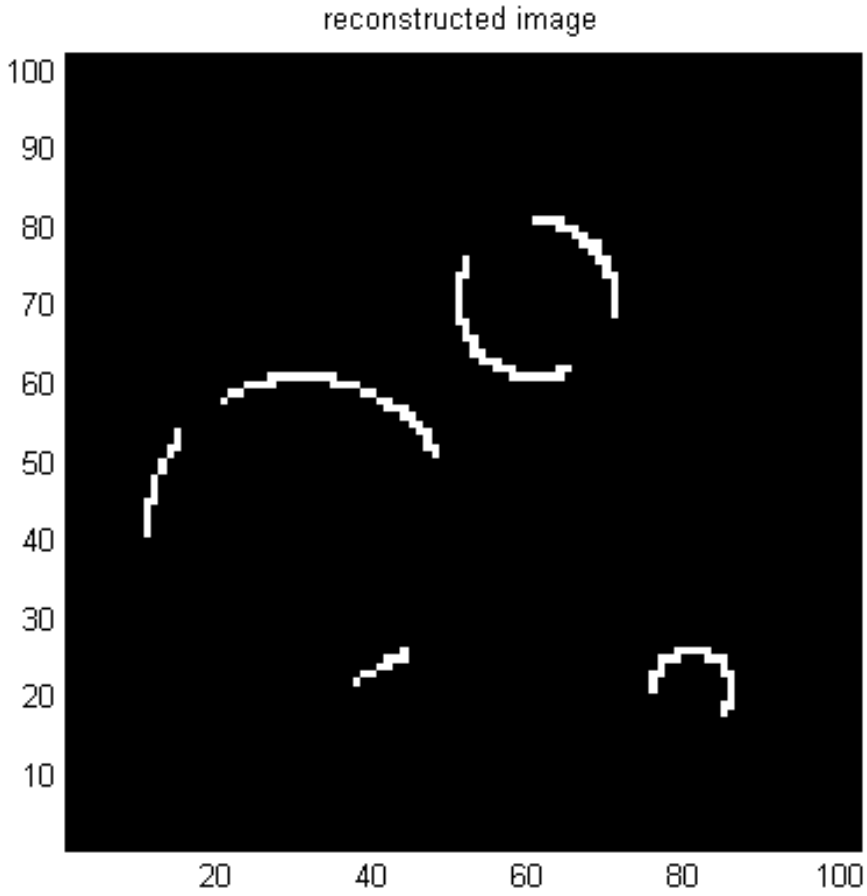

Figure 75. Reconstructed image of simple synthetic arcs

As shown in Figure 73, three sets of circular arcs have a number of gaps (marked with red circles) that can be detected by the circle overlaying method. Figure 74 shows recognized arcs by the 2D Cylinderlet based method. Different colors except red (blue, cyan, orange, yellow) indicate identified arcs shown in the original image while red colors represent gaps connected by the circle overlaying method. Gaps (red colored arcs in Figure 74) are detected by the circle overlaying method and connected. The reconstructed circular arcs are shown in Figure 75. All gaps are detected and connected. Using the 2D Cylinderlet based method; it is possible to recognize circular arcs in the image.

9.4.2 Example 2: Zirconia coated carbonyl iron particle

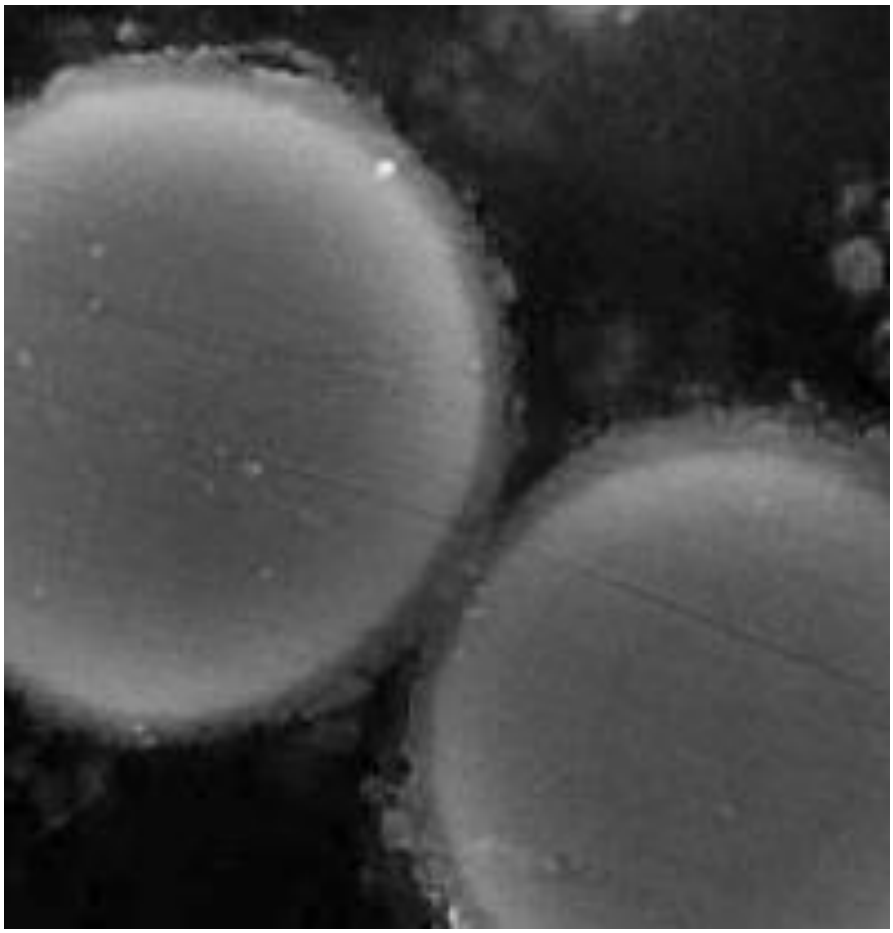

Figure 76. Zirconia coated carbonyl iron particle

This section shows that the 2D Cylinderlet based method works well for real microstructure image. As an example, zirconia coated carbonyl iron particle image taken by SEM is used [27] . Two circular arcs are presented in 200*200 zirconia coated carbonyl iron particle image as shown in Figure 76. Since the 2D Cylinderlet based method uses binary input image, simple edge detection image processing method is used to convert it to binary image. Well-known image detection algorithm 'Canny' [28] is used with the threshold and smoothness factor. Figure 77 shows conversion image of example.

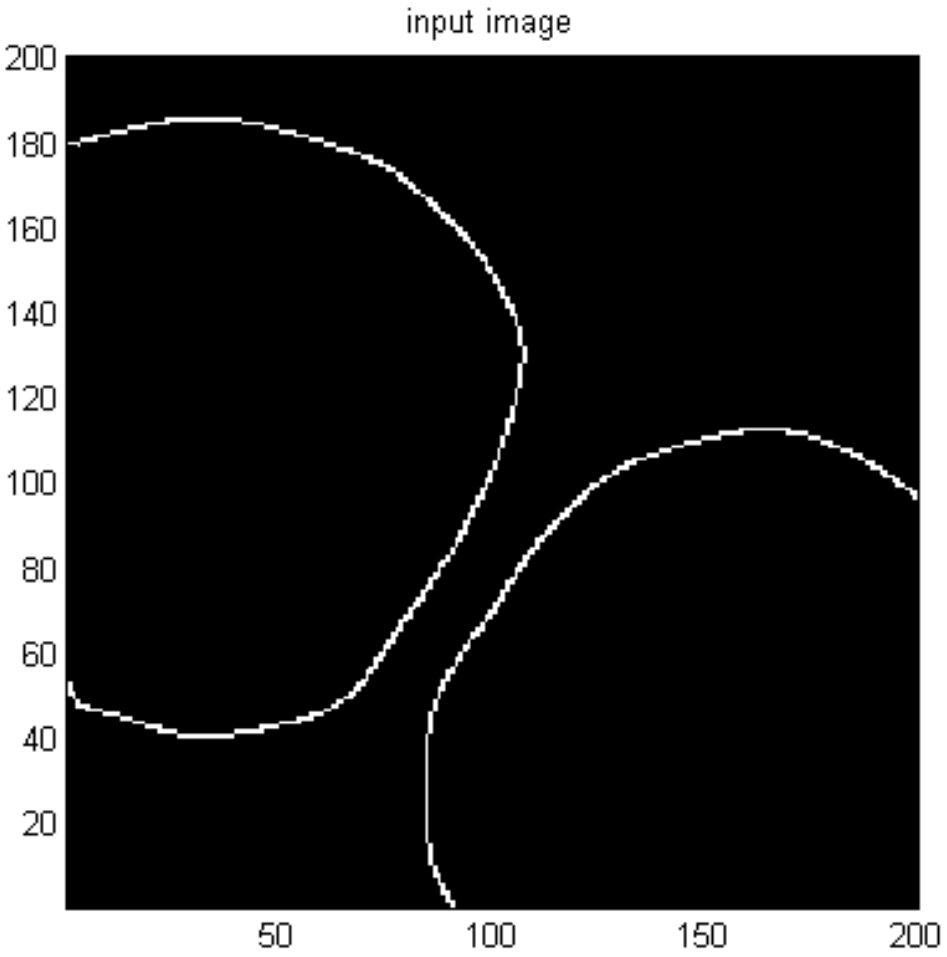

Figure 77. Zirconia coated carbonyl iron particle converted to binary image

Even though this image does not have gaps in the circular arc feature, the circle overlaying method plays an important role to recognize these arcs. The circular arcs are consisted with several small arcs with the different radii. Therefore, a several number of peaks are needed to be selected in the circular Radon-like transform domain in order to recognize the arc completely. When more than two arcs are recognized, it is very hard to reconstruct arcs smoothly together. Sometimes two arcs are overlapped or disconnected. In the case of disconnected two arc

segments, there must be a gap between arcs, which can be detected and connected by the circle overlaying method.

Table 14. Peak values correspond to circular features

	Recognized center coordinate	Recognized radius
Peak 1	(34.5, 99.3)	59
Peak 2	(163.4, 49.5)	63
Peak 3	(34.0, 108.7)	77
Peak 4	(171.2, 29.8)	84

Table 14 shows the peak values that correspond to circular arcs in the image. As mentioned above, a peak 1 only represents part of one arc as shown in Figure 78. In addition to that part of the arc shown in Figure 78 has several gaps inside due to the limitation of the resolution in the digital image domain. Therefore, it is needed to be connected by the circle overlaying method. The circle overlaying method identifies several arcs segments in the arc and these are represented as the different colors in Figure 79. Red circles represent the gaps between arc segments. By using the circle overlaying method, gaps can be detected and filled as shown in Figure 80.

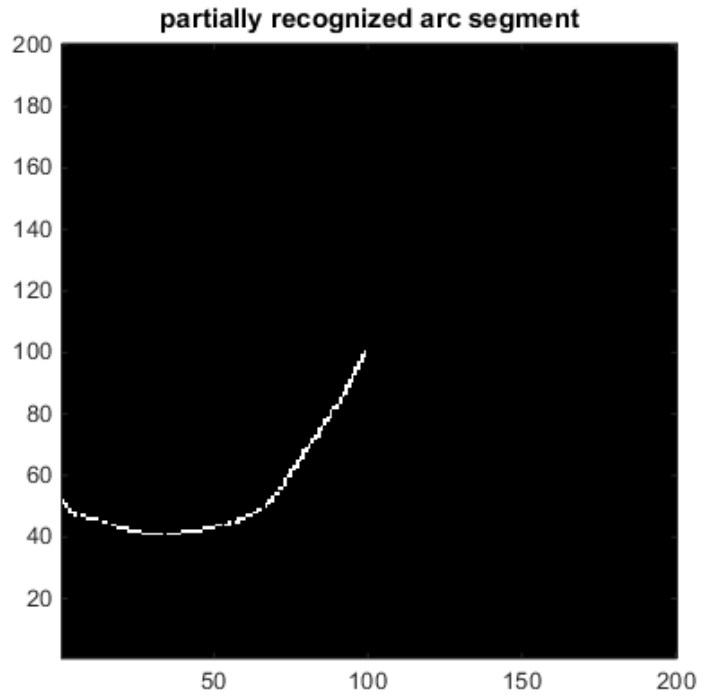

Figure 78. Partially recognized arc segment (peak 1)

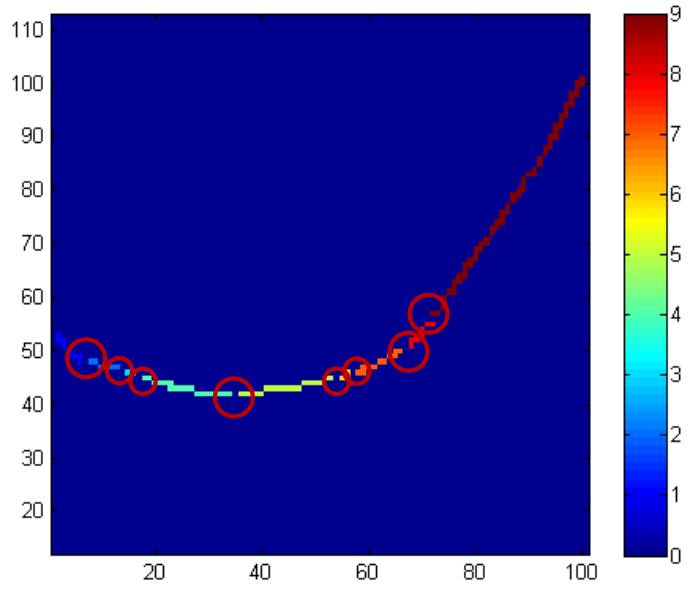

Figure 79. Identified arc segments with different colors (gaps are marked with red circles)

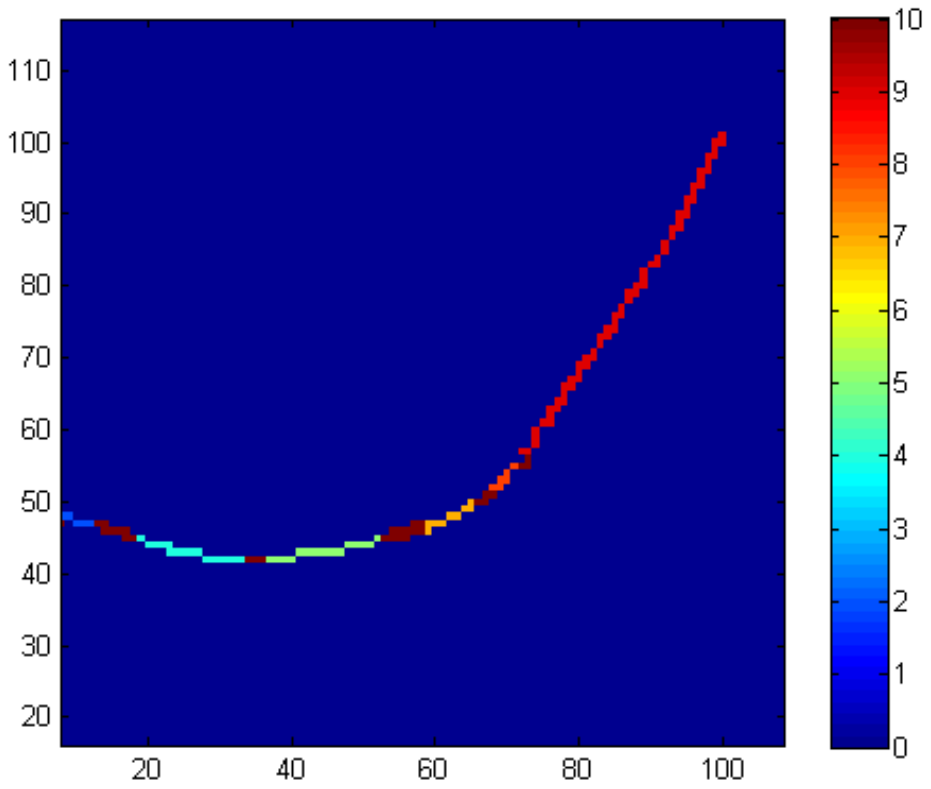

Figure 80. Identified connected arc segments (deep red color represents filled gap)

By using 4 peaks in Table 14, zirconia coated carbonyl iron particle image can be recognized. As shown in Figure 81, the recognized arc segments are represented peak by peak. If a gap size is larger than gap tolerance (gap_{max}), it is considered as disconnected two arcs shown in peak 2. Even though one peak cannot find entire circular arcs feature, combined 4 peaks represent good recognition of input image. Figure 82 shows the reconstructed microstructure of circular arc. This example indicates that the 2D Cylinderlet based method can be used as recognition of circular feature in 2D image domain. Furthermore, the peak values already provides the center coordinates, radii and start/end points of the arc, it is possible to construct explicit microstructure model using the 2D Cylinderlet based method.

Peak 1

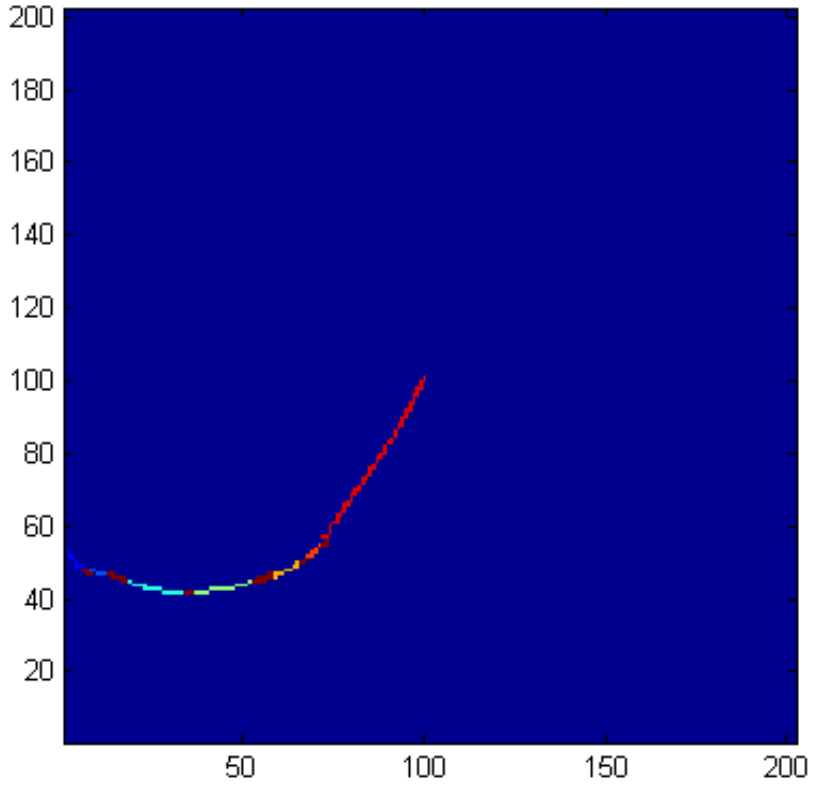
200
180
160
140
120
100
80
60
40
20
50
100
150
200

Peak 2

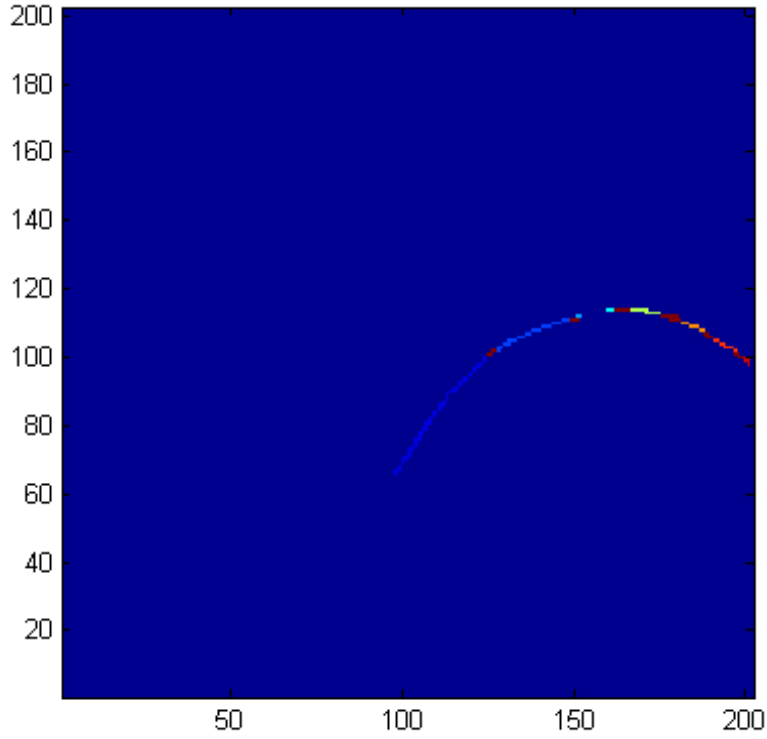
200
180
160
140
120
100
80
60
40
20
50
100
150
200

Peak 3

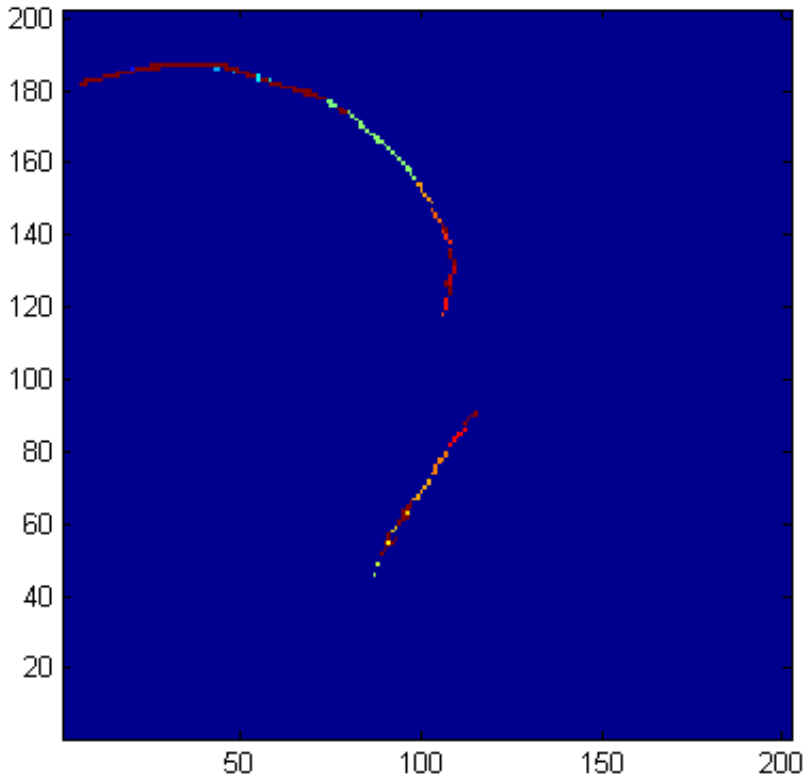

Peak 4

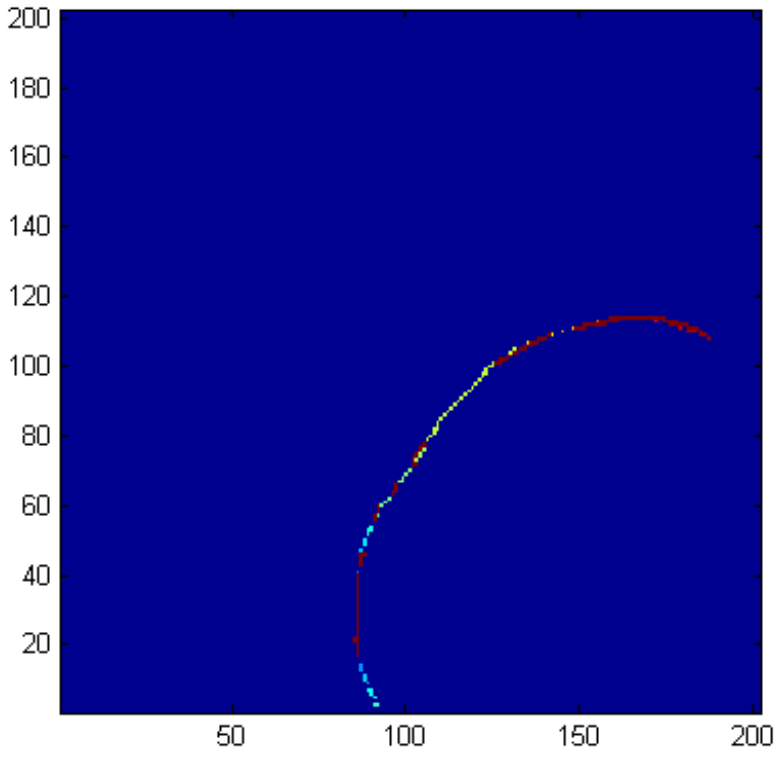

Figure 81. Recognized arc segments

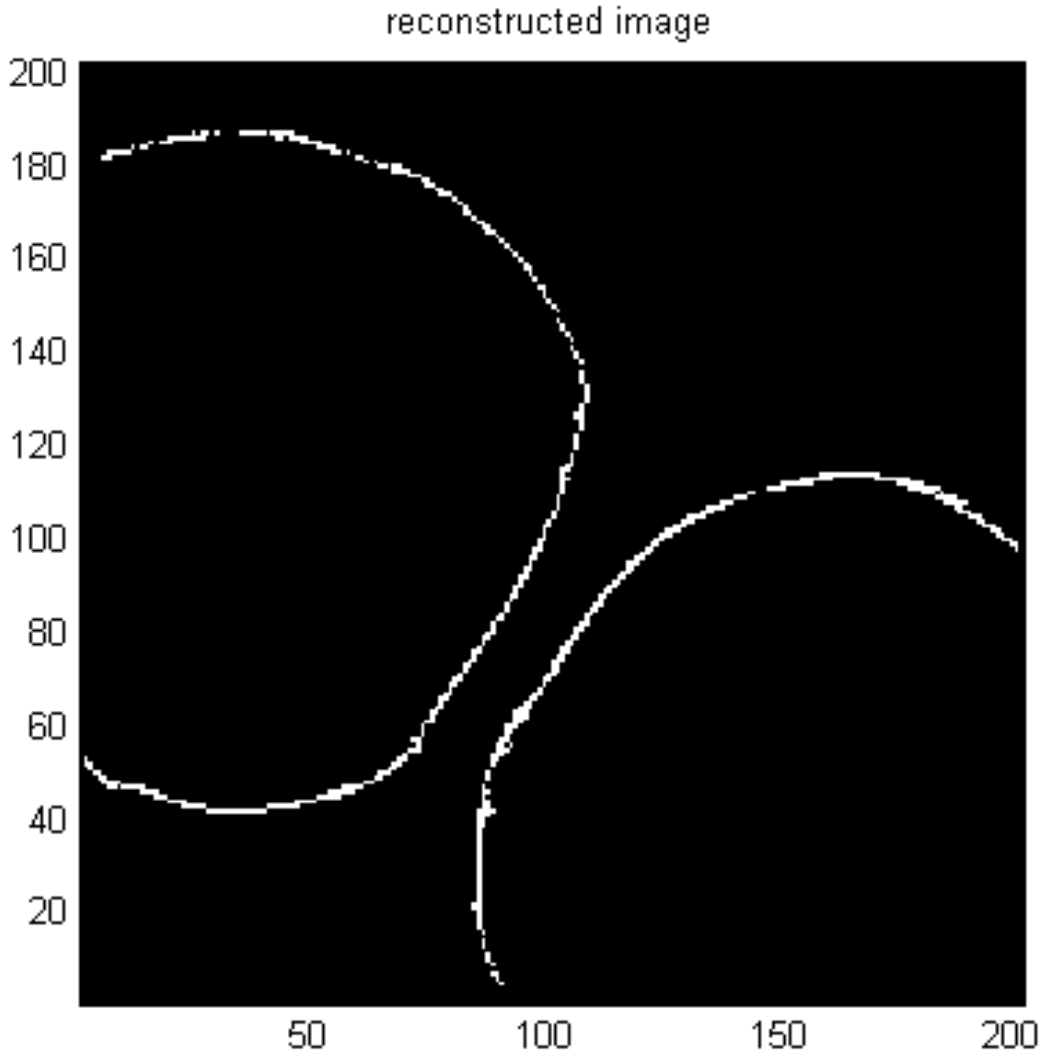

Figure 82. Reconstructed circular arcs

9.4.3 Example 3: Cross section of nano-fiber composite

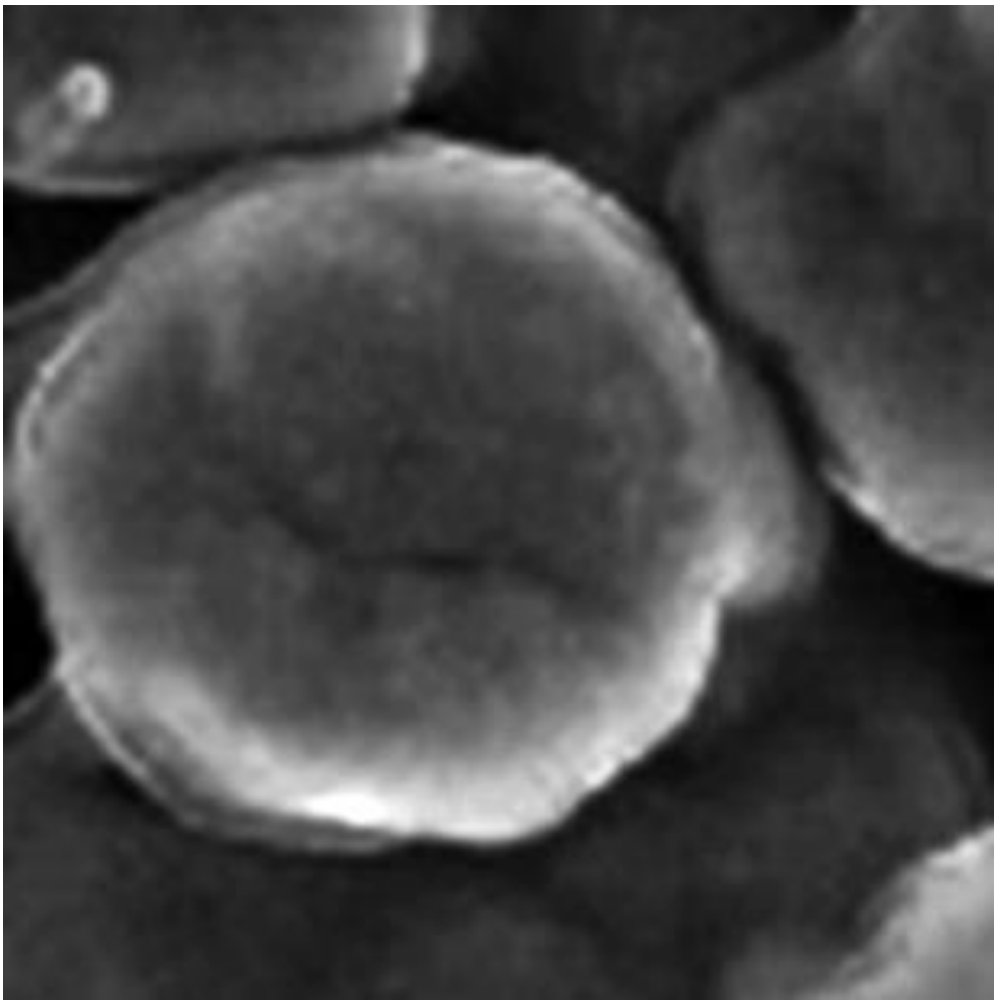

Figure 83. Cross section of nano-fiber composite

Another example image is used to demonstrate capability of the 2D Cylinderlet based method. Figure 83 shows a cross section of nano-fiber composite [26]. One circle is in the middle of the image can be identified by the 2D Cylinderlet based method. Since the 2D Cylinderlet based method uses binary input image, a simple edge detection image processing method is used to convert it to binary image. Canny algorithm [28] is used with threshold and smoothness factor. Figure 84 represents 250*250 size binary image of nano-fiber composite by canny image processing.

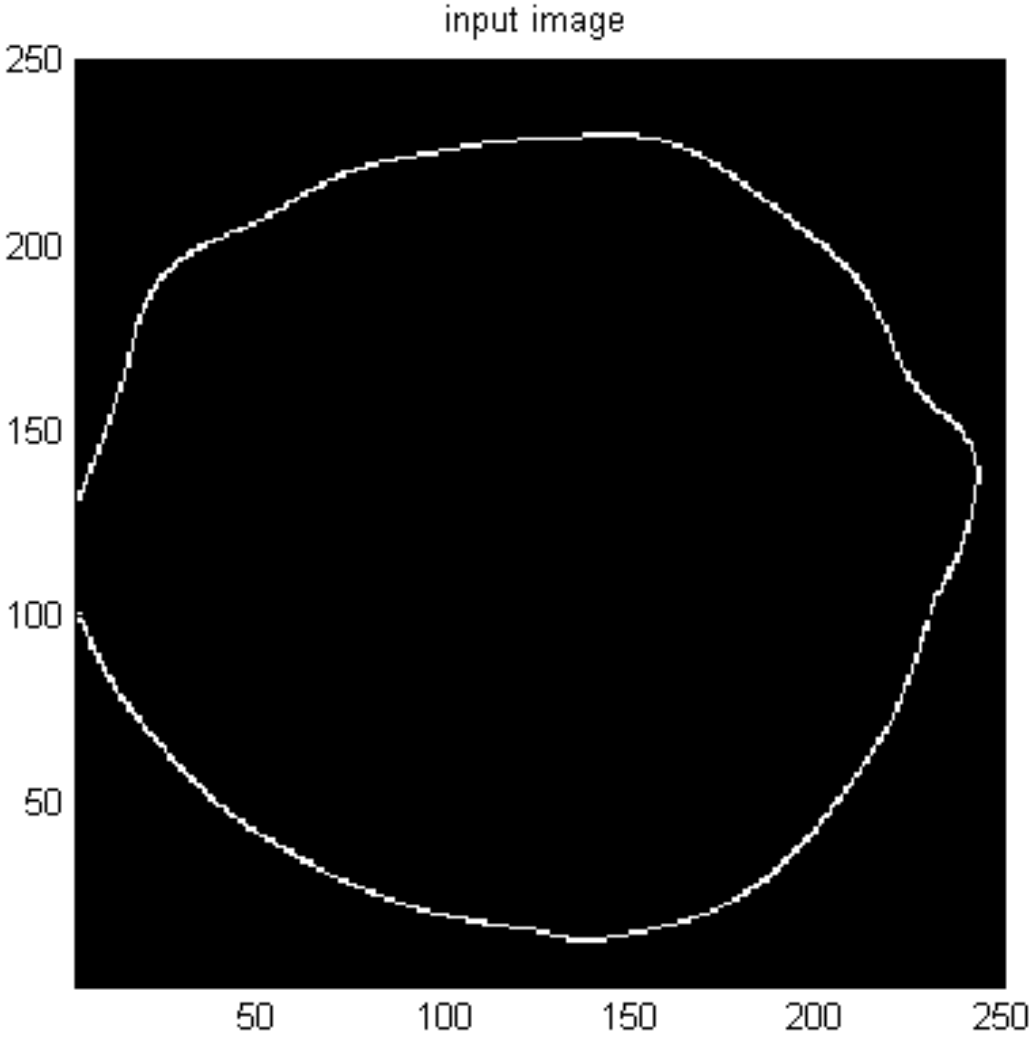

Figure 84. Cross section of nano-fiber composite binary image

This image is consisted with several small circular arcs, which can be recognized by the 2D Cylinderlet based method. When the small circular arcs are recognized to each other, gaps between circular arcs are inevitable. Therefore, the circle overlaying method plays an important role in the process of recognition. Table 15 shows center coordinates and radii from the circular Radon-like transform, which correspond to circular feature in the image Figure 84. By using

three peaks in Table 15, the circular feature in the image Figure 84 can be recognized. As shown in Figure 85, the recognized arc segments are represented. The arc segments are identified using the 2D Cylinderlet based method. If a gap exists in the arc segment, the circle overlaying method detects a gap and fills with same radius of the arc segment. Since the input image is not a perfect circle, it is impossible to recognize a circular arc with one peak value. However, three peaks in Table 15 can represent reconstructed circular feature in the 2D image domain shown in Figure 86.

Table 15. Peak values correspond to circular feature

	Recognized center coordinate	Recognized radius
Peak 1	(131.5, 125.8)	104
Peak 2	(126.4, 123.7)	108
Peak 3	(116.3, 121.6)	115

Peak 1

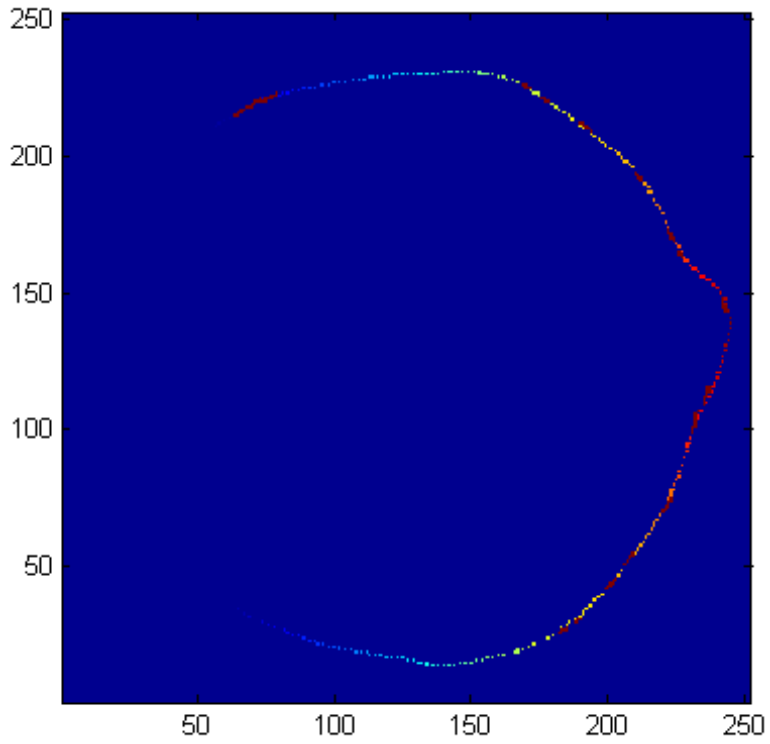
250
200
150
100
50
50
100
150
200
250

Peak 2

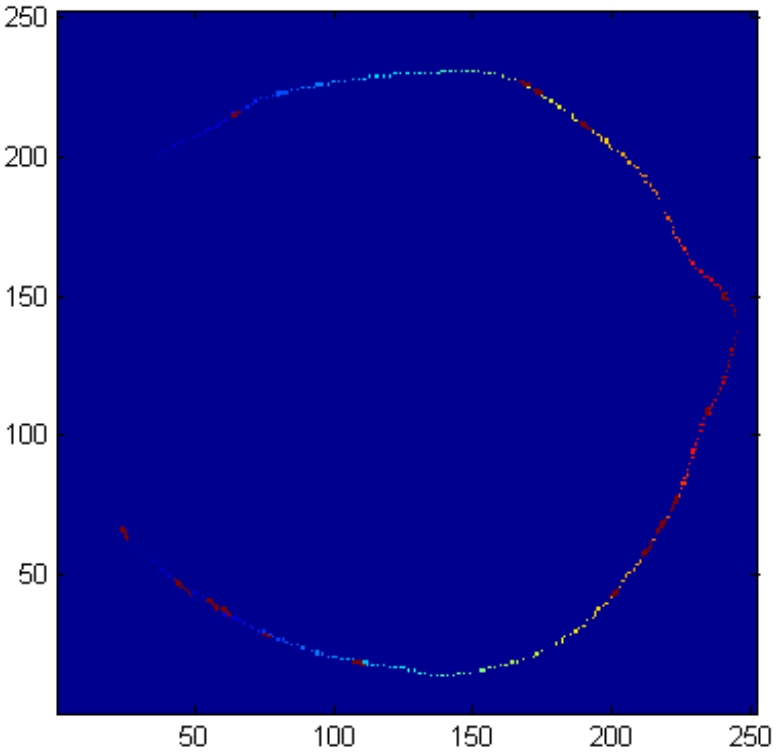
250
200
150
100
50
50
100
150
200
250

Peak 3

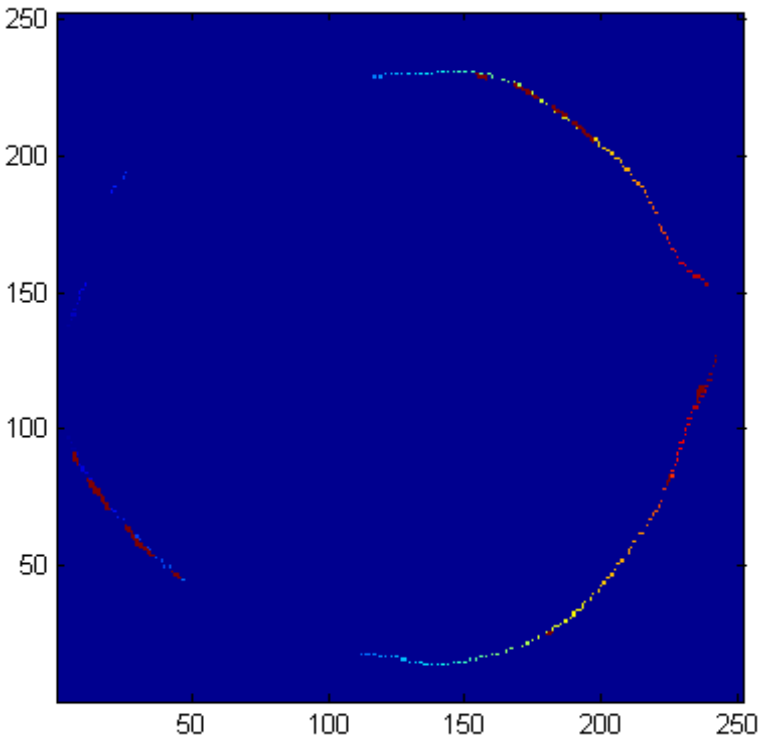

Figure 85. Recognized arc segments

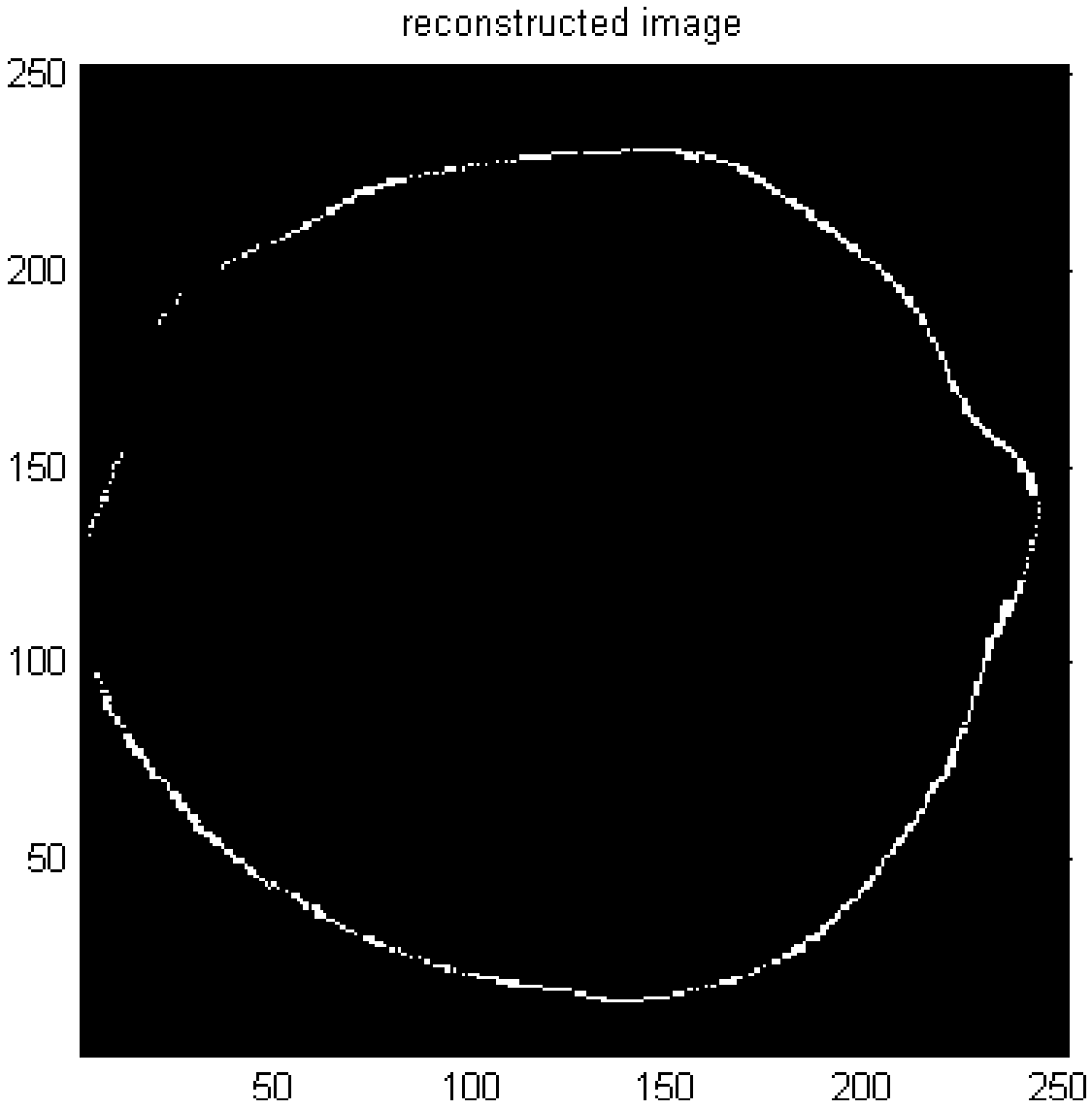

Figure 86. Reconstructed circular feature in 2D image domain

Even though three peaks recognize the circular feature, it still has unrecognized part shown in Figure 87. There is couple of reasons that why some features cannot be recognized. One reason is that if a circular feature has center coordinates outside of image domain, it could be unrecognizable. The other reason is intensity value. If a radius of a circular feature is too small

compare to the other radii of circular features in the same image domain, the intensity value of small circular feature also can be a smaller than the intensity value of large circular feature. Therefore, clustering technique may disregard the small radius of circular feature due to the small intensity value. A and B shown in Figure 86 are the example of the first case. Even though it has some unrecognizable portion, microstructure model of circular features can be constructed explicitly using the 2D Cylinderlet based method, providing center coordinates, radii, and start/end points of circular arcs.

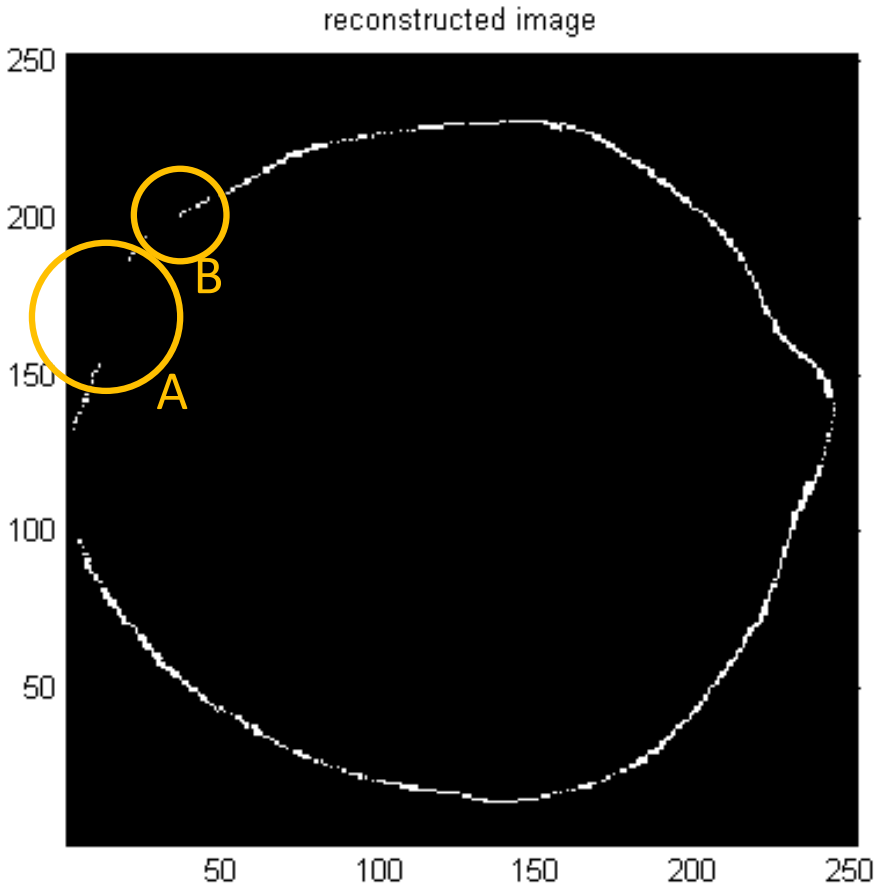

Figure 87. Un-recognized part in the circular feature

9.5 Summary

This chapter explains the recognition of 2D non-linear features in a microstructure domain. In order to do that, the 2D Cylinderlet based method is used. The 2D Cylinderlet based method includes the 2D circular Radon-like transform followed by the circle overlaying method. Each recognized 2D circular arc feature is used to construct explicit non-linear microstructure model. This chapter contributes to answer the research question 1 followed by the hypothesis 1b.

The hypothesis of this research question is validated in this chapter by showing the process of recognizing non-linear geometric features. Zirconia coated carbonyl iron particle and a cross section of nano-fiber composite are used as examples as well as the synthetic circular arc image. By using those examples, it is possible to demonstrate the recognition of non-linear features using 2D Cylinderlet based method. The 2D Cylinderlet based method allows constructing explicit microstructure model, providing center coordinates, radii, and start/end points of circular arcs.

Circular arcs are simple form of non-linear features. The 2D Cylinderlet based method recognizes the geometric features and it helps to achieve a reverse engineering of material process, shown in Figure 2. This method provides an explicit form of non-linear features, specifically circular arcs by giving center coordinates and radii. By completing this step, a heterogeneous CAD system can be achieved.

CHAPTER 10
STRUCTURE-PROPERTY RELATIONSHIP

This research aims to establish structure-property relationship of microstructure. In chapters 5 to 9, methods for recognizing geometric features in microstructure data are shown. Recognized geometric features are essential elements to build a structure-property relationship. By using achieved geometric features, a microstructure model can be constructed and its property information can be integrated. In this chapter, a structure-property relationship of a constructed microstructure model is explored. Specifically, the elastic modulus of the material for the structure-property relationship will be focused on this research.

10.1 Research question 2

The objective of this chapter is to answers research question 2.

> ***"Can the structure-property relationship of microstructures be established using the microstructure model from recognized geometry features?"***

In order to solve this question, the hypothesis is proposed.

> *"Recognized 2D linear features can be used to construct grain boundaries, which are used to form a microstructure model of grains. The microstructure model will be utilized as input to a computational engineering analysis tool so that effective mechanical properties can be calculated. By pursuing these processes, one can establish the structure-property relationship of microstructure"*

The proposed research question 2 and its hypothesis focus on the 2D linear features. To be specific, in this research IN100 material is used to prove hypothesis2. A specific polycrystalline

Ni-base superalloy, IN100, is widely used in high temperature application such as turbine engine components because of its enhanced strength, creep, fatigue and corrosion resistance at elevated temperatures [22]. Structure-property relationship for this material at micro-scale would be used to establish heterogeneous CAD system mentioned in chapter 1.

10.2 Structure: Construction of microstructure

In order to answer research question2, constructing a microstructure model is the first research task. Chapter 6.2 shows the constructed model of IN100 using the 2D surfacelet based method. All intersection points are identified and coordinates of intersection points are calculated. When line segments are placed close to each other, it is considered that they share the end points. By finding a shared point between two line segments within a tolerance, it is possible to connect line segments. Repeating this step produces a closed loop area, which can be considered as a grain shown in Figure 88. Figure 88 shows a microstructure model achieved by two different methods. An explicit microstructure model of IN100 can be provided by showing coordinates of each points and its connectivity information shown in Table 16, Table 17 and Figure 88. In Table 17, if more than 2 points are connected and share a vertex, the smallest number is used as the representative number.

Table 16. Coordinates of each point corresponding Figure 88 (a)

Point	Coordinate	Point	Coordinate	Point	Coordinate
1	(32.99, 82.50)	11	(194.33, 135.14)	21	(76.25, 132.00)
2	(32.00, 180.91)	12	(302.00, 181.91)	22	(170.78, 71.10)
3	(170.78, 71.10)	13	(32.99, 82.50)	23	(131.74, 135.40)
4	(132.42, 75.97)	14	(32.00, 180.91)	24	(159.58, 162.84)
5	(194.33, 135.14)	15	(0.00, 234.36)	25	(242.85, 180.81)
6	(76.25, 132.00)	16	(132.42, 75.97)	26	(0.00, 49.90)
7	(242.85, 180.81)	17	(95.51, 133.18)	27	(0.00, 0.00)
8	(131.74, 135.40)	18	(170.78, 71.10)	28	(302.00, 0.00)
9	(184.53, 0.00)	19	(32.26, 154.46)	29	(0.00, 253.00)
10	(159.58, 162.84)	20	(194.33, 135.14)	30	(302.00, 253.00)

Table 17. Cycle of line segments, forming grains

	Connected points in order
Grain 1	26, 1(=13), 19, 2(=14) , 15
Grain 2	15, 2(=14), 19, 6(=21), 17, 8(=23), 10(=24), 5(=11=20), 7(=25), 12, 30, 29
Grain 3	19, 6(=21), 17, 4(=16), 3(=18, 22), 9, 27, 26, 1(=13)
Grain 4	17, 8(=23), 10(=24), 5(=11=20), 3(=18=22), 4(=16)
Grain 5	3(=18=22), 5(=11=20), 7(=25), 12, 28, 9

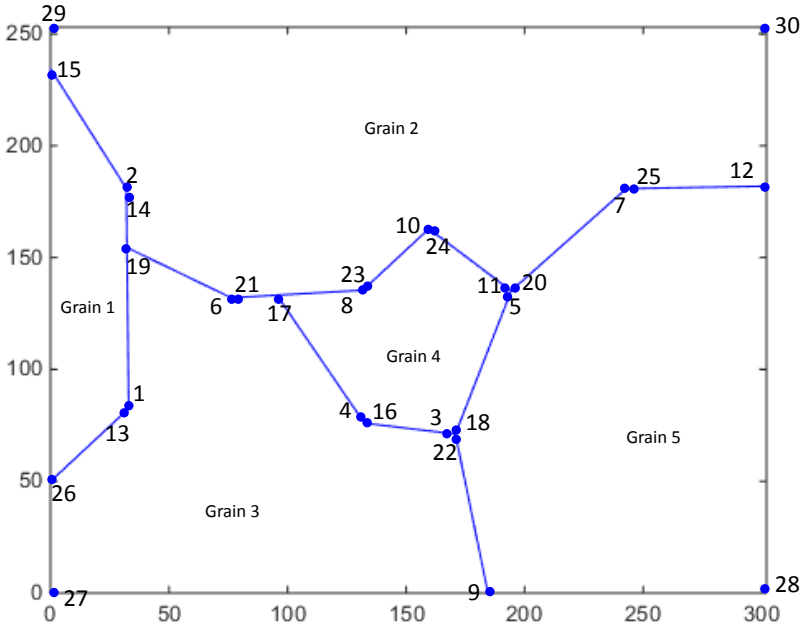

a) Butterfly wing method

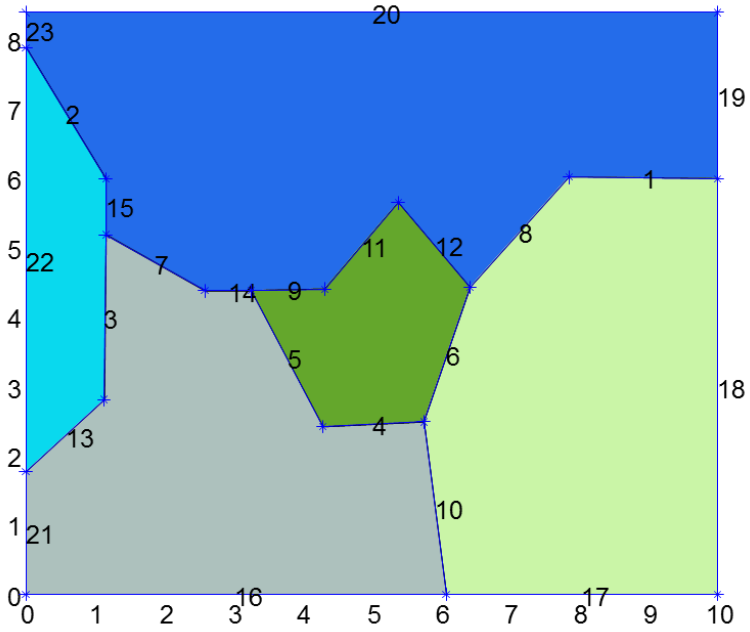

b) Line overlaying method

Figure 88. An explicit IN100 microstructure model, showing connectivity information

In the 3D microstructure model, a linear feature in 3D space is represented as large region. Therefore, a shared edge between two large regions is the most important feature to construct a 3D microstructure grain model. Detailed steps for finding a shared edge between 2 regions are explained in chapter 8.5. In order to find a shared edge, large regions in 3D space are needed to be determined first. Peak values from the 3D Radon transform are used in the plane overlaying method, yielding planes, which contains linear features. Then, the plane, produced by the plane overlaying method, is flattened onto the 2D domain and connectivity of each pixel is checked. Pixels that have a high connectivity value, form a large region. After a large region is found in 2D flattened plane, it is returned to 3D space. When large regions are recognized in 3D space, voxel indices shared between two linear features need to be found. By finding a line of shared voxels indices, a shared edge can be identified and a 3D microstructure model can be constructed.

10.3 Structure-property relationship

10.3.1 An explicit microstructure model and its orientations

In this research, structure-property relationship is established using IN100 2D linear example (2.68 X 3.90 μm). The Euler angles of each grain have been investigated by Leonhard Euler [1], which can represent each grain its own local orientation. The local orientations of each grain allow us to calculate rotation angles in global coordinate system for each grain.

Three elemental rotations in the Euler angles (α, β, γ) compose a rotation matrix R [1].

$$R = Z(\alpha)X(\beta)Z(\gamma) =$$

$$\begin{bmatrix} cos\alpha cos\gamma - cos\beta sin\alpha sin\gamma & -cos\alpha sin\gamma - cos\beta cos\gamma sin\alpha & sin\alpha sin\beta \\ cos\gamma sin\alpha + cos\alpha cos\beta sin\gamma & cos\alpha cos\beta cos\gamma - sin\alpha sin\gamma & -cos\alpha sin\beta \\ sin\beta sin\gamma & cos\gamma sin\beta & cos\beta \end{bmatrix} \quad (21)$$

By using this rotation matrix Equation (21), local orientations of each grain represented by global coordinate system can be obtained. Figure 88 (a) shows different grains in a 2D IN100 microstructure model recognized by the 2D surfacelet based method. Each grain has different orientations represented by Euler angles. Equation (21) is used to calculate rotation angles for each grain, shown in Table 18.

Table 18. Euler angles of each grain and its projected rotation angle

	α	β	γ	Projected rotation angle (°)
Grain 1	3.25	2.19	4.72	136.57
Grain 2	2.19	1.51	5.10	119.45
Grain 3	0.11	1.11	5.52	10.05
Grain 4	2.94	1.98	5.77	146.86
Grain 5	5.71	1.11	3.34	156.59

Each Coordinate of point is already determined shown in Table 16 and connectivity information of each line segment is also represented in Figure 88 (a) and Table 17. This information allows us to construct an explicit IN100 microstructure model. A cycle of line segments forms an area that can be meshed with higher order 2D 8node element. This type of element has quadratic displacement behavior and is well suited to modeling irregular meshes. When the mesh is created in the grain area, the orientations of each grain are also applied to the model. Finite element model for ANSYS is shown in Figure 89.

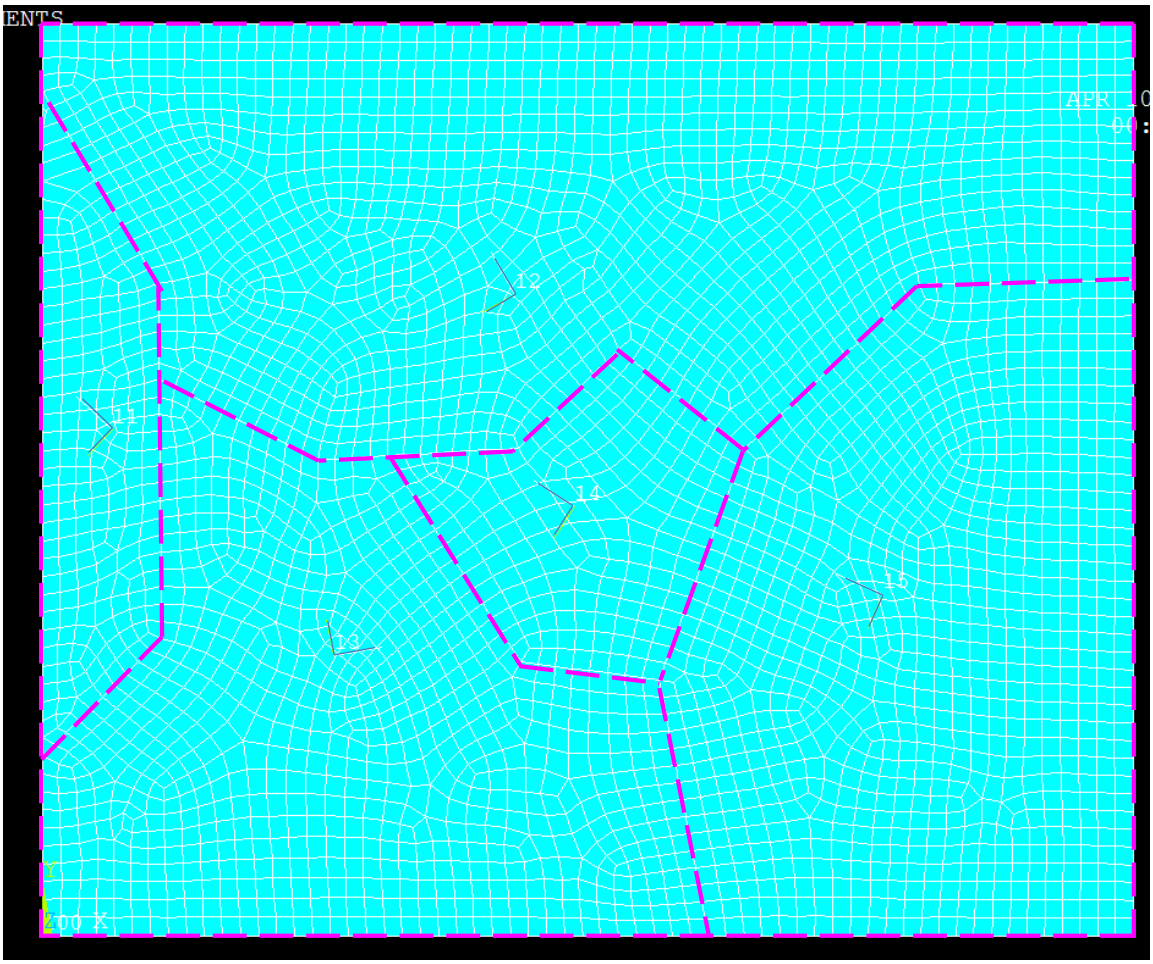

Figure 89. Finite element model of IN100 with grain boundaries and orientations

10.3.2 Cubic crystal material

If the material is cubic symmetry, the constitutive law for this material is particularly simple, and can be parameterized by only 3 material constants, shown in Equation (22) [29].

$$\begin{bmatrix}\sigma_{11}\\ \sigma_{22}\\ \sigma_{33}\\ \sigma_{23}\\ \sigma_{12}\\ \sigma_{13}\end{bmatrix} = \begin{bmatrix} C_{11} & C_{12} & C_{12} & 0 & 0 & 0 \\ & C_{11} & C_{12} & 0 & 0 & 0 \\ & & C_{11} & 0 & 0 & 0 \\ & & & C_{44} & 0 & 0 \\ & Sym & & 0 & C_{44} & 0 \\ & & & 0 & 0 & C_{44} \end{bmatrix} \begin{bmatrix}\varepsilon_{11}\\ \varepsilon_{22}\\ \varepsilon_{33}\\ 2\varepsilon_{23}\\ 2\varepsilon_{12}\\ 2\varepsilon_{13}\end{bmatrix} \quad (22)$$

This is virtually identical to the constitutive law for an isotropic solid, except that the shear modulus G is not related to the Poisson's ratio and Young's modulus through the usual relation in isotropic material. Three material constants of IN100 are given shown in Table 19 [22].

Table 19. Property of IN100 microstructure (γ')

C11 (MPa)	C12 (MPa)	C44 (MPa)
135,000	59,210	81,515

The relationship [29] between the elastic constants are

$$\mathrm{E} = \frac{C_{11}^2 + C_{12}C_{11} - 2C_{12}^2}{C_{11} + C_{12}} = 98.90\ GPa$$

$$\nu = C_{12}/(C_{11} + C_{12}) = 0.3049 \qquad (23)$$

$$\mathrm{G} = C_{44} = 81.52\ GPa$$

Using these elastic constants in ANSYS, the effective elastic moduli of x direction and y direction can be calculated. The effective elastic modulus of x direction (Ex_{eff}) is calculated with simple boundary conditions. A left vertical edge (y axis) is fixed while a right vertical edge is pulled 5 μm in x direction. Properties of each grain are applied depending on its orientations.

- Strain

$$\epsilon_x = \frac{\Delta l_x}{l_x} = \frac{5}{3.90} = 1.2813$$

- Pressure

$$\frac{F}{length_y} = \frac{594.24 * 10^9}{2.68} = 221.49\ GPa$$

Using the conditions above, the effective elastic modulus for the x direction is

$$Ex_{eff} = \frac{\sigma_x}{\epsilon_x} = 172.87\text{GPa}$$

Similar to Ex_{eff}, Ey_{eff} is also calculated using similar boundary conditions. A bottom horizontal edge (x axis) is fixed while a upper horizontal edge is pulled 5 μm in y direction. Properties of each grain are applied depending on its orientations.

- Strain

$$\epsilon_y = \frac{\Delta l_y}{l_y} = \frac{5}{2.68} = 1.8636$$

- Pressure

$$\frac{F}{length_x} = \frac{839.32 * 10^9}{3.90} = 215.08\ GPa$$

Using conditions above, the effective elastic modulus for the y direction is

$$Ey_{eff} = \frac{\sigma_y}{\epsilon_y} = 115.41\ Gpa$$

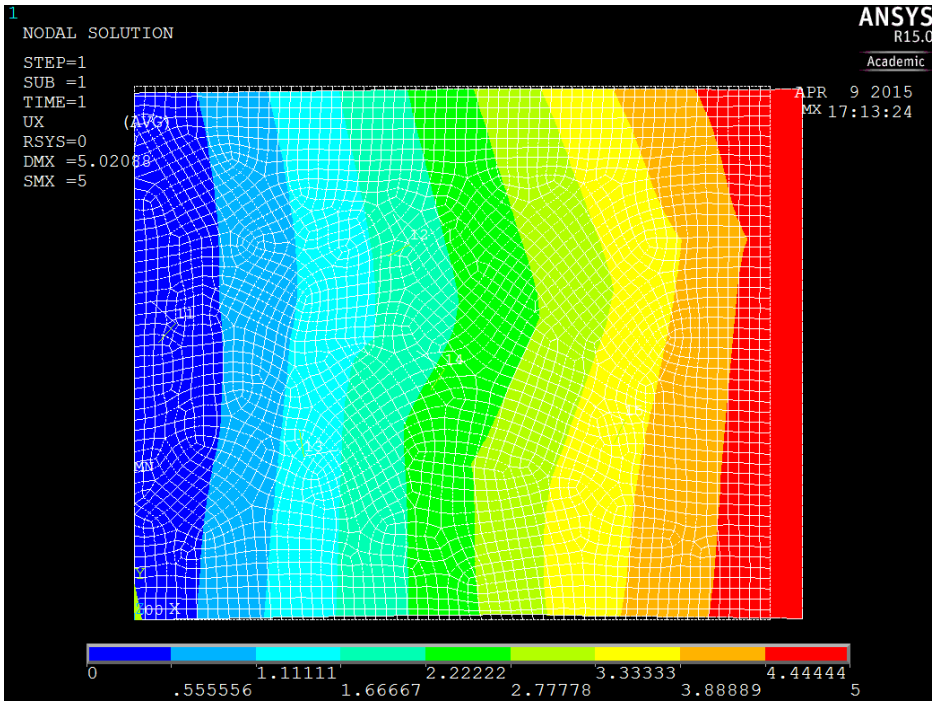

Figure 90. Displacement distribution of x direction (calculation of Ex_{eff})

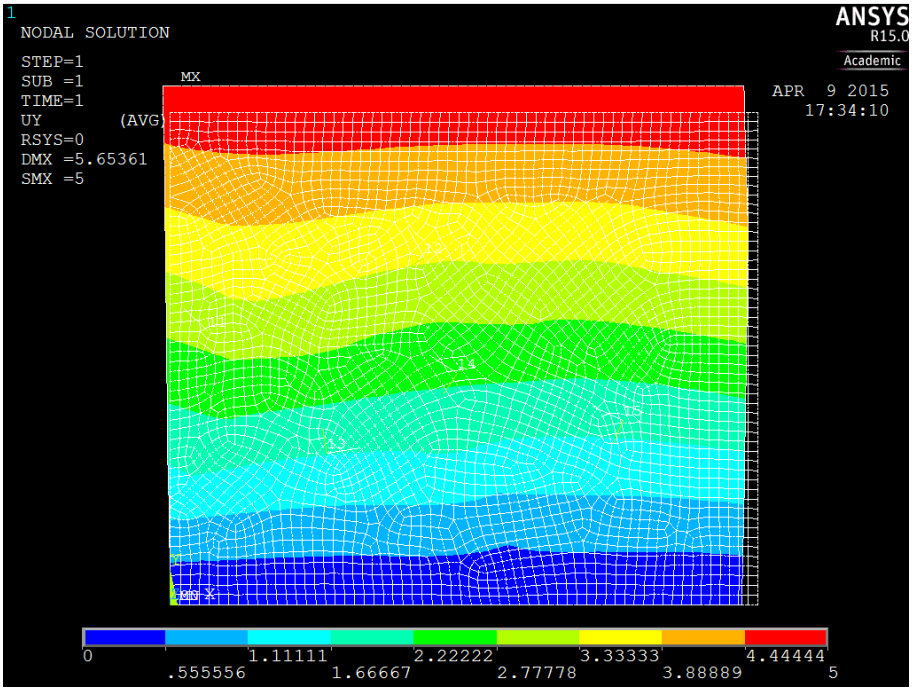

Figure 91. Displacement distribution of y direction (calculation of Ey_{eff})

Displacement field in x direction and y direction are shown in Figure 90 and Figure 91. It is a simple simulation but the displacements are distributed non-uniformly. Even though it is cubic symmetry material, which has same elastic constant on 3 axes, effective elastic moduli on x and y directions are different (Ex_{eff} = 172.87GPa, Ey_{eff} = 115.41GPa). The effective elastic modulus on x direction is increased 73.91% compare to input elastic modulus calculated in Equation (23) while the effective elastic modulus on y direction is increased 16.69%. This result indicates that the x direction is stiffer than the y direction. This is because the shear modulus G is not related to the Poisson's ratio and elastic modulus through the usual relation in isotropic material. In addition to that, the orientations of each grain affect elasticity for each grain.

The objective this research is to establish structure property relationship for microstructure. A property of the constructed microstructure model is calculated using orientations of each grain and elements of compliance matrix.

10.3.3 Orthotropic material

Hypothetically, if the material is an orthotropic material and has the same grain orientations introduced in section 10.3, it gives different results from cubic crystal material. In this section, the material is assumed to be an orthotropic material.

An orthotropic material has three mutually perpendicular symmetry planes so that its material properties are, in general, different along each axis. An example of this type of material is a metal which has been rolled to form a sheet. Since a rolled sheet metal develops an anisotropic structure during rolling, the properties of the two transverse directions and the property in the rolling direction will be different [30]. If IN100 material is assumed to be an orthotropic material, similar to rolled sheet metal, it can be expected that higher elasticity in one direction than the other 2 directions.

Orthotropic material has 9 independent material constants [31]. The constitutive law for this material is shown in Equation (24) [29].

$$\begin{bmatrix}\sigma_{11}\\ \sigma_{22}\\ \sigma_{33}\\ \sigma_{23}\\ \sigma_{12}\\ \sigma_{13}\end{bmatrix} = \begin{bmatrix} C_{11} & C_{12} & C_{13} & 0 & 0 & 0 \\ & C_{22} & C_{23} & 0 & 0 & 0 \\ & & C_{33} & 0 & 0 & 0 \\ & & & C_{44} & 0 & 0 \\ & Sym & & 0 & C_{55} & 0 \\ & & & 0 & 0 & C_{66} \end{bmatrix} \begin{bmatrix}\varepsilon_{11}\\ \varepsilon_{22}\\ \varepsilon_{33}\\ 2\varepsilon_{23}\\ 2\varepsilon_{12}\\ 2\varepsilon_{13}\end{bmatrix} \quad (24)$$

Assume that 9 elements are given the values shown in Table 20. These values allow calculating elastic constant using equation (24)[29].

Table 20. Independent element value of compliance matrix for orthotropic material

C_{11} [GPa]	C_{22} [GPa]	C_{33}[GPa]	C_{44} [GPa]	C_{55} [GPa]	C_{66} [GPa]	C_{12} [GPa]	C_{13} [GPa]	C_{23} [GPa]
14.4	14.2	137	7.2	6.2	3.6	7.4	7.7	7.4

$$\mathrm{E}_1 = \frac{(C_{11}C_{22}C_{33} + 2C_{23}C_{12}C_{13} - C_{11}C_{23}^2 - C_{22}C_{13}^2 - C_{33}C_{12}^2)}{(C_{22}C_{33} - C_{23}^2)} = 10.43GPa$$

$$\mathrm{E}_2 = \frac{(C_{11}C_{22}C_{33} + 2C_{23}C_{12}C_{13} - C_{11}C_{23}^2 - C_{22}C_{13}^2 - C_{33}C_{12}^2)}{(C_{11}C_{33} - C_{13}^2)} = 10.31GPa$$

$$\mathrm{E}_3 = \frac{(C_{11}C_{22}C_{33} + 2C_{23}C_{12}C_{13} - C_{11}C_{23}^2 - C_{22}C_{13}^2 - C_{33}C_{12}^2)}{(C_{11}C_{22} - C_{12}^2)} = 131.74GPa$$

$$\upsilon_{32} = \frac{(C_{11}C_{23} - C_{12}C_{13})}{(C_{11}C_{22} - C_{12}^2)} = 0.3322$$

(24)

$$\upsilon_{21} = \frac{(C_{12}C_{33} - C_{13}C_{23})}{(C_{11}C_{33} - C_{13}^2)} = 0.5000$$

$$v_{31} = \frac{(C_{13}C_{22} - C_{12}C_{23})}{(C_{11}C_{22} - C_{12}^2)} = 0.3645$$

$$G_{12} = C_{66} = 7.20GPa$$

$$G_{23} = C_{44} = 6.20GPa$$

$$G_{13} = C_{55} = 3.60GPa$$

Note that notation of this system is not conventional x, y, and z order. Notation 1 refers a normal vector direction, and notation 2 refers a vertical direction (conventionally y direction) while notation 3 refers a horizontal direction of the material (conventionally x direction) shown in Figure 92.

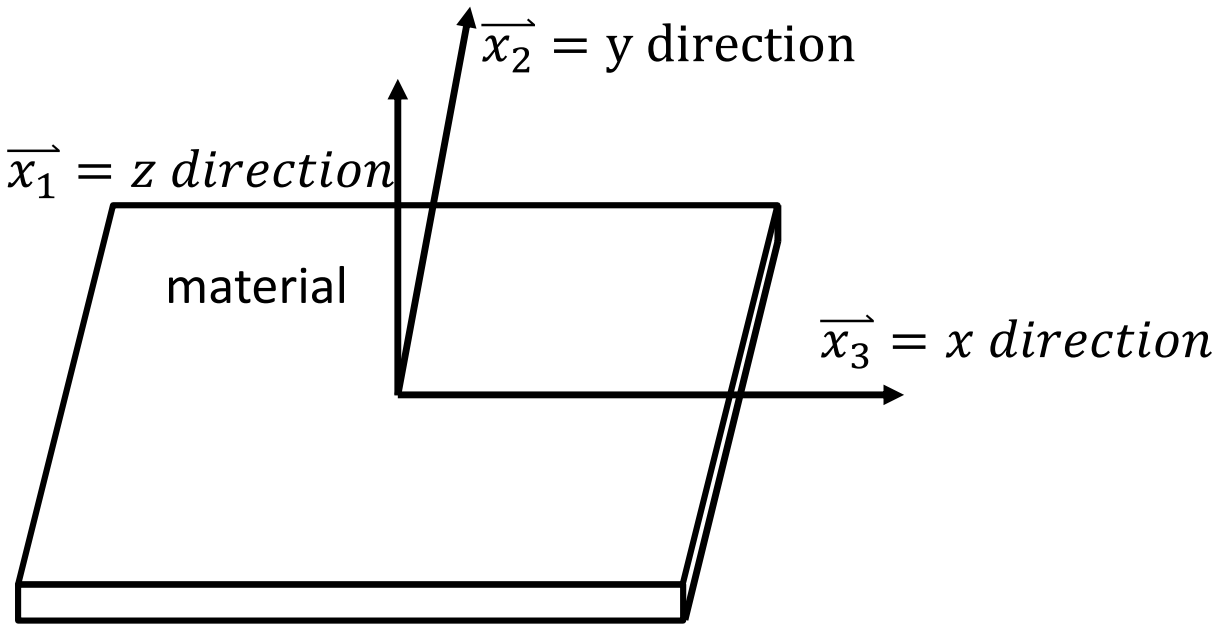

Figure 92. Notation used in orthotropic analysis

By using these, effective elastic moduli can be calculated with same boundary conditions described section 10.3.1. Stress and strain results are shown in Table 21.

.

Table 21. Stress, strain and effective elastic modulus on both x and y direction (Orthotropic material)

	X-direction	Y-direction
Strain	$\epsilon_x = \frac{\Delta l_x}{l_x} = \frac{5}{3.90} = 1.2813$	$\epsilon_y = \frac{\Delta l_y}{l_y} = \frac{5}{2.68} = 1.8636$
Stress	$\frac{F}{length_y} = \frac{141.41 * 10^9}{2.68}$ $= 52.71\ GPa$	$\frac{F}{length_x} = \frac{104.41 * 10^9}{3.90} = 26.76\ GPa$
Effective elastic modulus	$Ex_{eff} = 41.14Gpa$	$Ey_{eff} = 14.36Gpa$

The material is assumed to be an orthotropic material, which has aligned grain in x-direction. Therefore, elastic modulus in x direction is much larger than the other directions, indicating that this material is stiff in x-direction. When the orientation of each grain is applied, aligned grains have different orientations, affecting elastic moduli in both x and y directions. Hence, the distribution of displacement of both x and y directions (shown in Figure 93 and Figure 94) are non-uniform patterns. The effective elastic modulus in x direction decreases 68.77% while elastic modulus in y direction increases 39.28%. Before applying the orientation angles the material has aligned grains in x direction, and then the orientation affects alignment of the grains, causing reducing elastic modulus in x direction. On the other hand, y direction elastic modulus increases due to the orientations of the grain by having un-organized aligned grains.

The research objective is to achieve structure-property relationship for microstructure model. The geometric features of the microstructure are extracted by the proposed method in Chapters 5, 6, 8, and 9. An explicit geometric model of microstructure using captured geometric features

is successfully performed in previous sections. If material constant and orientation of the grain microstructure are given, it is possible to have structure-property relationship.

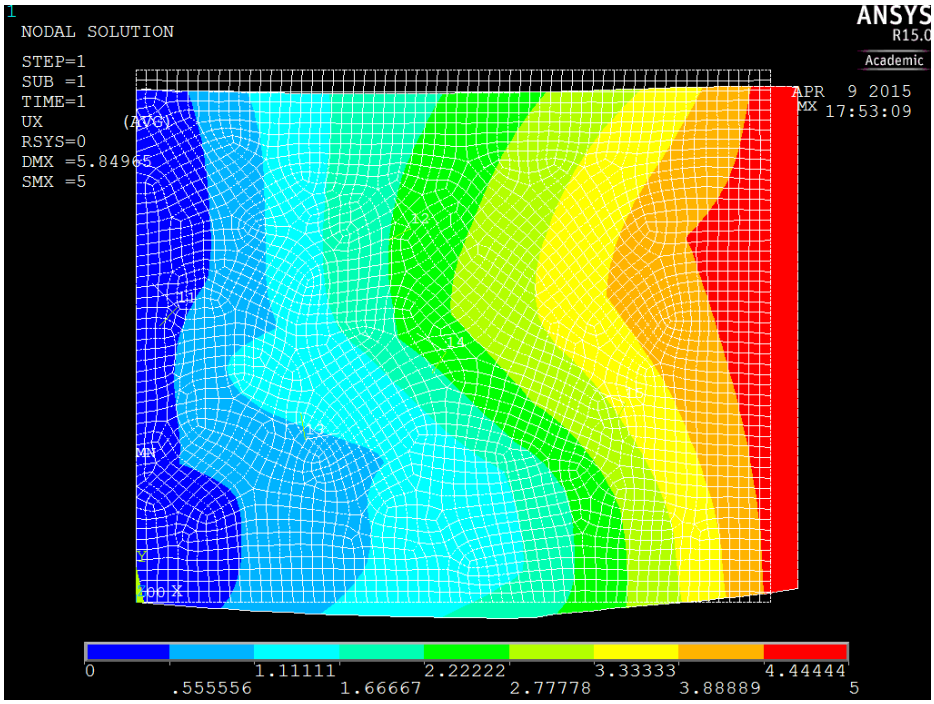

Figure 93. Displacement distribution of orthotropic material in x direction

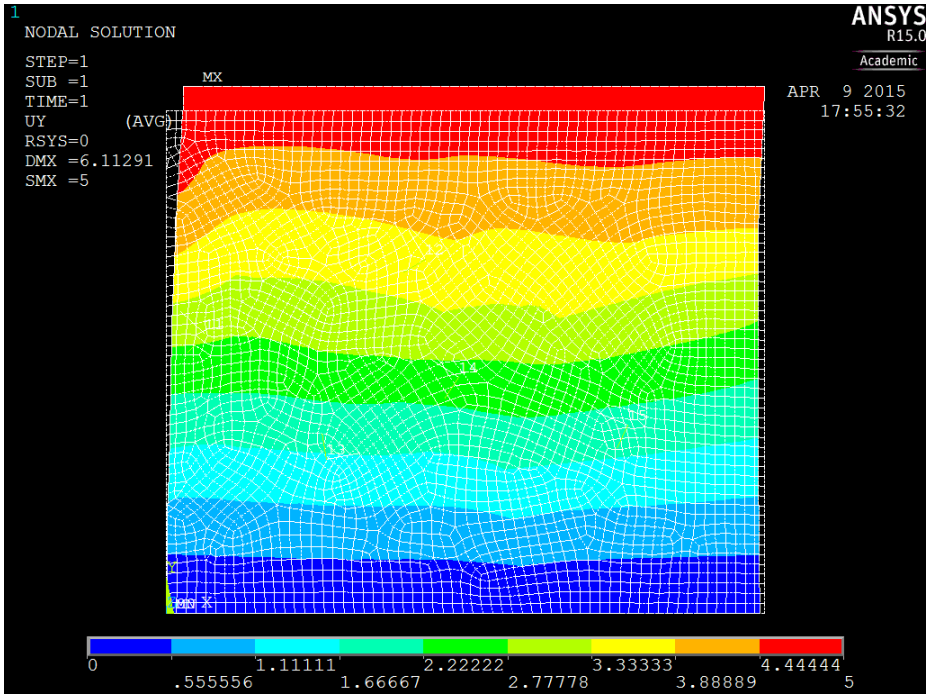

Figure 94. Displacement distribution of orthotropic material in y direction

10.4 Summary

This chapter explores structure-property relationship of microstructure. Structure of microstructure can be obtained using proposed method explained in chapter 5, 6, 8, and 9. Recognized geometric features using different kinds of surfacelet based methods form an explicit microstructure model by finding shared points or edges.

In this chapter, IN100 material is used to demonstrate a structure-property relationship. A structure model is constructed by the 2D surfacelet based method and each grain has different orientations. When the material has cubic crystal structure, effective elastic moduli in x direction and y directions increase compared to input elastic constants. This is because the shear modulus G is not related to the Poisson's ratio and elastic modulus through the usual relation in isotropic material. In addition, the material is assumed to be orthotropic material,

which requires 9 independent elements in compliance matrix to calculate elastic constants. This type of material produces different values of effective elastic moduli in x and y directions. These simulations provide one relationship, structure-elastic modulus of material.

The most important factor in this research is that an explicit microstructure model is used. An explicit microstructure model can provide specific coordinates of each vertices, points, and edges. This representation is consistent with the representation that is used in current CAD system. A microstructure model with property relationship can be integrated into a current CAD system and this enables the development of a heterogeneous CAD system.

CHAPTER 11
COMPARISON AND CONTRAST OF THE METHOD

This research aims to develop a new method of geometric reconstruction for microstructure. The method, a surfacelet-based method, represents a different approach to microstructure quantification methods than conventional statistical and voxel modeling approach. This chapter compares the surfacelet-based method with conventional microstructure quantification methods used in the Material Science area.

11.1 Statistical approach

Mathematically, local state is defined at the length scale of interest by averaging the information over all the length scales below the selected length scale [32]. The form of a probability distribution at a particular material point describes a local state, explaining means of finding a particular local state in some small neighborhood around a material point. The local state distribution summarizes volume fraction information and, is the most well-known statistical measure of microstructure. Orientation distribution function (ODF) is one of the most studied local state distributions in metal alloy for representing processing/property relationships [33]. By using ODF, each distinct lattice orientation can be explained as an independent local state. The spatial distribution of local states in the material internal structure would be limited even if the user had defined the local states of interest and the corresponding local state space. *N*-point correlations provide a rigorous statistical framework to define the spatial correlations of local states in the microstructure [34]. Since distributions on local state spaces reflect the probability density associated with finding a specific local state of interest, *h*, at a point selected randomly in the microstructure, they often are termed 1-point statistics. 2-point correlations are

expanded versions of the basic concept that capture the probability density associated with finding local states *h* and *h*' at each end of finite-length vectors thrown randomly into a microstructure image. 1-point probability function represents the phase volume fraction that is commonly used in classical homogenization methods to capture material's heterogeneity [35]. 2-point correlation is useful for characterization of phase distribution, morphology, and spatial arrangement and heterogeneity of microstructure feature. Also, it has been used in statistical mechanics based models for computation of mechanical and physical properties of heterogeneous material [35, 36]. 2-point correlation function describes grain size distribution and hierarchy of statistical measures of the microstructure. Furthermore, it can incorporate distribution and interaction of two phases as well as information on the shape and morphology of each individual phase.

Mathematically, local state is defined at the length scale of interest by averaging the information over all the length scales below the selected length scale [32]. 2-point correlation function is good enough to provide information for microstructure reconstructions, where reconstructed microstructures are statistically accurate. Different reconstructions can span the range of real microstructures. However, 2-point correlation functions give only probability of finding two points in given positions separated by a given distance. Therefore the design of heterogeneous material from only 2-point correlation functions can result in several microstructure cases [35]. In terms of modeling, the surfacelet based method generates an explicit geometric reconstruction model, which provides coordinates of vertices for linear features, center coordinates, radius for non-linear features. Additionally, the surfacelet based method generates consistent results using explicit equations because the reconstruction model is based on the image. Therefore, microstructure model can be easily converted to current CAD system. However, the surfacelet based method highly depends on the quality of image.

Furthermore, the surfacelet based method cannot capture the range of microstructures that actually occur while 2-point methods can.

11.2 Dream3D

It is important to obtain accurate microstructure model in 3D because it allows predicting structure-property relations. The accurate microstructure model contains size, shape, orientation, and spatial arrangement of grains, which can have a significant influence on the microstructure properties of materials. Dream3D is a program, providing quantification of microstructural features in 3D and generating of statistically equivalent microstructures. Dream3D is intended to design quantification of microstructural parameters as well as their correlations to define morphological characteristics. Then it generates statistically equivalent synthetic microstructure model. The input data are the form of statistical characterization data obtained from serial-sectioning of microstructure. The size and shape measurement collected from 2D sections and then extrapolated to 3D, can have potential error in representing the actual 3D distribution [37] [38].

Similar to Dream3D, the surfacelet based method also uses 2D images to reconstruct microstructure models. The reconstruction method in Dream3D uses the statistical models to generate a model of grains, where each grain is modeled using a collection of polygons. Dream3D grain representation is the same as the surfacelet based method in which explicit geometric equations are constructed for grain boundaries. The difference is that the surfacelet based method uses mathematical conversion in the process of generating microstructure model, instead of using statistical information. Therefore, geometric features in the constructed microstructure model have each mathematical equation so that it can be easily converted to parametric form used in current CAD system. The advantage of using the surfacelet based

method is providing consistent results for users whereas the Dream3D constructs a statistically equivalent, but different microstructure model. The surfacelet based method directly extracts geometric features from image so that it will produce the same results when it runs. However, the Dream3D will construct a different microstructure since it samples the statistical distributions each time it runs.

11.3 Voxel modeling

The research about reconstruction with voxel modeling for microstructure has been conducted. Representations of microstructure using voxel modeling provide physical location within a 3D volume so that its properties, density, color and more can be described [39]. Most of CAD systems are simply unable to manage spatial variations in material properties. This is because that most design programs have been built upon a surface modeling paradigm where a 'solid' object is defined as an object enclosed by a set of discrete boundaries. This is known as Boundary Representation or Brep [17]. On the other hand, voxel representations offer a new paradigm where objects can be defined as a dense representation of material properties throughout a 3D volume. The voxel modeling converts microstructure data directly to the 3D modeling, including its material property information. The surfacelet-based method, on the other hand, uses microstructure data mathematically to convert microstructure models and then its properties are connected to the model using another process. It is much more complicated process to establish structure-property relationships compare to voxel modeling.

The advantage of the surfacelet based method is accuracy. For example, the surfacelet based method generates explicit information of each geometric feature so it provides specific center coordinate, radius and start, end point of the curvature. On the other hand, the voxel modeling is a fast and fully automated mesh generation technique, where the elements are directly

created from the 3D dataset [40]. However, representation of curvature with jagged inner and outer surfaces might cause numerical problems. Marks and Gardner showed that the use of unsmoothed geometry could result in a lack of convergence for elements with sharp geometrical discontinuities[41]. In addition, if a voxel modeling achieves a moderate accuracy then, it requires a large number of freedoms [42].

11.4 Compression

Material image requires a large storage space especially for computational material design. For example, a small 3D material image with the size of 1000×1000×1000 resolution has 1 billion pixels [26]. Therefore, this image may have a size of hundreds of megabytes even with a compressed format such as JPEG. Therefore, data compression for material images is important. The surfacelet based method includes the Radon transform and the peak values are selected from the Radon transform coefficient domain. From the input image to the selected peak value, data are compressed to reconstruct geometric features. Data compression by the surfacelet based method will be described in this chapter, comparing compression ratio with different data compression method.

The 2D surfacelet based method uses gray scale JPEG image with size of n x m pixel. In order to reconstruct geometric features from a microstructure image, the 2D surfacelet based method only requires peak values in the Radon transform coefficient domain. The peak value provides the angle of the linear feature (α) and the distance of the feature from the origin (b). By using α and b, it is possible to reconstruct a linear feature. Therefore, the number of geometric features (k) require k x (α, b) numbers of data for reconstructing the geometric features in n x m pixel image domain.

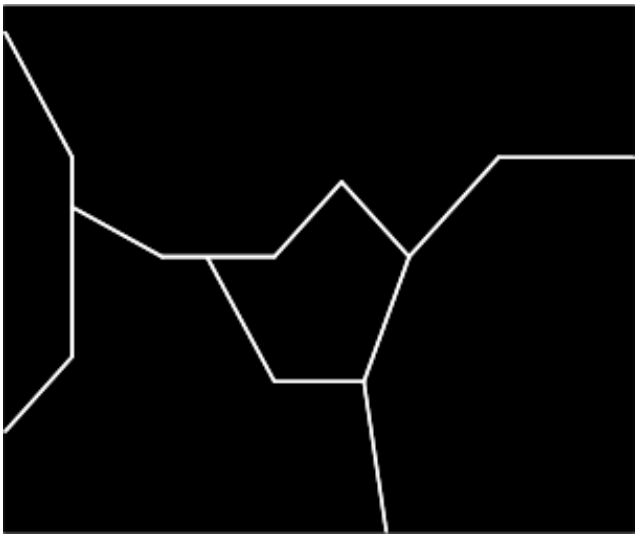

Figure 95. 2D IN100 image (smoothed)

IN100 2D image used in chapter 6 will be used as an example shown in Figure 95. The image size is 302 x 253 pixels with gray scale, which is 611,246 (8 x 302 x 253) bytes. The image of IN100 is applied to the Radon transform. The Radon transform generates 363 x 181 coefficient domain, which is 525,624 (8 x 363 x 181) bytes. Data compression ratio is defined as the ratio between the uncompressed size and compressed size [43].

$$compression\ ratio = \frac{uncompressed\ size}{compressed\ size}$$

Therefore, the compression ratio is 1.162. Then, peak values are selected in order to reconstruct microstructure model. In this example only 14 peaks are selected and each peak value is represented (α, b). Therefore, since only 28 floating points are required, the compression ratio is 21,830.

Huang conducted a research about retrieving the image pixels from the surface integrals based on feature identification results [26]. By the complete of forward and inverse surfacelet transform, the compression material image data was reconstructed. In the surfacelet transform,

surface integrals are obtained from image pixels. Huang et al. tried to use three different constrained conjugate-gradient-based methods with combinations of boundary constraints and inner constraints on internal distributions to solve the inverse problem of retrieving image pixel values from surface integrals[26]. They used a gray scale nano-fiber composite image. The cylindrical surfacelet is used to reconstruct circular geometric features. Total number of pixel for image is 3600 (20 x 20 x 9) and the number of pixel for the surfacelet is 1875. The compression ratio he obtained is 1.92, which is very small number compared to the compression ratio from the surfacelet based method (21,830).

11.5 Summary

This chapter compares the surfacelet based method with different approaches, which are designed to reconstruct microstructure models. The surfacelet based method provides consistent reconstructed model meanwhile statistical approaches, n-point correlation and the Dream3D, generate different microstructure models since it samples the statistical distributions each time it runs. Additionally, the surfacelet yields an explicit geometric model, which is convenient form to be converted to CAD system. Then, properties of the microstructure model will be connected. Therefore, the heterogeneous CAD system can be achieved.

CHAPTER 12
CONCLUSION

The central goal of this dissertation was the development of a heterogeneous CAD system, which integrates parameters related to material composition, microstructure, and mechanical properties with geometry information. Structure-property-process relationships of material need to be built and integrated into current CAD system in order to support the heterogeneous CAD system. The relationships allow detailed composition of actual material to be captured. This research only focuses on a structure-property relationship of micro scale. A new method for reverse engineering of material is presented to construct an explicit geometric model that can be used as CAD representations to support a heterogeneous part modeling. An explicit microstructure model can be achieved by capturing geometric features in the microstructure image. The geometric features in the image can be defined as the structure, represented by lines, angles, curves, and other geometric primitives. These geometric features are captured by the proposed methods, Surfacelet based method, and used for constructing a microstructure model.

12.1 Answering the research question 1

This chapter answers research question 1 and its hypotheses. Research question 1 is

"Can an entire geometric feature in the microstructure image be extracted as an explicit geometric model using the surfacelet method?"

12.1.1 Linear geometric feature model in 2D

Hypothesis 1.a: *"A surfacelet based method that includes the Radon transform can be used to detect linear features using infinite lines, for 2D images, or bounded planes, for 3D datasets, and this can provide* ***an explicit geometric model*** *of these microstructure features."*

Hypothesis 1.a states to extract linear geometric features in the 2D image and 3D voxel data set. In chapters 5 and 6 explain the method to capture linear geometric information from the 2D image domain and its examples. Chapter 5 completes how to recognize geometric feature in 2D image domain. Orientation, position, and length of 2D linear geometric features are determined by using proposed approaches, the surfacelet based method, which includes butterfly wing method and line overlaying method. This method is proposed to answer this research question1. By using masking, clustering, and high frequency component of the wavelet transform, it is possible to select appropriate peak values, which correspond to linear feature in the image domain. Then, analyzing peak values using 2 approaches, a butterfly wing method and a line overlaying method, allows recognizing geometric feature completely.

In chapter 8, 3D linear geometric features are recognized by the 3D surfacelet based method. The 3D Surfacelet based method includes a 3D Radon transform followed by a plane overlaying method. Each recognized 3D linear feature is used to construct a 3D microstructure. The hypothesis of this research question is validated in chapter 8 by showing the process by which the voxel data was constructed microstructure using the proposed method, 3D Surfacelet-based method. The 3D Surfacelet-based method can be successfully used to recognize 3D linear features with **explicit form,** which is the same representation system that current CAD systems use. Therefore, the hypothesis has been validated and the research question has been answered.

12.1.2 Linear geometric feature in 3D

Hypothesis 1.b: *"Non-linear geometry features, such as circles or circular arcs, can be recognized by the cylindrical surfacelet based method, which can be used to represent cylindrical singularities. The cylindrical surfacelet based method extracts circular or cylindrical microstructure features as explicit geometry model from 2D or 3D dataset."*

Microstructure includes not only linear features but also non-linear features, such as cylinders or circles. A cylindrical surfacelet based method enables users to extract 2D and 3D non-linear features from the microstructure. The cylinderlet based method uses a cylinder shape to extract the curvature boundary of the microstructure feature.

Hypothesis 1.b states to extract non-linear geometric features in the 2D image. Chapter 9 explains the recognition of 2D non-linear feature in a microstructure domain. In order to do that, the 2D Cylinderlet based method is used. The 2D Cylinderlet based method includes the 2D circular Radon-like transform followed by the circle overlaying method. Each recognized 2D circular arc feature is used to construct explicit non-linear microstructure model. Chapter 9 contributes to answer the research question 1 followed by the hypothesis 1b. The hypothesis 1.b of this research question is validated in chapter 9 by showing the process of recognizing non-linear geometric features. The 2D Cylinderlet based method allows constructing an explicit microstructure model, providing center coordinates, radii, and start/end points of circular arcs. The research question is also answered.

12.2 Research question 2

This chapter answers research question 1 and its hypotheses. Research question 2 is

> ***"Can the structure-property relationship of microstructures be established using the microstructure model from recognized geometry features?"***

12.2.1 Structure-Property relationship

> Hypothesis 2: *"Recognized 2D linear features can be used to construct grain boundaries, which are used to form a microstructure model of grains. The microstructure model will be utilized as input to a computational engineering analysis tool so that effective mechanical properties can be calculated. By pursuing these processes, one can establish the structure-property relationship of microstructure"*

Integration of microstructure, material composition, and mechanical properties with geometry information aids many product development activities. Structure-property relationships enable users to model heterogeneous CAD systems, which support not only geometry information but also material composition. By using features extracted from research question #1, a microstructure model can be constructed.

Chapter 10 explores structure-property relationship of microstructure. Structure of microstructure can be obtained using proposed method explained in chapter 5, 6, 8, and 9. Recognized geometric features using different kinds of surfacelet based methods form an explicit microstructure model by finding shared points or edges.

In this research, IN100 material is used to demonstrate a structure-property relationship. A structure model is constructed by the 2D surfacelet based method and each grain has different

orientations. The effective elastic modulus can be calculated depending on the material crystal structure. The orientations of microstructure model and its elastic constants are applied to an explicit microstructure model.

The most important factor in this research is that an explicit microstructure model is used. An explicit microstructure model can provide specific coordinates of each vertices, points, and edges. This representation is consistent with the representation that is used in current CAD system. A microstructure model with property relationship can be integrated into a current CAD system and this enables the development of a heterogeneous CAD system.

12.3 Contributions

To summarize, the major contributions of this work include:

- This research contributes development of feature recognition for geometric primitives (e.g., lines, circular arcs)
- The overlaying methods determine geometric primitives quantitatively so it can be utilized to construct an explicit microstructure model.
- This research provides a framework to establish an explicit microstructure model using the Surfacelet based method.
- This research construct a structure-elastic property relationship of microstructure model, which can be greatly used to develop a heterogeneous CAD system.

12.4 Future work

As with any other research, this work has limitations. Outlined here are some of the future work that are worth exploring future.

- Constructing an entire 3D linear geometric model of microstructure

This research provides a feasibility of constructing grain model in the 3D space. Partially recognized real data set is shown in the research. The entire grains in the 3D voxel data set can be found using the proposed method. However, this requires extensive mathematical model for the 3D space and also huge computational resources. We do believe this work will fulfill the completion of an explicit model of linear geometric features.

- Recognizing a non-linear feature other than circular arc (ellipsis, artery shape)

A circular arc in the 2D image domain is focused on this research regarding non-linear geometric features in this research. A real microstructure image contains various types of geometric features other than a circular arc. It is worth to develop a mathematical model for various geometric features so it can be applied on the Surfacelet based method.

- Automation of recognizing the geometric feature in both 2D and 3D

The Surfacelet based method includes the Radon transform followed by overlaying method (for 2D linear case, a butterfly wing method can be substituted for a line overlaying method). During the process, tolerance values, threshold values, or other parameters are needed to be adjusted feature by feature in one image domain. However, if one can use optimization method to find universal numbers for each parameters for one image domain, it would greatly aid the proposed method to be automated.

- Exploring various effective mechanical properties, which can be integrated into an explicit geometric model

This research explored the effective elastic modulus for establishing structure-property relationship. The elastic modulus is one of the common mechanical property in Mechanical Engineering field. On the other hand, other common mechanical properties, such as thermal expansion coefficient, compressive strength, or hardness etc., can be also investigated. This would help to accomplish a structure-property relationship for microstructure model.

REFERENCES

1. Weisstein, E.W., *Euler angles.* 2009.

2. Torquato, S., *Random heterogeneous materials: microstructure and macroscopic properties*. Vol. 16. 2001: Springer.

3. Kumar, V. and D. Dutta, *An approach to modeling & representation of heterogeneous objects.* Journal of Mechanical Design, 1998. **120**(4): p. 659-667.

4. Kumar, A.V. and A. Wood. *Representation and design of heterogeneous components*. in *Proceedings of SFF Conference, Austin, Texas*. 1999.

5. Ganter, M., et al. *H-ISM: An implementation of heterogeneous implicit solid modeling*. in *ASME Desigh Automation Conference*. 2002. Montreal.

6. Pratap, A. and R.H. Crawford, *Implementation of a functionally gradient material modeling and design system*. 2003, University of Texas at Austin.

7. Schmid, S., M. Casey, and J. Starkey, *An illustration of the advantages of a complete texture analysis described by the orientation distribution function (ODF) using quartz pole figure data.* Tectonophysics, 1981. **78**(1): p. 101-117.

8. Saheli, G., H. Garmestani, and B. Adams, *Microstructure design of a two phase composite using two-point correlation functions.* Journal of computer-aided materials design, 2004. **11**(2): p. 103-115.

9. Niezgoda, S.R., et al., *Applications of the Phase-Coded Generalized Hough Transform to Feature Detection, Analysis, and Segmentation of Digital Microstructures.* Computers, Materials, & Continua, 2010. **14**(2): p. 79-98.

10. Leavers, V. and J. Boyce, *The Radon transform and its application to shape parametrization in machine vision.* Image and Vision Computing, 1987. **5**(2): p. 161-166.

11. Leavers, V., *Use of the Radon transform as a method of extracting information about shape in two dimensions.* Image and vision computing, 1992. **10**(2): p. 99-107.

12. Kak, A.C. and M. Slaney, *Principles of computerized tomographic imaging*. Vol. 120. 2001: Siam Philadelphia:.

13. Do, M.N. and M. Vetterli, *The finite ridgelet transform for image representation.* Image Processing, IEEE Transactions on, 2003. **12**(1): p. 16-28.

14. Lanzavecchia, S., P.L. Bellon, and M. Radermacher, *Fast and accurate three-dimensional reconstruction from projections with random orientations via radon transforms.* Journal of structural biology, 1999. **128**(2): p. 152-164.

15. Jiang, X., et al., *Linear feature extraction based on complex ridgelet transform.* Wear, 2008. **264**(5): p. 428-433.

16. Daubechies, I., O. Runborg, and W. Sweldens, *Normal multiresolution approximation of curves.* Constructive Approximation, 2004. **20**(3): p. 399-463.

17. Wang, Y. and D.W. Rosen, *Multiscale Heterogeneous Modeling with Surfacelets.* Computer-Aided Design & Applications, 2010. **7**(5): p. 759-776.

18. David W. Rosen, N.J., Yan Wang, *A Method for Reverse Engineering of Material Microstructure for Heterogeneous CAD.* Computer-Aided Design, 2013.

19. MacQueen, J. *Some methods for classification and analysis of multivariate observations*. in *Proceedings of the fifth Berkeley symposium on mathematical statistics and probability*. 1967. Oakland, CA, USA.

20. Chui, C.K., *Wavelets: a tutorial in theory and applications*. Vol. 2. 2012: Academic Press.

21. Kaur, J., *Properties of biologically relevant nanocomposites: effects of calcium phosphate nanoparticle attributes and biodegradable polymer morphology.* 2010.

22. Shenoy, M., Y. Tjiptowidjojo, and D. McDowell, *Microstructure-sensitive modeling of polycrystalline IN 100.* International Journal of Plasticity, 2008. **24**(10): p. 1694-1730.

23. Wang, F., J. Mei, and X. Wu, *Microstructure study of direct laser fabricated Ti alloys using powder and wire.* Applied Surface Science, 2006. **253**(3): p. 1424-1430.

24. Jeong, N., D.W. Rosen, and Y. Wang. *A Comparison of Surfacelet-Based Methods for Recognizing Linear Geometric Features in Material Microstructure*. in *ASME 2013 International Design Engineering Technical Conferences and Computers and Information in Engineering Conference*. 2013. American Society of Mechanical Engineers.

25. Smistad, E., A.C. Elster, and F. Lindseth, *Real-time gradient vector flow on GPUs using OpenCL.* Journal of Real-Time Image Processing, 2012: p. 1-8.

26. Huang, W., Y. Wang, and D.W. Rosen, *Inverse Surfacelet Transform for Image Reconstruction With Constrained-Conjugate Gradient Methods.* Journal of Computing and Information Science in Engineering, 2014. **14**(2): p. 021005.

27. Shafrir, S.N., et al., *Zirconia-coated carbonyl-iron-particle-based magnetorheological fluid for polishing optical glasses and ceramics.* Applied optics, 2009. **48**(35): p. 6797-6810.

28. Canny, J., *A computational approach to edge detection.* Pattern Analysis and Machine Intelligence, IEEE Transactions on, 1986(6): p. 679-698.

29. Bower, A.F., *Applied mechanics of solids*. 2009: CRC press.

30. Tong, W., *A planar plastic flow theory of orthotropic sheet metals and the experimental procedure for its evaluations.* Proceedings of the Royal Society A: Mathematical, Physical and Engineering Science, 2005. **461**(2058): p. 1775-1809.

31. Hosten, B., *Elastic characterization of orthotropic composite materials from ultrasonic inspection through non-principal planes*, in *Review of Progress in Quantitative Nondestructive Evaluation*. 1991, Springer. p. 1437-1444.

32. Kalidindi, S.R., S.R. Niezgoda, and A.A. Salem, *Microstructure informatics using higher-order statistics and efficient data-mining protocols.* JOM Journal of the Minerals, Metals and Materials Society, 2011. **63**(4): p. 34-41.

33. Fullwood, D.T., S.R. Niezgoda, and S.R. Kalidindi, *Microstructure reconstructions from 2-point statistics using phase-recovery algorithms.* Acta Materialia, 2008. **56**(5): p. 942-948.

34. Kalidindi, S.R., S.R. Niezgoda, and A.A. Salem, *Microstructure informatics using higher-order statistics and efficient data-mining protocols.* Jom, 2011. **63**(4): p. 34-41.

35. Mikdam, A., et al., *A new approximation for the three-point probability function.* International journal of solids and structures, 2009. **46**(21): p. 3782-3787.

36. Lin, S. and H. Garmestani, *Statistical continuum mechanics analysis of an elastic two-isotropic-phase composite material.* Composites Part B: Engineering, 2000. **31**(1): p. 39-46.

37. Groeber, M., et al., *A framework for automated analysis and simulation of 3d polycrystalline microstructures.: Part 1: Statistical characterization.* Acta Materialia, 2008. **56**(6): p. 1257-1273.

38. Groeber, M., et al., *A framework for automated analysis and simulation of 3D polycrystalline microstructures. Part 2: Synthetic structure generation.* Acta Materialia, 2008. **56**(6): p. 1274-1287.

39. Hosoi, F., Y. Nakai, and K. Omasa, *3-D voxel-based solid modeling of a broad-leaved tree for accurate volume estimation using portable scanning lidar.* ISPRS Journal of Photogrammetry and Remote Sensing, 2013. **82**: p. 41-48.

40. Lengsfeld, M., et al., *Comparison of geometry-based and CT voxel-based finite element modelling and experimental validation.* Medical engineering & physics, 1998. **20**(7): p. 515-522.

41. Marks, L. and T. Gardner, *The use of strain energy as a convergence criterion in the finite element modelling of bone and the effect of model geometry on stress convergence.* Journal of biomedical engineering, 1993. **15**(6): p. 474-476.

42. Viceconti, M., et al., *A comparative study on different methods of automatic mesh generation of human femurs.* Medical engineering & physics, 1998. **20**(1): p. 1-10.

43. Poynton, C., *Digital video and HD: Algorithms and Interfaces*. 2012: Elsevier.